Brain Oscillatory Signal Analyses in Chronic Pain

by

Henry Fu

M.A.Sc., University of British Columbia, 1991

B.Sc.E., University of New Brunswick, 1986

Thesis Submitted in Partial Fulfillment of the

Requirements for the Degree of

Doctor of Philosophy

in the

School of Engineering Science

Faculty of Applied Sciences

SIMON FRASER UNIVERSITY

Fall 2023

Declaration of Committee

Name:	**Henry Fu**
Degree:	**Doctor of Philosophy**
Title:	**Brain Oscillatory Signal Analyses in Chronic Pain**
Committee:	**Chair: Mirza Faisal Beg** Professor, Engineering Science
	Teresa Cheung Co-Supervisor Assistant Professor, Engineering Science
	Ash Parameswaran Co-Supervisor Professor, Engineering Science
	Sam Doesburg Committee Member Associate Professor, Biomedical Physiology and Kinesiology
	Urs Ribary Examiner Professor Emeritus, Psychology
	Naznin Virji-Babul External Examiner Associate Professor, Physical Therapy University of British Columbia

Ethics Statement

The author, whose name appears on the title page of this work, has obtained, for the research described in this work, either:

a. human research ethics approval from the Simon Fraser University Office of Research Ethics

or

b. advance approval of the animal care protocol from the University Animal Care Committee of Simon Fraser University

or has conducted the research

c. as a co-investigator, collaborator, or research assistant in a research project approved in advance.

A copy of the approval letter has been filed with the Theses Office of the University Library at the time of submission of this thesis or project.

The original application for approval and letter of approval are filed with the relevant offices. Inquiries may be directed to those authorities.

Simon Fraser University Library
Burnaby, British Columbia, Canada

Update Spring 2016

Abstract

Pain lasting three months or longer is generally referred to as Chronic Pain (CP). According to Health Canada, approximately 20% of the Canadian population experience CP within their lifespan. CP also greatly burdens society. For example, in 2019 alone, $40 billion was spent on CP. CP research includes the search for diagnostic tools and pain intervention methods. My thesis examined the use of EEG/MEG brain rhythms in CP and explored non-traditional intervention, which focused on two main goals. The first goal was to explore the inclusion of age in CP analysis, as age can influence brain rhythm properties. The second goal was to use virtual reality (VR)-guided meditation as a mindfulness-based stress reduction alternative intervention for CP.

To study CP and aging, a MEG database of 474 healthy controls and 22 CP participants was used. The methods included finding the participants' brain rhythm properties in four alpha generation regions of interest (ROIs) and the rhythm property correlations with age. A CP case study demonstrated how to include age using support vector regression (SVR). The results showed the brain rhythm properties in the four ROIs were significantly independent, and negative correlations with medium effect size were found between peak alpha frequency (PAF) and age in the frontal, temporal, and parieto-occipital ROIs. In the case study, SVR prediction helped identify slowed PAF in the posterior brain area of the CP participants. This novel SVR prediction approach helps to include age in CP analysis without using age-matched controls.

To study the VR-guided meditation, ten adult patients with chronic cancer pain were recruited. The patients underwent a VR-guided meditation experience in a specially designed therapy sequence. Brain rhythm changes measured in EEG before, during, and after meditation were compared using topography, coherence, and cluster-based permutation techniques. EEG power changes were compared with the patient-reported numerical pain rating scores before, during and after meditation. During the therapy, increased power was found in β and γ bandwidths, and coherence changes between the frontal, parietal, and occipital regions in the θ, α, and γ bands were observed. No significant relationships between pain scores and EEG power variations were found. The novel EEG recording and analysis methods help reveal specific therapy-related EEG changes and can be used to investigate neurophysiological changes in VR pain applications.

Keywords: aging; chronic pain (CP); electroencephalography (EEG); magnetoencephalography (MEG); support vector regression (SVR); virtual reality (VR)-guided meditation

Dedication

I dedicate this thesis to my Lord and Saviour, Jesus Christ.

Acknowledgements

I would like to thank my co-supervisors, Dr. Teresa Cheung and Dr. Ash Parameswaran, for their valuable guidance, support, and encouragement throughout the research.

I would also like to thank my committee member, Dr. Sam Doesburg, for his feedback on improving my thesis.

Special thanks to Dr. Bernie Garrett for giving me the chance to collaborate with his excellent research team at UBC, and the financial support for me to go to a conference.

Table of Contents

List of Tables

List of Figures

List of Acronyms

ACC	Anterior Cingulate Cortex
AD	Alzheimer's Disease
AI	Anterior Insula
AMY	Amygdala
ASD	Autism Spectrum Disorder
BEM	Boundary Element Method
BG	Basal Ganglia
CamCAN	Cambridge Centre for Ageing and Neuroscience
CCA	Canonical Correlation Analysis
CMS	Command Mode Sense
CNN	Convolutional Neural Network
CNS	Central Nervous System
CP	Chronic Pain
DMN	Default Mode Network
DRL	Driven Right Leg
dSPM	Dynamical Statistical Parametric Mapping
EC	Eyes Closed
ECG	Electrocardiogram
EEG	Electroencephalography
EMG	Electromyogram
EO	Eyes Open
EOG	Electrooculogram
ERF	Event-Related Field
ERP	Event-Related Potential
FDR	False Discovery Rate
FEM	Finite Element Method
FFT	Fast Fourier Transform
FM	Fibromyalgia
fMRI	Functional Magnetic Resonance Imaging

fNIRS	Functional Near-Infrared Spectroscopy
FPN	Frontoparietal Network
FWER	Family-Wise Error Rate
HMD	Head-Mounted Display
HPI	Head Position Indicator
HSP	Head Shape Point
IAB	Individual Alpha Bandwidth
IAPF	Individual Alpha Peak Frequency
IC	Insular Cortex
ICA	Independent Component Analysis
ICD-11	International Classification of Diseases, Revision 11
LORETA	Low-Resolution Electromagnetic Tomography
MAE	Mean Absolute Error
MANOVA	Multivariate Analysis of Variance
MBSR	Mindfulness-Based Stress Reduction
MCI	Mild Cognitive Impairment
MEG	Magnetoencephalography
mPFC	Medial Prefrontal Cortex
MRI	Magnetic Resonance Imaging
NPR	Numerical Pain Rating
NRS	Numerical Rating Scale
OLS	Ordinary Least Square
OMEGA	Open MEG Archive
PAF	Peak Alpha Frequency
PAG	Periaqueductal Grey
PB	Parabrachial Nucleus
PCA	Principal Component Analysis
PCC	Posterior Cingulate Cortex
PFC	Prefrontal Cortex
PNS	Peripheral Nervous System
PSD	Power Spectral Density

RBF	Radial Basis Function
RCT	Randomized Controlled Trial
RVR	Relevance Vector Regression
S1	Primary Somatosensory Cortex
S2	Secondary Somatosensory Cortex
SCI	Spinal Cord Injury
SFU	Simon Fraser University
SN	Salience Network
SVR	Support Vector Regression
TCD	Thalamocortical Dysrhythmia
TD	Typically Developing
Th	Thalamus
VR	Virtual Reality

Chapter 1.

Introduction

1.1. Background

According to Health Canada, almost 8 million people in Canada or around one-fifth of the population, experience chronic pain (CP) (Canada, 2021; Schopflocher, 2011). CP refers to pain lasting over three months (Canada, 2021). Examples are lower back pain, spinal cord injury pain, arthritis and cancer pain (Treede et al., 2015). CP can impair function and significantly impact the patient's quality of life (Government of Canada, 2018). It also greatly burdens society, for instance, a total direct and indirect cost of around $40 billion was spent on CP in 2019 in Canada (Canada, 2020). CP becomes more prevalent as people age. According to the USA National Health Interview Survey, 2016, the prevalence of CP in the 18-24 age group was 7.0%, 25-44 was 13.2%, 45-64 was 27.8%, 65-84 was 27.6%, and in the 85+ age group was 33.6% (Dahlhamer, 2018) (Table 1.1).

Table 1.1. Prevalence of chronic pain in the USA in 2016.

Age Group	Percentage	Ratio
18 - 24	7.0%	≥ 1/15
25 - 44	13.2%	≥ 1/8
45 - 64	27.8%	≥ 1/4
65 - 84	27.6%	≥ 1/4
85+	33.6%	≥ 1/3

1.2. Motivation

Two CP research topics interest us: CP assessment and CP intervention. Even with today's advanced medical technology, assessing CP in patients is still challenging. It often relies on the patients to estimate and report pain, such as using the numerical pain rating scale (NPRS) (Williamson & Hoggart, 2005). However, using a pain scale to self-report the pain level is rather subjective, and an objective solution to CP assessment is desired. In recent years, there has been much research on objective CP assessment based on CP biomarkers, and the use of resting-state electroencephalography (EEG) and

magnetoencephalography (MEG) as biomarkers are potential ones (Pinheiro et al., 2016; Zebhauser et al., 2022). EEG and MEG are neuroimaging tools with high temporal resolution which can detect brain rhythm changes. The implementation methodology usually requires comparing CP patients' EEG/MEG data with that of matched healthy controls. As age can significantly affect the brain's oscillatory signal properties (Chiang et al., 2011), age-matched controls are required to minimize false positive results. An aging model to extend general future large database studies is desired. This leads to our first objective in this thesis: to explore an aging model to overcome the age-matched control requirement in CP studies.

The primary CP intervention approach in North America is through medications, such as opioids. However, medications can cause complications and side effects for the patients, and alternative CP interventions are highly desired. Mindfulness-based stress reduction (MBSR) (Kabat-Zinn, 2003; Rosenzweig et al., 2010) is a potential solution, and it is non-invasive, safe, has no side effects and is easy to apply. An implementation of MBSR using virtual reality (VR)-guided meditation for CP intervention is of interest to us. However, this brings out a new problem in assessing the intervention effect. Our second objective in this thesis is to verify VR-guided meditation as an alternative intervention for CP and use EEG for the intervention effect assessment.

1.3. Pain

Pain is sensory and affective (Talbot et al., 2019), and this thesis only refers to sensory pain. Pain involves sensory, motivational and cognitive activities (Melzack & Casey, 1968; Ploner et al., 2017) and is a unique experience from sight, hearing, or touch (Melzack & Casey, 1968). Pain can be caused by noxious stimuli (physiological) or arise from tissue or nerve damage and diseases (pathological) (Kuner, 2004; Liu & Kelliher, 2022). Physiological pain is to alert that the body is being invaded or damaged, which triggers a biological response to escape danger or quit doing something harmful (Melzack & Casey, 1968; Kuner, 2004). Pathological pain is due to nociceptive hypersensitivity or spontaneous pain, including neuropathic pain, chronic inflammatory pain, etc. (Kuner, 2004).

The pain pathway can be described in four processes: the transduction and transmission processes in the peripheral nervous system (PNS) and the modulation and

perception processes in the central nervous system (CNS) (Christiansen & Cohen, 2018). The transduction process starts from a noxious stimulus that triggers the peripheral nociceptors. In the transmission process, the signal transmits through the first-order neuron and the synapse at the dorsal horn, then to the second-order neuron and ascends the spinal cord to the thalamus. The signal further broadcasts to other cortical sites from the thalamus, including the somatosensory cortex, the cingulate and the insula. The modulation process transforms the signal biologically, and the perception process interprets the signal in the brain. The brain can control through the periaqueductal grey in the midbrain to stop the perception of pain from being transmitted to the second-order neuron with enkephalin (Baller & Ross, 2017). The brain areas which are involved in the pain network are anterior cingulate cortex (ACC), primary somatosensory cortex (S1), secondary somatosensory cortex (S2), insular cortex (IC), thalamus (Th), prefrontal cortex (PFC), nucleus accumbens, amygdala (AMY), basal ganglia (BG), periaqueductal grey (PAG), parabrachial nucleus (PB) and cerebellum (Apkarian et al., 2005; Bushnell et al., 2013).

In addition to physiological and pathological pain, pain can be classified into five types: acute, chronic, neuropathic, nociceptive, and radicular (McLaren, 2023). Acute pain lasts relatively short, from minutes to three months, and is typically related to soft-tissue injury or temporary illness (McLaren, 2023). Pain that lasts longer than three months or beyond the expected healing time, such as lower back pain, spinal cord injury pain, arthritis and cancer pain, is referred to as CP (Treede et al., 2015; Canada, 2021). Neuropathic pain is related to the damage of the nerves or nervous system. Nociceptive pain is caused by damage to body tissue. Radicular pain happens when a spinal nerve is compressed or inflamed (McLaren, 2023). Another mechanism classifies pain types as nociceptive, inflammatory, and neuropathic pain (Yang & Chang, 2019), where Inflammatory pain relates to tissue damage and inflammation.

Pain diagnosis is mainly through self-reporting with clinical questionnaires or a numerical pain rating scale (NPRS) (Williamson & Hoggart, 2005). This method could be subjective and inconsistent, and self-reporting may not be applicable if patients cannot communicate properly. Objective pain measures are desired in diagnosis, patient condition monitoring and treatment delivery. Some objective approaches reported are by analyzing (1) pain behaviour, such as facial expression recognition and electrical activity of muscles and movement, and (2) physiological signals, such as changes in heart rate,

skin conductance, and pupillary dilation, etc. (3) pain brain activity, such as functional connectivity (FC) and power changes in theta and alpha brain wavebands (Zhang & Seymour, 2014).

1.4. Chronic Pain

CP is a pathological condition due to central sensitization, which refers to hypersensitization in the spinal cord's dorsal horn (Latremoliere & Woolf, 2009; Woolf, 2011; Greenwald & Shafritz, 2018). The transition from acute to CP is mainly related to neural plasticity: (1) The regrowth of a pain fibre after an injury can be abnormal. The nonselective growth factors released by macrophages can cause the non-pain and sympathetic fibres to grow. As a result, they could all synapse on a cell that should respond to pain only. (2) In an injury, C fibres at the synapse may misfire continuously and cause dorsal horn neurons to become more sensitive to stimulation. (3) The CP signal projects to the nucleus accumbens may cause the nucleus accumbens to become hypersensitive to pain signals (Baller & Ross, 2017).

CP can alter the brain's chemistry, generating abnormal neurotransmitter levels. CP also triggers changes in brain structure and functionality, such as decreased grey matter volume and abnormal FC within the salience network (SN) and default-mode networks (DMN) (Borsook, 2012; Hemington et al., 2016; Greenwald & Shafritz, 2018). For instance, the dorsolateral prefrontal lobe circuits can be altered in CP conditions and affect a patient's cognition and emotion, leading to increased fear, anxiety and depression (Borsook, 2012).

The brain functional networks are specific brain regions that are interconnected together. DMN comprises brain regions involved in cognitive functions, including the posterior cingulate cortex (PCC), precuneus, medial prefrontal cortex (mPFC), and inferior parietal cortices (Broyd et al., 2009). SN acts as a switch of the other brain networks in information processing and comprises the anterior insula (AI) and dorsal anterior cingulate cortex (ACC) (Seeley, 2019). CP causes less anticorrelated FC between DMN and SN, and cross-network FC can be a biomarker of CP (Hemington et al., 2016).

CP can result from a large number of pain syndromes. Table 1.2 shows a classification mechanism of CP conditions defined by the International Classification of

Diseases, Revision 11 (ICD-11) as a reference. There are six basic conditions of CP, and all the others not classified by the first six types are grouped in the primary type.

Table 1.2. A category of chronic pain (Treede et al., 2015)

Chronic Pain Condition	Description
Cancer	Caused by cancer or cancer treatments
Postsurgical and post-traumatic	Pain occurs after surgery or tissue trauma that lasts for more than three months
Neuropathic	Caused by damage to the somatosensory nervous system
Headache and orofacial	Headache and orofacial pain that lasts for more than three months and 50% of the days
Visceral	Long-lasting pain in an internal organ
Musculoskeletal	Prolonged lasting nociceptive pain in the bones, joints, muscles, or tissue
Primary	Chronic pain not caused by the other chronic pain conditions above

Interventions for CP can be through medications and alternative interventions. The main medication types available are (1) opioids, such as morphine; (2) nonsteroids, such as aspirin and ibuprofen; (3) antidepressants, such as amitriptyline; and (4) antiepileptics, such as gabapentin (Borsook, 2012).

Alternative interventions include invasively stimulating the spinal cord, brain and motor cortex and non-invasively stimulating the scalp using magnetic and electric fields (Zhang & Seymour, 2014). Other interventions for CP include mindfulness meditation, acupuncture, massage, and supplements. Pain management using a virtual reality (VR) environment (Mohammad & Ahmad, 2018; Garrett et al., 2020) and VR-guided meditation (Fu et al., 2021) have also been investigated recently.

1.5. Brain Oscillations

Neurons are nerve cells that transmit messages within the nervous system using electrical and chemical signals. A neuron receives messages through its dendrites and transmits them along its axon membrane in ion flows. At a synapse which connects the axon to another neuron, the electrical signals are converted to chemical neurotransmitters,

which can travel through the synaptic gap and reach the receptors of the dendrite of another neuron and recreate the electrical signals.

The human brain neuron impulses generate oscillations and interest researchers greatly. The brain oscillation/wave frequency range of 1 to 100 Hz (Buzsáki & Draguhn, 2004) is related to many neurological, physiological and pathological conditions. Brain waves are divided into wave bands that reflect different brain functions. The conventional wave bands are delta (1-4 Hz), theta (4-8 Hz), alpha (8-12 Hz), beta (12-30 Hz) and gamma (30-100 Hz). Generally, the delta rhythm happens in the sleep state. The theta rhythm relates to light sleep, meditation, or a deeply relaxed condition. The alpha rhythm appears during wakefulness and relaxation and is more apparent when the eyes are closed. The beta rhythm links to light brain activity. The gamma rhythm happens when the brain is highly active in information processing (Abhang et al., 2016; Siuly et al., 2016).

In healthy human adults, spontaneous brain rhythms in the 8-12 Hz (Foster et al., 2017; Scally et al., 2018) frequency range are generally called alpha rhythms. They are generated primarily in the frontal, central, temporal, and parieto-occipital brain regions. More specifically, the brain rhythms generated in these regions are frontal alpha, mu, tau, and posterior alpha, respectively (Richard Clark et al., 2004; Chiang et al., 2011; Jensen et al., 2013; Niedermeyer, 1997).

The posterior alpha rhythm is likely the most prominent feature of spontaneous neurophysiological activity, and it was discovered using EEG almost a century ago by Berger (1929). Visual stimuli or merely eyes open conditions can attenuate the rhythm amplitude (Ciulla et al., 1999; Barry et al., 2007). The posterior alpha typically has a spectral power peak frequency and amplitude higher than frontal alpha, mu, and tau (Chiang et al., 2011). Split alpha peaks sometimes occur, possibly associated with variations in interhemispheric connectivity (Olejarczyk et al., 2017). The frontal alpha might be linked to pain perception and suppression, where the increase in frontal alpha activity could be related to increased pain intensity and less successful pain suppression attempts (Jensen et al., 2013). The mu rhythm is typically in the frequency range of 7-11 Hz and originates in the sensorimotor cortex in the central area. Its amplitude attenuates with movement and even movement planning (Chatrian et al., 1959). The tau rhythm is in the frequency range of 8-10 Hz and originates in the auditory cortex in the temporal lobe.

Tau amplitude is related to emotion, and auditory stimuli can suppress the rhythm (Yokosawa et al., 2020).

1.6. EEG and MEG

EEG and MEG are essential neuroimaging techniques for measuring brain oscillatory signals. They have a high temporal resolution and are non-invasive and direct neurophysiological measures, unlike functional magnetic resonance imaging (fMRI) and functional near-infrared spectroscopy (fNIRS). EEG/MEG can detect the electric/magnetic fields produced by the neurons' electric current in the cortex. The electrical impulses of a single neuron are too weak to be detected by the EEG/MEG sensors. When many neurons work synchronously, EEG/MEG can detect the cortical electrical impulses through rhythms or oscillations.

EEG/MEG recordings are usually performed in either a resting or event-related state. In the resting state, the subject is awake and not performing any task. It contrasts with the event-related potential (ERP) state for EEG or the event-related field (ERF) state for MEG, a task-performing state for measuring brain response to an event. In the resting state, subjects are usually asked to either open their eyes and focus on a mark or to close their eyes but not fall asleep. Some brain regions show consistent activity patterns in the resting state, such as the default mode network (DMN) (Raichle et al., 2001) and sensorimotor, executive control, visual, lateralized fronto-parietal, auditory, and temporo-parietal components (Rosazza & Minati, 2011).

EEG/MEG sensors are susceptible to noise, which can contaminate the EEG/MEG signals and harm EEG/MEG analyses. Environmental noise, including AC power line noise (60 Hz in North America and 50 Hz in Europe, and the harmonics), room lighting, electromagnetic interference from nearby equipment, etc., can be reduced using shielding and DC-operated equipment. Physiological noise from the patient, including eye blinks, eye movement, heartbeat, muscle movement, etc., is sometimes unavoidable. However, clear instructions, comfortable resting positions, and short recording sessions could minimize this noise.

EEG/MEG recordings are usually performed with built-in noise cancellation and detection features. For instance, a notch filter to attenuate powerline noise, and the use

of special detection sensors such as an electrocardiogram (ECG) for heartbeats, electrooculogram (EOG) for eyeball movement, electromyogram (EMG) for muscle contraction, head-coil position (HCP) for head movement, etc. A preprocessing pipeline is usually used to prepare the raw data for analysis, which involves a sequence of cleaning and processing steps, such as loading the data, extracting the interested segments, fixing bad channels, cleaning the data, removing artifacts and performing source localization. The sessions below describe the preprocessing and analysis techniques necessary to extract and interpret the critical information in the EEG/MEG data. Also, statistical analysis techniques are crucial in evaluating the effectiveness of the analysis results.

1.7. Data Preprocessing

1.7.1. Bad Channels and Repair

During the EEG/MEG brain imaging process, it is common to see that some data channels may not function properly, such as being extremely noisy or appearing as a flat line. For EEG, causes include electrode malfunctioning, electrodes having bad contact with the scalp, cables picking up noise, bad electric contact between electrode and cable, etc. For MEG, causes include sensor malfunctioning, electromagnetic interference, etc.

Bad channels can be identified by observing and manually marking during data acquisition or by visually inspecting recorded data using a data browsing tool afterward. Bad channels can also be identified automatically. Some advanced software tools can detect if the signal amplitude exceeds a predefined threshold value. If a channel shows a flat line with no signal, using it in the analysis may cause a biased result as a very low noise level is weighted on the flat channel. Noisy channels can cause problems in averaging, such as in EEG electrode average reference and unnecessary rejections of epochs.

Eliminating bad channels in an analysis may cause an inaccurate overall signal-to-noise ratio. Bad channels can be replaced using interpolated signals from the neighbourhood channels (Perrin et al., 1989). If only some portions of the bad channels appear noisy, removing only the bad portions instead of the whole channels is feasible. Bad segments can be identified and removed manually or automatically. Manual approaches include inspecting the data using a data viewer and examining the recording

notes of the participant's movements. Automated approaches include comparing the signal amplitudes with a threshold level in the data channels and/or the ECG, EOG, and EMG channels.

1.7.2. Digital Filtering

A digital filter is a mathematical algorithm that attenuates the amplitude of discrete signals at the desired frequency range. Common EEG/MEG signal processing filter types include high-pass, low-pass, bandpass, and notch filters. Below are some usages of digital filtering in EEG/MEG preprocessing pipelines.

(1) Notch filtering is required to remove powerline noise and its harmonics. For data recorded in North America, cut-off frequencies are set to 60 Hz, 120 Hz, 180 Hz, etc. For data recording in Europe, the cut-off frequencies are set to 50 Hz, 100 Hz, 150 Hz, etc. (2) Resampling data to a lower sampling rate can significantly reduce data preprocessing time. Before downsampling, an anti-aliasing filter is required to ensure the bandwidth complies with the Nyquist frequency requirement. For instance, to downsample a 1,000 Hz signal to 250 Hz, a prior low-pass filtering with a cut-off at 125 Hz or lower has to be used to avoid signal distortion due to aliasing. (3) For the independent component analysis (ICA) artifact removal process, applying a 1 Hz high-pass filter to remove slow drifts that ICA is sensitive to is common (Winkler et al., 2015).

Digital filters can introduce unwanted distortion to the signal, such as amplitude and phase distortion, and then affect brain rhythm and connectivity analyses. The amplitude distortion can be minimized by designing a filter with a flat passband or steep transition band (fast roll-off). The phase delay can be compensated using a zero-phase filter that uses a two-pass (applied twice) approach, once forward and backward.

1.7.3. Artifact Removal

Artifacts are noises that mix with the signals of interest during recording. Environmental and physiological noises are common artifacts in EEG and MEG recordings. ICA and signal-space projection (SSP) are useful artifact removal approaches, which are especially effective in identifying ocular and cardiac artifacts that cannot be easily removed using frequency filtering.

SSP assumes signal sources are spatially distributed and the artifact sources have a low dimension. SSP projects signals recorded at the sensors into multidimensional components. The artifact components with a low dimension are removed, and the remaining components are converted back to sensor channels (Uusitalo & Ilmoniemi, 1997).

ICA is a blind source separation technique. During EEG/MEG recordings, the spatially distributed independent sources project signals to the sensors, where signals are linearly mixed. ICA decomposes signals at the sensors back to their independent source components, and the artifact components can then be identified and removed. The remaining source components are converted back to sensor channels to achieve clean data (Bell & Sejnowski, 1995).

1.7.4. Source Localization

EEG/MEG sensors can detect the scalp's electric and magnetic brain signals. These recorded sensor space signals only reflect the mixed neuronal activity underneath the sensors and their adjacency. Source localization is a technique for localizing source neuronal activities in the brain.

Source localization is a complex process consisting of many steps. The first step is to reconstruct the structural MRI data from the format of a brain volume into a cortical surface. This is required for setting up the source model (source space) and head model. The distributed approach uses the source model to represent the EEG/MEG signal source locations with a grid of dipoles. The head model defines the geometry of the head and the conductivity of different layers of the head. The geometry of the head can be separated into tiny elements to match the segmentation of the MRI data using the finite element method (FEM) or boundary element method (BEM) (Gramfort et al., 2014).

Co-registration is a process to align the EEG/MEG sensor locations with the head model so they are on the same coordinate system. This requires identifying the fiducial landmarks: nasion, left and right preauricular points on the head model and fitting the fiducials with the head shape points (HSP) (Gramfort et al., 2014).

The forward solution describes how the EEG potential or MEG field distributes from sources to the head and the sensors. Once the co-registration alignment is done, the

source and head models form the forward solution. With the help of the noise-covariance matrix derived from the empty room noise recording to provide the noise source information, the source localization can be prepared using an inverse operator on the forward solution and noise-covariance matrix. Familiar inverse operators include minimum-norm, dynamical statistical parametric mapping (dSPM) (Dale et al., 2000), and standardized low-resolution brain electromagnetic tomography (sLORETA) (Pascual-Marqui, 2002). The tools for source localization are readily available in some neuroimaging analysis software packages such as MNE-Python (Gramfort et al., 2013).

1.8. Data Analysis Techniques

1.8.1. Power Spectral Density

Power spectral density (PSD) represents the power level of a signal at each frequency point in a frequency spectrum. The unit of the sensor space PSD is the square of the signal amplitude unit divided by frequency in Hz. The source space PSD can be expressed in decibels (dB), a ratio on a logarithmic scale. To obtain PSD for resting-state EEG/MEG measurement, data are usually first segmented into epochs of equal length, usually between 1 to 10 seconds, then computed using a Fast Fourier Transform (FFT) method for each epoch, and the results are averaged to get an improved signal-to-noise ratio (Welch, 1967). The discontinuity at the start and end points of the epochs can lead to spectral leakage in FFT. Window functions, such as Hanning, Hamming, and discrete prolate spheroidal sequence (DPSS) (Slepian, 1978) tapers, can taper the signal amplitude at the epoch edges to reduce information loss before computing PSD.

Normalization is usually used before averaging the PSD of subjects to avoid bias. There are several approaches for normalization: (1) dividing by average or total power across frequency bins on each channel, (2) dividing by average power across all channels for each frequency bin, (3) computing z-score across all channels (Sprecher et al., 2016), or (4) applying logarithm in addition to the approaches mentioned above.

1.8.2. Peak Alpha Frequency and Bandwidth

Peak alpha frequency (PAF) specifies the frequency in the alpha band with the highest amplitude. PAF can also be represented using the centre of gravity or the mean

alpha frequency (Klimesch et al., 1997; Klimesch, 1999). The alpha rhythm centre of gravity is the weighted sum of spectral estimates divided by alpha power: $\sum(a(f) \times f) / \sum a(f)$, where f is a frequency bin within the alpha band, a(f) is the PSD amplitude at f (Klimesch, 1999). The centre of gravity representation is more applicable for multiple alpha peak situations.

Due to neurological conditions, such as CP, aging and cognitive performance tasks, PAF can shift off the conventional alpha bandwidth of 8-12 Hz. For PSD analysis, the use of individual alpha peak frequency (IAPF) and individual alpha bandwidth (IAB) might be more practical (Bazanova, 2012). IAPF specifies the eyes-closed, posterior cortex dominant peak frequency and is not restricted to 8-12 Hz. IAB is based on the upper and lower frequency points at which amplitude suppression transited between eyes-closed and eyes-open conditions. PAF was found not dependent on the left or right hemisphere, eyes-closed or eyes-open condition (Bazanova, 2011). Other alpha bandwidth approaches include the use of an extended fixed alpha range, such as 5-14 Hz (Moretti et al., 2011), 4-14 Hz (Chiang et al., 2008), 6-14 Hz (Scally et al., 2018), etc., and a flexible alpha bandwidth using IAPF as the centre frequency and a fixed bandwidth based on the centre frequency, such as ±2 Hz or ±2.5 Hz of IAPF (Bazanova & Vernon, 2014).

1.8.3. Alpha Peak Amplitude

In EEG recording, the amplitude of the alpha rhythm is usually below 10^2 μV, and in MEG recording, below 10^3 fT for magnetometer sensors and below 10^3 fT/cm for gradiometer sensors. The alpha peak amplitude refers to the PSD value at PAF. It signifies the EEG/MEG power content at the peak frequency. The alpha peak amplitude suppression is the amplitude drop from the eyes-closed condition to the eyes-open condition at PAF (Bazanova 2012). The alpha peak amplitude unit is $(\mu V)^2$/Hz for EEG and fT^2/Hz for MEG magnetometer sensors, and $(fT/cm)^2$/Hz for MEG gradiometer sensors. For normalized PSD, alpha peak amplitude has no unit.

1.8.4. Alpha Band Power

Alpha power can be represented in absolute or relative form. Absolute alpha power is the original computed alpha band power, expressed by the sum of the PSD amplitudes across the alpha band frequency bins. The sensor space absolute power unit is $(\mu V)^2$ for

EEG, fT^2 for MEG magnetometer sensors, and $(fT/cm)^2$ for MEG gradiometer sensors. Relative alpha power relates the band power to the total power as a reference, expressed by dividing absolute alpha power by total spectrum power. Relative power has no unit.

1.8.5. Functional Connectivity

Functional connectivity (FC) is the statistical relationship in neurophysiological signal changes between brain regions. Metrics for FC include coherence, Granger causality, phase synchronization, phase-slope index, etc. (Bastos & Schoffelen, 2016), and coherence is a commonly used method for FC analysis. Coherence is the linear relationship of the frequency spectra power between two brain regions. If the signals are directly related, the coherence value equals one. If they are not related, coherence equals zero. For signals x and y, their coherence equals the squared cross-spectral density of x and y divided by the product of the auto-spectral density of x and the auto-spectral density of y (Unde & Shriram, 2014).

Volume conduction and magnetic field spread can disturb the EEG and MEG coherence measurements (Holsheimer & Feenstra, 1977; Winter et al., 2007). For EEG, coherence is contributed by neocortical source correlations and volume conduction (Srinivasan et al., 1998). Volume conduction can be reduced by the surface Laplacian method (Srinivasan et al., 1998) or with electrodes more than 10-12 cm apart (Winter et al., 2007). For MEG, coherence is contributed by neocortical sources and the magnetic field effect defined by the Biot-Savart law, and the field-spread effect can be minimized with sensor pairs more than 20 cm apart (Winter et al., 2007).

1.9. Statistical Analysis Techniques

1.9.1. Parametric Methods

Parametric statistical methods are based on the assumption of the normality of the data. That is, the data has the property of normal distribution. Student's t-test compares the means between two samples, and linear regression, which fits sample data using a straight line, are examples of parametric methods.

1.9.2. Non-parametric Methods

Non-parametric methods do not require making any assumption of the data distribution as for the parametric methods. These methods are suitable for data with unknown distribution, outliers, attributes, or data which are not necessarily independent. The Shapiro-Wilk, Kolmogorov-Smirnov, or Anderson-Darling tests can be applied to check data normality. The non-parametric methods have to be used for neuroimaging data for which the distribution is unknown. Non-parametric methods require data to be ranked and sorted in ascending order, then work on the data ranks instead of the data values. Wilcoxon rank sum test, K-sample Anderson-Darling test, and support vector regression are examples of non-parametric tests. Table 1.2 shows a list of parametric tests and their non-parametric equivalence.

Table 1.3. Some standard parametric tests and non-parametric equivalence (McDonald, 2014; De Smith, 2021).

Type	Parametric	Non-parametric
statistical significance	one-sample t-test	Kolmogorov-Smirnov test
	unpaired t-test	Mann-Whitney U test
	paired t-test	Wilcoxon signed-rank test
ANOVA[a]	ANOVA	Kruskal-Wallis test
	one-way repeated measures ANOVA	Friedman test
regression	linear regression	Support-vector regression (linear kernel)
	polynomial regression	Support-vector regression (polynomial kernel)
correlation	Pearson correlation	Spearman rank correlation
		Kendall rank correlation
the goodness of fit test	Chi-squared test	Anderson-Darling test
		Shapiro-Wilk test

[a]ANOVA: analysis of variance.

1.9.3. Multiple comparisons

When a statistical inference test involves multiple comparisons, there is a chance of a false positive, also known as the type I error, where the null hypothesis is true but

rejected because of a P-value less than or equal to the significance level (α) by chance. The family-wise error rate (FWER) or the probability of false positives increases as comparisons increase. This could generate misleading results that could cause hypotheses to be rejected when they should not.

One commonly used method for resolving the multiple comparisons error is to apply Bonferroni correction (Holm, 1979; Cabin & Mitchell, 2000) by dividing α by the number of comparisons to compensate for the false positive rate. The P-value of the results has to be equal to or lower than this new α to be significant.

For the tests with a large number of comparisons, Bonferroni correction may lower α too much and cause many false negatives. The false discovery rate (FDR) is a method to control the false positive rate. This approach ranks the P-values of the individual tests and compares the P-values with (i/m)q, where i is the rank, which starts from 1, m is the number of comparisons, and q is the chosen false discovery rate, such as 0.1, 0.2, etc. If k is the largest i that $P(i) \leq (i/m)q$, then all H(i) are rejected for i = 1, 2, …, k (Benjamini & Hochberg, 1995).

EEG/MEG data are multidimensional as they contain multiple channels and multiple time points. Statistical EEG/MEG data analysis inherently involves multiple comparisons (Maris & Oostenveld, 2007). Cluster-based permutation is a method of resolving multiple comparisons in neuroimaging analysis. Examples include comparing PSD topographies and comparing time-frequency responses. The Monte Carlo method is used to estimate the P-value. The trials in different conditions are randomly partitioned. Samples in different conditions are first quantified using a t-test, and the samples with a t-value higher than a threshold are selected. Selected samples are clustered by neighbourhood, and each cluster's maximum summed t-values are the cluster-level statistics. This procedure is repeated many times to form a histogram of cluster-level statistics. The P-value is the proportion of test statistics in the histogram with a value greater than the observed one (Maris & Oostenveld, 2007).

1.9.4. Sample Size, Effect Size and Power

The sample size is the number of samples used in an experiment. Before experimenting, it is essential to estimate the number of participants (N) required for the

results to be effective, especially for pilot studies. A larger N can provide better statistical results. Factors in studies like cost, pain, and difficulties may keep N to a minimum. For pilot studies, N = 24 to 36 from a population is a reasonable minimum (Johanson & Brooks, 2010), and N = 12 per group with two or three groups is also recommended (Julious, 2005). A possible minimum of N = 10 was also reported (Johanson & Brooks, 2010).

The P-value shows if an effect exists, where effect size (d) shows the size of the effect and the magnitude of differences (Sullivan & Feinn, 2012). d is defined as: 0.01 = very small, 0.2 = small, 0.5 = medium, 0.8 = large, 1.2 = very large, 2.0 = huge (Sawilowsky, 2009).

Statistical power is the probability of finding an effect if it exists. A larger sample size increases the chance of finding an effect, and an increase in effect size will increase the statistical power. The correlations between power, effect size and sample size can be computed using power analysis tools such as G*Power (Faul et al., 2007).

1.10. Machine Learning

Artificial intelligence (AI) is the field of science that uses algorithms to simulate human consciousness and to match or exceed human intelligence. AI can discover, infer, and reason and is able to solve many problems, such as natural language processing, vision, text-to-speech, and motion, which are human abilities.

Machine learning (ML) is a subset of AI. ML simulates human learning and uses statistical algorithms to learn from data sets to improve accuracy over time without being explicitly programmed. The output of ML is the trained models. ML has three main categories: supervised, unsupervised, and reinforcement learning.

Supervised Learning uses data labelled with a tag to train an algorithm to recognize the desired patterns. The outcome is a trained model which can predict or decide on further unlabelled data input. For instance, pictures of animals with their types tagged are used for training, and then the trained algorithm is able to classify further unlabelled pictures. Supervised learning is often used in active learning, classification and regression. Examples of supervised learning algorithms include support vector machines, random forest models and neural networks.

When using supervised learning algorithms, data is divided into two parts for training and testing. For instance, 80% is for training, and 20% is for testing. However, bias may sometimes occur due to how the data are distributed. Cross-validation is an approach used to mitigate bias in ML training. K-fold, repeated K-fold, and stratified K-fold are commonly used cross-validation methods. K-fold cross-validation divides the data into K number of subsets, and in each training, one subset is used as test data, the remaining subsets are used as training data, and K times of training are done. Repeated K-fold repeats the K-fold cross-validation n number of times and shuffles the data each time. Stratified K-fold cross-validation is used in an imbalanced data set. It is similar to K-fold cross-validation but with the data rearranged such that each fold represents the whole data well.

Unsupervised Learning uses unlabeled data to train an algorithm. The algorithm is required to find the patterns by itself. The outcome is that data are grouped according to their characteristics or features. Unsupervised learning is helpful when the patterns are unknown or unspecified. For instance, a large number of human portraits are input, and the algorithm groups the portraits according to complexion, hair and eye colour. One common application of unsupervised learning is clustering.

Reinforcement learning uses rewards and punishments to train an algorithm to learn the desired and undesired actions. The outcome is an algorithm that can optimize its actions to achieve the desired goals. For instance, a chess-playing algorithm can learn how to win from past successes or failures. Reinforcement learning often sequences actions or decisions to achieve a goal.

Deep learning (DL) is a subset of ML. DL simulates human neural processes using a neural network algorithm with multiple layers. A neural network uses connected nodes to loosely model the neurons in a brain. The connections simulate synapses to transmit signals from one node to another. The nodes are called artificial neurons, and the connections are called edges. The artificial neurons are organized in layers. The first layer is the input layer for data input, the last layer is the output layer for the final results or prediction, and the middle layers are hidden layers that process and transmit signals to other layers. Different hidden layers may perform different processes. Deep learning refers to using at least two hidden layers in a neural network (Artificial Neural Network, 2023). DL is often used to solve complex tasks with high accuracy — for instance, autonomous

driving, facial recognition, and medical imaging. Examples of DL algorithms include convolution neural networks (CNNs) and recurrent neural networks (RNNs).

In neuroimaging studies, ML has gained importance rapidly since the early 2000s (Davatzikos, 2019). The most used algorithms in neuroimaging include support vector machines, random forests, and deep learning models. Support vector machines (Schölkopf & Smola, 2002) possess advantages like robustness, flexible kernel and parameter adjustments, and ease of use. Random forests (Breiman, 2001) have been another favoured family of methods due to their good generalization properties and noise removal ability (Davatzikos, 2019). Deep learning models benefit from their ability to deal with complex features, good accuracy and nonlinear usages (Davatzikos, 2019). ML has been used in neuroimaging to reveal biomarkers for diseases and disorders, brain development, aging, and brain states (Davatzikos, 2019).

1.10.1. Support Vector Regression

Support vector regression (SVR) is used in Chapter 4 for prediction purposes. SVR is a robust machine-learning model with good accuracy (Xu et al., 2015). Although deep learning models such as CNNs often generate results with the best accuracy (Fisch et al., 2021; Guerrero et al., 2021), SVR is non-parametric and has the advantages of easy implementation and exemplary performance in terms of a sample size of hundreds in this study. Also, SVR is tailored for correlation fittings and is more flexible than the popular linear regression. SVR can take linear and non-linear kernels, such as polynomial and “radial basis function” (RBF). SVR uses a hyperplane to represent the line of best fit and a tube around the hyperplane with a width ε representing the acceptable maximum error or margin of tolerance. Points outside the tube are support vectors. The distance from the support vectors to the tube is slack (ξ) and ξ can be controlled by the regularization parameter (C). The SVR algorithm tries to find the best-fit function to maximize the number of points in the tube while minimizing ε and ξ.

1.11. Thesis Objectives and Outline

We planned to collect magnetoencephalography (MEG) data from CP patients and healthy controls. However, due to the pandemic and an extended closedown, we instead obtained CP datasets from the Open MEG Archive (OMEGA) (Niso et al., 2016) and

Simon Fraser University's (SFU) internal MEG dataset. These datasets help to verify the CP properties in brain rhythm with previous findings. Therefore, it is an essential part of achieving the thesis goals.

There are two primary goals to tackle in this thesis. First, to investigate how to include age in CP analysis. Second, to explore using VR-guided meditation on chronic cancer patients as an alternative intervention and to investigate the brain oscillatory signal variations. The following chapters describe the works in this thesis.

This thesis starts with an introduction to CP and the methodology for processing and analyzing EEG and MEG data in this chapter. The specific software tools, analyzing and statistical techniques for particular datasets and studies are to be further illustrated in the related chapters respectively.

Chapter 2 presents a literature review of brain rhythm properties related to CP, aging, other pathophysiological conditions, and ML prediction. This chapter provides essential information on the previous findings that this research can refer to and compare with.

Chapter 3 investigates the brain oscillations of CP using the OMEGA and SFU datasets. The aim is to find the trend of neuroimaging properties in CP and verify results found in previous studies. The null hypothesis is that alpha rhythm properties and CP have no statistically significant relationship.

Chapter 4 aims to find a novel method to include age in CP analysis. The Cambridge Centre for Ageing and Neuroscience (CamCAN) aging datasets are analyzed in alpha generation sites to investigate the alpha rhythm properties. When doing CP analysis, it is necessary to include age to avoid false significance. We explore SVR, a machine-learning regression approach, for this purpose. The null hypothesis is that age and alpha rhythm properties have no statistically significant relationship.

To our knowledge, this is the first exploration of correlations between alpha rhythm properties and age in MEG source space PSD regarding multiple alpha generation sites using support vector regression (SVR). Also, the first to use SVR-predicted controls in a CP study and provide a novel method to include age in CP analyses.

Chapter 5 aims to verify a novel therapeutic approach for CP intervention. We apply VR-guided meditation to cancer CP patients and explore EEG activities recorded in the pre, during and post-meditation conditions. The null hypothesis for inferential statistical analysis is that the probability distribution of the condition-specific averages for power spectral density and coherence would be identical for all conditions.

To our knowledge, this is the first exploration of EEG alterations in the brain's electrophysiological signals associated with VR-guided meditation in patients with CP. This exploration provides novel EEG recording and analysis methods that can be used to investigate neurophysiological changes in VR pain applications

1.12. Contributions

Fu, H., Garrett, B., Tao, G., Cordingley, E., Ofoghi, Z., Taverner, T., Sun, C., & Cheung, T. (2021). Virtual Reality–Guided Meditation for Chronic Pain in Patients With Cancer: Exploratory Analysis of Electroencephalograph Activity. JMIR Biomedical Engineering, 6(2), e26332. https://doi.org/10.2196/26332

Garrett, B., Fu, H., Tao, G., Cordingley, E., Ofoghi, Z., Sun, C., Cheung, T., Taverner, T. (2022). Chronic Pain Management in Cancer: An exploratory analysis of electroencephalograph activity during virtual reality pain distraction therapy. CPS 42nd Annual Scientific Meeting, Montreal, Canada. (I worked on the methods, analyses, results and part of the discussion.)

Garrett, B., Fu, H., Tao, G., Cordingley, E., Ofoghi, Z., Sun, C., Cheung, T., Taverner, T. (2022). Chronic Pain Management in Cancer: An exploratory analysis of electroencephalograph activity during virtual reality pain distraction therapy. IPOS 2022 World Congress, Toronto, Canada. (I worked on the methods, analyses, results and part of the discussion.)

Fu, H., Doesburg, S. M., Cheung, T. (2023). Including Age in Chronic Pain MEG Analysis Using Support Vector Regression (in the process of submission for publication).

Chapter 2.

Literature Review

2.1. Introduction

There has been evidence for brain rhythm changes in resting state activity in chronic pain (CP). However, other neurophysiological conditions also reveal similar rhythm changes. It is desired to find the trend in how CP is associated with brain rhythm variations and how to differentiate it from the trends of other neurophysiological conditions. A literature review of past studies is presented for this purpose.

Some brain rhythm properties have been recognized as associated with neurophysiological conditions, such as CP (Sarnthein et al., 2006; De Vries et al., 2013), aging (Chiang et al., 2011; Scally et al., 2018), dementia (Hughes et al., 2019; Moretti et al., 2011; Sitnikova et al., 2018), cognitive and working memory performance (Clark et al., 2004; Klimesch W., 1999). Below is a brief description of some recent findings of brain oscillatory rhythm variations for neurophysiological conditions in electroencephalography (EEG) / magnetoencephalography (MEG) neuroimaging.

2.2. Chronic Pain Studies

Some previous reviews on EEG/MEG CP studies in the resting state summarized some waveband changes, such as increased theta and alpha power (Pinheiro et al., 2016) and increased theta and beta power (Ploner et al., 2017; Zebhauser et al., 2022). Where the increase in theta power is consistent in all three reviews. Ploner et al. (2017) pointed out that the abnormal increase in theta power could be caused by a central nervous system dysfunction known as thalamocortical dysrhythmia (TCD) and might represent the slowing of PAF. Pinheiro et al. (2016) and Ploner et al. (2017) also indicated that the theta power increase was mainly in the frontal cortex.

2.2.1. Studies Using EEG

Previous findings about band power changes in CP patients included decreased alpha power, especially in the posterior lobe (Tran et al., 2004), increased power in the 2-

25 Hz range, especially in 7-9 Hz (Sarnthein et al., 2006), increased power in the high theta and low beta bands (Stern et al., 2006), decreased lower absolute and relative alpha power (Jensen et al., 2013), increased absolute delta and theta power, relative delta power, and reduced relative alpha power (Buchanan et al., 2021), an inverse correlation between normalized alpha central lobe power and pain intensity (Feng et al., 2021), and decreased beta and gamma power (Fu et al., 2021). For these studies based on EEG, the results mostly agreed on increased theta power and decreased alpha band power.

Findings about peak amplitude and peak frequency changes included lower peak alpha amplitude, especially in central and posterior lobes in patients (Tran et al., 2004;), slowed PAF, especially in the posterior lobe (Tran et al., 2004; Sarnthein et al., 2006; Stern et al., 2006; De Vries et al., 2013), and peak theta and alpha band frequency slowing (Boord et al., 2008). Only one study mentioned a lower peak alpha amplitude for amplitude change; most agreed on a slowed PAF.

2.2.2. Studies Using MEG

For pain studies based on MEG, findings included decreased power in alpha and beta activities in the sensorimotor (mu generation site) and occipital cortices (posterior alpha generation site) (Ploner et al., 2006), an increase in theta, beta and gamma power and a slowing in PAF (Lim et al., 2016) and a significantly higher alpha-power ratio (power 7-9 Hz divided by power 9-11 Hz) in patients (Witjes et al., 2021). These studies based on MEG depicted results similar to the EEG studies of increased theta power, decreased alpha power, and slowed PAF. However, gamma power, seldom mentioned in all the studies, showed inconsistency with an increase in MEG (Lim et al., 2016) and a decrease in EEG (Fu et al., 2021).

2.2.3. Summary

Table 2.1 summarizes the EEG and MEG pain studies above. Despite the heterogeneous results of the spectrum analysis, many showed increased theta power, decreased alpha power and slowed PAF in CP. The theta power increase likely represented slowed PAF (Ploner et al. 2017).

Table 2.1. A summary of the chronic pain studies.

Source	Pain	Patient (M/F, Age)	Control (M/F, Age)	Method	Statistical Analysis	Pain Results
Tran et al., 2004	spinal cord injury (SCI) pain	20 (18M/2F, mean 34.3, SD 10.6)	20 (18M/2F, mean 33.7, SD 11.2)	EEG - 14 channels, resting state, eyes-open (EO) & eyes-closed (EC)	ANOVA, Mann-Whitney U-test, sign test	decreased alpha power and peak amplitude, slowed PAF
Sarnthein et al., 2006	neurogenic pain	15 (9M/6F, 38-75, median 64)	15 (7M/8F, 41-71, median 60)	EEG - 60 channels, resting state, EC & EO	Wilcoxon test	increased power in 2-25 Hz, slowed PAF
Stern et al., 2006	neurogenic pain	16 (9M/7F, 63±10)	16 (8M/8F, 56±12)	EEG - 60 channels, resting state, EC & EO, LORETA	non-parametric test	increased high theta and low beta power, slowed PAF
Boord et al., 2008	neuropathic pain	16 paraplegia patients, 8 (7M/1F, 33.5±10.3) with chronic pain, 8 (8M, 34.3±10.7) without pain	16	EEG - 14 channels, EC & EO	ANOVA, sign test	slowed theta and alpha frequency
Jensen et al., 2013	SCI pain	54 SCI patients, 38 (27M/11F, mean 51.24, SD 12.04) with pain, 16 (15M/1F, mean 49.00, SD 12.82) without pain	28 (18M/10F, mean 44.57, SD 13.96)	EEG - 19 channels, resting state, EC	ANOVA	decreased absolute and relative alpha power
De Vries et al., 2013	pancreatitis pain	16 (10M/6F, 24-59)	16 (10M/6F)	EEG - 26 channels, resting state, EC & EO	repeated measures ANOVA	slowed PAF in the parietal and occipital regions

Source	Pain	Patient (M/F, Age)	Control (M/F, Age)	Method	Statistical Analysis	Pain Results
Buchanan et al., 2021	post-concussive syndrome and chronic pain	57 (21M/36F, mean 44.6, SD 11.2)	54 (16M/38F, mean 43.5, SD 9.4)	EEG - 19 channels, resting state, EO	Mann-Whitney U test, support vector machine	increased absolute delta and theta power, relative delta power, and decreased relative alpha power
Feng et al. 2021	low-back pain	27 (7M/20F, mean 44.6, SD 2.3)		EEG - 64 channels, resting state, EC & EO, Visual Analogue Scale	linear regression	normalized alpha central lobe power inversely correlated with pain intensity
Fu et al. 2021	cancer pain	7 (3M/4F, 37-66)		EEG - 64 channels, EO, resting state and VR-guided meditation, numerical rating scale	cluster-based permutation, MANOVA	increased beta and gamma power during meditation (the opposite at rest)
Ploner et al., 2006	laser pain stimuli (acute pain)		12 (12M, 22-41, mean 33)	MEG - 122 channels, laser pain stimuli, resting state, EC	Wilcoxon signed-rank test	decreased alpha and beta power in the sensorimotor and occipital cortices
Lim et al., 2016	fibromyalgia	18 (18F, mean 45.1, SD 8.5)	18 (18F, mean 44.7, SD 8.8)	MEG - 306 channels, MRI, sLORETA, resting state, EC & EO	permutation test	increased theta, beta and gamma power, slowed PAF
Witjes et al., 2021	back or leg chronic pain	21 (10M/11F, mean 48, SD 10)	25 (15M/10F, mean 49, SD 11)	MEG - 275 channels, resting state, EO	permutation test	higher alpha power ratio (7-9 Hz power divided by 9-11 Hz power)

2.3. Aging Studies

2.3.1. Studies using EEG

Some typical findings in EEG properties related to aging are described here. The alpha rhythm frequency range for healthy adults is in the range of 8-12 Hz. Alpha rhythm of 7-8 Hz was observed at one year old (Samson-Dollfus et al., 1997). PAF increased from early childhood to adulthood around age 20 (Cellier et al., 2021), and decreased from around age 20 gradually (Köpruner et al., 1984; Chiang et al., 2011), or decreased from age 45 (Aurlien et al., 2004), there was an indication of a PAF decrease from 20 to 55, then increased with aging (Samson-Dollfus et al., 1997). Also, a comparison of an older adult group (mean age 69.8) with a young adult group (mean age 20.3) found that the older group had a lower PAF (Scally et al., 2018). In summary, PAF decreased gradually during adulthood.

2.3.2. Studies using MEG

Some findings in aging studies using MEG included a significant decrease in relative power in the delta and theta bands from childhood to age 50 and an increase after age 60. The alpha, beta, and gamma bands showed the opposite, with significance found in the beta band (Gómez et al., 2013), also in relative power, a decrease in the delta, theta and alpha bands and an increase in the beta and gamma bands with age (Xifra-Porxas et al., 2021). Both of these studies agreed on the decrease in relative power in the delta and theta bands and an increase in the beta and gamma bands with aging, although the first study showed a change to this after age 60.

2.3.3. Summary

Table 2.2 summarizes some aging studies. Generally, an increase in PAF from childhood to around age 20 was found. PAF started to decrease in frequency from adulthood, though the starting age was inconsistent in the studies from 20 to 45. One study found that PAF started to increase again after age 60. Regarding relative power, a decrease in delta and theta and an increase in beta and gamma were found with aging. The results showed that the property of aging overlaps with CP in PAF slowing.

Table 2.2. A summary of the aging studies.

Source	Subject (M/F, Age)	Method	Statistical Analysis	Aging Results
Aurlien et al., 2004	4651 (2423M/2228F, 0-100 appx)	EEG, resting state, eyes-closed (EC)	polynomial regression	PAF decreased gradually from age 45
Chiang et al., 2011	1498 (763M/735F, 6-86)	EEG - 19 channels, resting state, EC, automated peak identification	smooth asymptotically linear fits, Gaussian fits	increased PAF from childhood to approximately age 20 and decreased gradually
Scally et al., 2018	37 young (13M/24F, mean 20.3, SD 2.06) and 32 older adults (11M/21F, mean 69.75, SD 4.91)	EEG - 64 channels, resting state, EC	ANOVA, priori t-test	a slowed PAF in older adults
Gómez et al., 2013	220 (99M/121F, 7-84)	MEG - 148 magnetometer channels, resting state, EC	polynomial regression	a decrease in the delta and theta relative power from childhood to the age of 50 and an increase after age 60, the opposite for alpha, beta and gamma
Xifra-Porxas et al., 2021	652 (322M/330F, 18-88, mean 54.3, SD 18.6), 613 used	MEG - 306 channels, MRI, resting state, EC, principal component analysis (PCA), canonical correlation analysis (CCA)	Gaussian process regression	a decrease in the delta, theta and alpha relative power and an increase in the beta and gamma relative power

2.4. Dementia Studies

2.4.1. Studies using EEG

Moretti et al. recruited 13 patients with Alzheimer's disease (AD). The EEG recordings showed an increase in alpha3 (10.7–12.7 Hz) power, and the alpha3 / alpha2 (8.7–10.7 Hz) power ratio was negatively correlated with the hippocampal volume in AD (Moretti et al., 2011).

2.4.2. Studies using MEG

Hughes et al. (2019) selected 84 patients with mild cognitive impairment (MCI) and 84 healthy controls. The MEG recordings found a decrease in PAF in patients compared to controls. There was also a decrease in relative alpha power in patients, possibly due to a shift of the alpha peak. Mandal et al. (2018) reviewed some MEG studies in AD. Slowing oscillation frequency and decreased connectivity in AD were the most common finding.

2.4.3. Summary

The brain rhythm changes related to dementia include a change in alpha power, though inconsistent in either an increase or decrease. The trends of slowing PAF and decreased connectivity were also reported. As a result, the slowed PAF property was common in dementia, CP and aging.

2.5. Cognition and Memory Performance Studies

2.5.1. Studies using EEG

Previous studies on cognition and memory performance showed relationships with brain rhythm properties. Here is a list of some studies and their findings: (1) Angelakis et al. (2004) recruited 19 undergraduate students to participate in a reading test. The EEG recording analysis found a positive correlation between PAF and cognitive ability. (2) Clark et al. (2003) selected 550 normal subjects aged 11-70 to participate in memory tests. The EEG analysis showed that the frontal PAF positively correlated with test performance. (3) Bazanova & Aftanas (2006) recruited 129 male students and teachers aged 16-50 to participate in a learnability test. The results showed that PAF and alpha power in the EEG spectrum were positively correlated with performance. (4) Dickinson et al. (2018) recruited 59 children with autism spectrum disorder (ASD) and 38 typically developing (TD) children to participate in a cognitive test. From the analysis of the EEG recording, in children with ASD, PAF was found to be lower and strongly related to non-verbal cognition. (5) Rathee et al. (2020) selected 300 healthy subjects for a reading comprehension task. From the EEG recording analysis, PAF significantly correlated with a high score in the task.

2.5.2. Summary

Cognitive and memory abilities were found to be positively correlated with PAF. Also, one analysis showed that alpha power positively correlated with learnability. These results might reveal that alpha rhythm is related to brain performance, especially in cognition and memory performance. One interesting point by Clark et al. was that spontaneous PAF slowed more in the anterior than the posterior region in aging (Clark et al., 2004).

2.6. Machine Learning Prediction

The exploratory study in Chapter 4 uses the support vector regression (SVR) (Vapnik, 1995; Drucker et al., 1996) approach to predict brain rhythm properties according to age. This is a novel approach and no previous examples have been found in using SVR or other ML algorithem for the same purpose.

For reference, we investigated some related approaches used in age prediction. Dosenbach et al. (2010) used a support vector machine-based multivariate pattern analysis to predict brain maturity, using functional connectivity magnetic resonance imaging (FC MRI) data with 238 typically developing subjects aged 7 to 30. The fitting had a coefficient of determination (R^2) of 0.553. Franke et al. (2012) used relevance vector regression (RVR) (Tipping, 2001) to predict age on structural T1-weighted MRI data, with N = 394 healthy children and adolescents. The results indicated a mean absolute error (MAE) of 1.1 years and a correlation between predicted and chronological age with r = 0.93. Fisch et al. (2021) described the works of several research teams in a competition to predict chronological age using structural T1-weighted MRI data with N = 3,307 healthy subjects. The results obtained from deep learning models, such as 3D convolutional neural networks (CNNs), were better than those using other algorithms, such as support vector machines, relevance vector machines, or Gaussian process regression. The best result showed an MAE of 2.90 years (Gong et al., 2021). Xifra-Porxas et al. (2021) used two dimensionality reduction techniques: canonical correlation analysis and principal component analysis, and Gaussian process regression on structural T1-weighted MRI and resting state MEG data, with N = 613 healthy subjects aged 18-88 years. The best result was MAE = 4.88 years while combining features of both MRI and MEG using the canonical correlation analysis approach. Also, the results were better using spectral properties than

connectivity in MEG. Klymenko et al. (2023) used a random forest regression model on EEG data, with N = 5785 aged 15 to 99. The results showed an MAE of 15.7 years.

2.6.1. Summary

SVR is robust, has good accuracy (Xu et al., 2015) and is tailored for correlation fittings. The literature review above showed CNNs had the best performance in a competition (Fisch et al., 2021; Guerrero et al., 2021). However, SVR is non-parametric, easy to implement and is effiicient for a sample size of hundreds as in the study in Chapter 4, it is then chosen as the ML algorithm to use for prediction in Chapter 4.

2.7. Discussion

In the literature reviewed, the trend of brain rhythm oscillatory variations found in CP is mainly a slowed PAF, increased theta power, and decreased alpha power. The following factors could cause this phenomenon: (1) The power changes could be due to the alpha rhythm shifting to a lower frequency. Hence theta power increased, and alpha power decreased (Witjes et al., 2021). (2) Thalamocortical dysrhythmia (TCD) can cause abnormalities in theta and alpha wavebands due to specific neurological disorders (Llinás et al., 1999; Sarnthein et al., 2006), the increased theta and decreased alpha activity in CP could be related to TCD (Sarnthein et al., 2006; Witjes et al., 2021). (3) CP can disrupt sleep patterns or other homeostatic mechanisms, causing drowsiness and increasing theta activity (Jensen et al., 2013). (4) Drowsiness can cause the resting posterior alpha and central mu rhythms to shift to the frontal cortex, increasing frontal alpha but decreasing overall alpha activity (Jensen et al., 2013). As frontal brain structures may be linked to pain sensation suppression, the increase in frontal alpha could indicate unsuccessful suppression attempts (Jensen et al., 2013).

The trend of brain oscillatory variations in adult aging is similar to CP in slowed PAF, so age has to be included in CP studies. The trend for dementia is an increase in high alpha power, decreased functional connectivity, and a slowed PAF. The trend for cognition and memory performance is a positive correlation with PAF. As CP, dementia, and cognitive and memory decline all share the property of slowed PAF, where cognitive and memory decline are symptoms of dementia, and cognitive impairment is commonly linked with pain and analgesic medications (Moriarty et al., 2011; Khera & Rangasamy,

2021), it may require a thorough design in a chronic study to avoid the above-mentioned pathophysiological conditions in causing false positive results.

As the main rhythm variation found in CP is a shift of the alpha activity to a lower frequency, Chapter 3 aims to verify the alpha rhythm properties in CP further and focus on PAF, peak alpha amplitude, absolute alpha power and relative alpha power. Chapter 4 aims to understand further the rhythm properties related to aging. The alpha rhythm properties will be examined as the primary shared trend between aging and CP is slowed PAF. The correlations between aging and alpha rhythm will be explored to derive a method to include age in CP analysis. Chapter 5 investigates the rhythm property changes in CP when a VR-guided meditation approach is used as an alternative therapy. The delta, theta, alpha, beta and gamma band power and coherence will be analyzed as some previous findings mentioned changes in band power and coherence in mindfulness meditation studies (Lomas et al., 2015; Lee et al., 2018; Cahn and Polich, 2006; Delmonte, 1984).

Chapter 3.

Alpha Rhythm Property Changes in Chronic Pain

Abstract

Previous works on chronic pain (CP) analyses revealed various resting-state brain rhythm property changes, such as in dominant peak frequency, band power, and peak amplitude. However, the findings were heterogeneous. This work aims to explore the brain rhythm properties of CP using MEG data from two sources and to verify the results with previous findings.

The OMEGA data has 7 CP patients (6 males, aged 42-66, and 1 female, aged 74) and 158 pain-free, non-Parkinson, healthy controls (41 males, aged 26.96 - 83.78, and 117 females, aged 22.53 - 82.84). For the SFU data, dataset 1 has 1 male CP patient (aged 47.5) and 1 pain-free male control (aged 53.1); dataset 2 has 24 pain-free, healthy controls (17 males, aged 21.0 - 42.5, and 7 females, aged 23.7 - 33.0). Peak alpha frequency (PAF), peak amplitude, absolute alpha power and relative power are compared between the patients and controls. Mann-Whitney U test is used to verify the significance of the results. The Crawford-Howell single-case test verifies if the individual patient differs from the controls. Topographies are plotted to reveal the rhythm generation sites.

The analyses in the OMEGA data showed slowed PAF, decreased power and peak amplitude in CP patients, but no significance was found in the Mann-Whitney U test. Slowed PAF was also found in the SFU CP data. The Crawford-Howell single-case test found significance in slowed PAF in the CP patient in eyes closed condition compared to the controls. The topographies demonstrated the posterior alpha, the central mu and the temporal tau rhythm generation sites.

The results matched previous findings in CP studies in slowed PAF, decreased alpha power and peak amplitude. No significance was found in the OMEGA data, likely due to the limitation of small CP sample sizes. The results, however, might motivate further explorations into brain oscillatory activity in CP, especially in using MEG.

3.1. Introduction

Apart from acute pain, pain that lasts more than three months or beyond the expected healing time is called CP (Canada, 2021). Some examples are low back pain, spinal cord injury, and cancer pain (Treede et al., 2015). The most used pain diagnosis approach is based on a numerical pain rating scale or clinical questionnaires (Williamson & Hoggart, 2005), where patients self-report their pain level or severity. This approach is known to be subjective and inconsistent. Some objective pain assessments include measuring the patients' pain behaviour and physiological signals and analyzing pain brain activity (Zhang & Seymour, 2014). However, these objective pain diagnosis approaches are still mainly in the research stage.

CP interventions in North America are primarily through medications, and the main types are opioids, nonsteroids, antidepressants and antiepileptics (Borsook, 2012). Non-medication pain interventions include invasively stimulating the spinal cord, brain and motor cortex or non-invasively stimulating the scalp using magnetic and electric fields (Zhang & Seymour, 2014). Other pain intervention approaches include a VR environment (Mohammad & Ahmad, 2018; Garrett et al., 2020), mindfulness meditation, acupuncture, massage, and supplements. A novel VR-guided meditation approach (Fu et al., 2021) was recently explored. The VR-based approaches are non-invasive, safe, and easy to self-operate.

In recent years, much research has explored brain oscillatory signal properties in CP (Pinheiro et al., 2016; Zebhauser et al., 2022). Distinct variations were found, including dominant peak frequency, band power and peak amplitude. However, the results might match or differ between studies. This chapter aimed to verify the brain rhythm properties in CP using magnetoencephalography (MEG) datasets. Analyses were performed on CP patients and healthy controls to compare brain oscillation properties. The results were verified with previous findings.

3.1.1. Literature Review

Animal Models

Emotional and ethical issues may exist when using human models in pain assessment tasks. As pain modulates brain oscillation in humans and animals, it is

common to use rat models as an alternative to human models, where pain experiments using rat models can be more accessible to design and perform (Deuis et al., 2017). LeBlanc et al. (2016) used rat models to test the correlation between EEG and pain. The results showed an increase in EEG power with pain in the 3-30 Hz range over the primary somatosensory cortex (S1) and prefrontal cortex (PFC) and also an increase in coherence between PFC and S1 (LeBlanc et al., 2016). These results match previous findings in human models with CP (Sarnthein et al., 2006; Stern et al., 2006) and may signify the possibility of using rat models to mimic the pain response of humans in brain imaging analysis. However, there are factors to consider when using rat models. For instance, using isoflurane as anesthesia in EEG electrode implant surgery may induce slow-wave activity and increase delta band power (MacIver & Bland, 2014).

Human Models

Previous studies showed an association between peak alpha frequency (PAF) slowing with pain and CP (Furman et al., 2020; Wydenkeller et al., 2009; De Vries et al., 2013; Lim et al., 2016). For instance, Lim et al. recorded MEG from 18 females with fibromyalgia (FM) and 18 control subjects of matching ages and sex. The finding showed a slowing of the dominant alpha peak in the FM patients. De Vries et al. recorded EEG from 16 patients with chronic pancreatitis and 16 healthy controls with matching ages, sex, and education. The chronic pancreatitis patients showed a slower average PAF. Other than slowed PAF, the other most consistent findings in CP patients were increased theta power and decreased alpha power (Tran et al., 2004; Stern et al., 2006; Jensen et al., 2013; Ploner et al., 2006; Lim et al., 2016; Ploner et al., 2006; Witjes et al., 2021; Sarnthein et al., 2006; Buchanan et al., 2021). The increased theta and decreased alpha power were related to the shift of the alpha rhythm to a lower frequency, and thus, this study focused on exploring the alpha rhythm variations.

3.2. Methods

3.2.1. Participants

In the first study, the Open MEG Archive (OMEGA) (Niso et al., 2016), Release 3.0.0 (March 2022), was used, which had 7 CP patients (6 males, aged 42-66, mean 52.66, SD 9.02, and 1 female, aged 74) and 158 pain-free, non-Parkinson healthy controls

(41 males, aged 26.96-83.78, mean 64.22, SD 12.71, and 117 females, aged 22.53-82.84, mean 63.99, SD 10.64). The participants were resting, sitting upright, eyes open, focusing on a fixed cross for 5 minutes. The data were collected using CTF MEG (CTF MEG, Coquitlam, Canada) with 275 axial gradiometers. The sampling rate was 2400 Hz with a hardware low-pass filter at 600 Hz for anti-aliasing, and CTF 3rd-order gradient compensation was applied (Niso et al., 2016; 2019).

The second study used the SFU MEG data, which had two datasets collected in 2018-2019 using CTF MEG with 275 gradiometer channels and a sampling rate of 1200 Hz. CTF 3rd-order gradient compensation was applied. Dataset 1 has two participants: a CP patient (male, aged 47.5) and a healthy, pain-free control (male, aged 53.1). The scanning duration was 8 minutes in resting state and for separate eyes open and eyes closed conditions. Dataset 2 has 24 pain-free participants (17 males, aged 21.0-42.5, mean age = 28.07, SD = 5.71, and 7 females, aged 23.7-33.0, mean age = 26.86, SD = 3.18). The scanning duration was 3 minutes in resting state and eyes open condition. Dataset 2 was used as a control group for the second study.

3.2.2. Analysis

The OMEGA and SFU data studies were performed at different stages of this thesis and based on different analysis technologies. The analysis of the OMEGA data was performed using MNE-Python (Gramfort et al., 2013). Data were band-pass filtered at 1 Hz and 55 Hz and cleaned with signal-space projection (SSP) to remove ocular and heartbeat artifacts. The alpha rhythm properties were extracted from PSD and compared between the CP and control groups. A null hypothesis was set that there was no correlation between brain rhythm properties and CP. The brain rhythm properties for exploration included PAF, peak amplitude, absolute and relative power. Mann-Whitney U test (Mann & Whitney, 1947) was used to verify the significance of the results.

The SFU data analysis was performed using FieldTrip (Oostenveld et al., 2011). The data were band-pass filtered at 1 Hz and 150 Hz to remove slow drifts and high-frequency noise and notch-filtered at 60 Hz, 120 Hz and 180 Hz to remove power line noise and harmonics. Bad channels, muscle artifacts, and head movement were marked and removed using a data browser. Ocular and heartbeat artifacts were cleaned using independent component analysis (ICA). Topography was plotted to identify the alpha peak

generator locations. The Crawford-Howell single-case method (Crawford & Howell, 1998; Crawford & Garthwaite, 2004) was applied to verify the SFU data. A null hypothesis was set that the PAF of the CP patient was not statistically different from the controls.

3.3. Results

3.3.1. OMEGA Data

After eliminating the participants who showed no prominent alpha peak in PSD (determined by alpha band relative power < 10%), only 1 female and 4 male CP patients and 91 female and 30 male controls remained. Table 3.1 shows the analysis results of the CP patients and matched controls. Lower values of PAF, alpha peak amplitude, absolute alpha power and relative alpha power were found in patients though no significance in the Mann-Whitney U test was found.

Table 3.2 shows the comparison between patients and the whole control group, and similar results as in Table 3.1 were found.

Table 3.1. A comparison of the OMEGA chronic pain patients and matched controls in alpha rhythm properties.

	Age	Abs Power	Rel Power	Peak Amp	PAF
Female patient (1)	74.0	3.44E+03	26.30%	1.69E+03	9.4
Matched control (1)	74.5	1.47E+04	62.80%	2.80E+04	9.6
	Mean Age	**Abs Power**	**Rel Power**	**Peak Amp**	**PAF**
Male patients (4)	53.3	3.14E+03	18.04%	1.46E+03	9.3
Matched controls (4)	57.2	4.67E+03	22.45%	2.33E+03	10.0

Table 3.2. A comparison of the OMEGA chronic pain patients and all controls in alpha rhythm properties.

	Mean Age	Abs Power	Rel Power	Peak Amp	PAF
Chronic Pain Female (1)	74.0	3.44E+03	26.30%	1.69E+03	9.4
Control Female (91)	63.5	6.16E+03	28.24%	3.40E+03	9.7
	Mean Age	**Abs Power**	**Rel Power**	**Peak Amp**	**PAF**
Chronic Pain Male (4)	53.3	3.14E+03	18.04%	1.46E+03	9.3
Control Male (30)	64.7	6.48E+03	24.17%	4.32E+03	9.8

3.3.2. SFU MEG Data

Three participants with no alpha peak found in PSD and one outliner were eliminated from the comparison. This reduced the healthy controls to 21. Table 3.3 shows that the patient's PAF was lower than the matched and mixed controls. For the Crawford-Howell single-case test, the null hypothesis was rejected for the patient in the eyes-closed condition but not the eyes-open condition. The same test was repeated for the individual controls in the control group. Only one control was rejected. This reflected that the controls had very similar PAF values.

Table 3.3. A comparison of the ImageTech patient and matched control/all controls in PAF.

	Male Patient (N = 1) (Eyes Closed)	Male Patient (N = 1) (Eyes Open)	Male Age-Matched-Control (N = 1) (Eyes Closed)	Male Age-Matched-Control (N = 1) (Eyes Open)	Mixed Controls (N = 21) (Eyes Open)
PAF	8.91 Hz	9.22 Hz	9.40 Hz	9.77 Hz	10.47 Hz
Mean Age	47.5	47.5	53.1	53.1	27.2
Crawford-Howell Test	P = 0.021	P = 0.058	Not tested	P = 0.245	P = 0.494 (mean)

For the SFU data topography plots, the healthy control subjects generated an alpha rhythm at around 10 Hz in the parieto-occipital alpha generator site. An example is shown in Figure 3.1; the matched control of the patient had a PAF at 9.77 Hz in the parieto-occipital region. In Figure 3.2, the patient showed a slower PAF at 9.22 Hz in the same region.

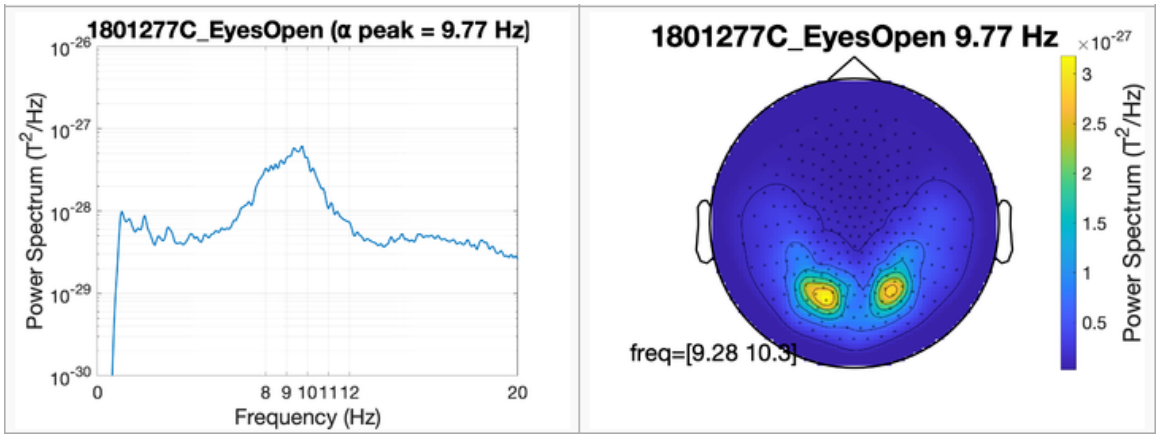

Figure 3.1. In the SFU data, the matched control of the patient had a PAF at 9.77 Hz in the parieto-occipital region.

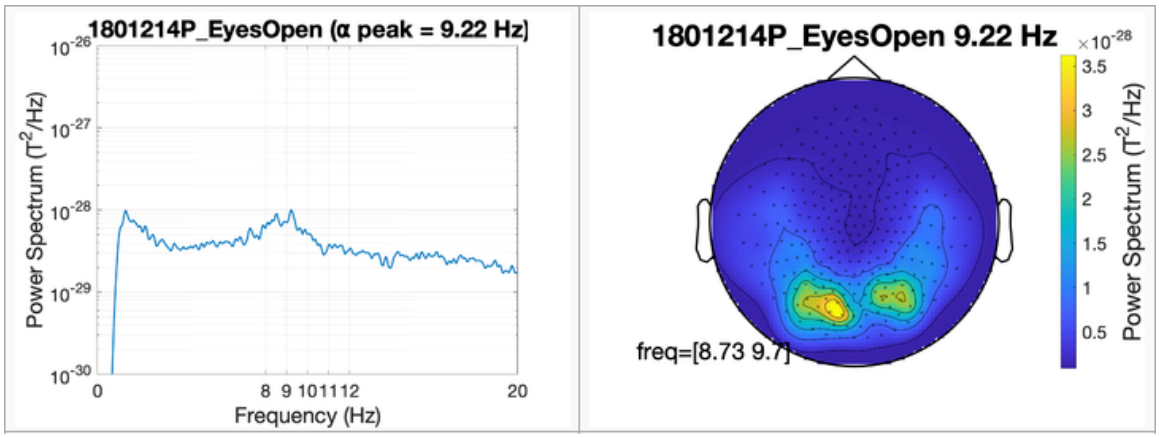

Figure 3.2. In the SFU data, the chronic pain patient had a PAF at 9.22 Hz in the parieto-occipital region.

Figure 3.3 shows the mu wave in the centro-parietal region (the sensorimotor region) (see Chapter 1.5. for explanation of mu and tau waves). The PAF at 10.93 Hz was in the mu-wave range of 7-11 Hz (Chatrian et al., 1959). Figure 3.4 shows the tau wave in the temporal/auditory region. The PAF at 9.52 Hz was in the tau wave range of 8-11 Hz (Yokosawa et al., 2020).

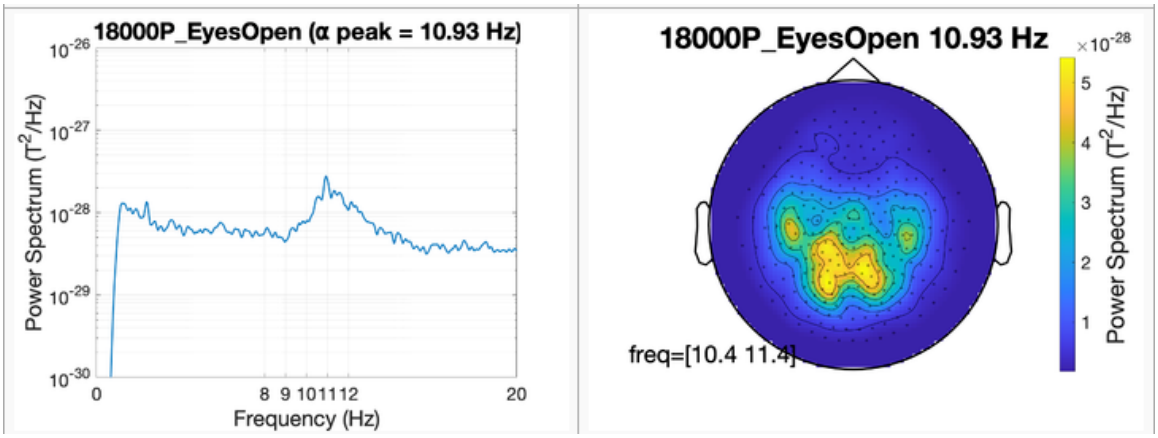

Figure 3.3. A mu wave in the centro-parietal region.

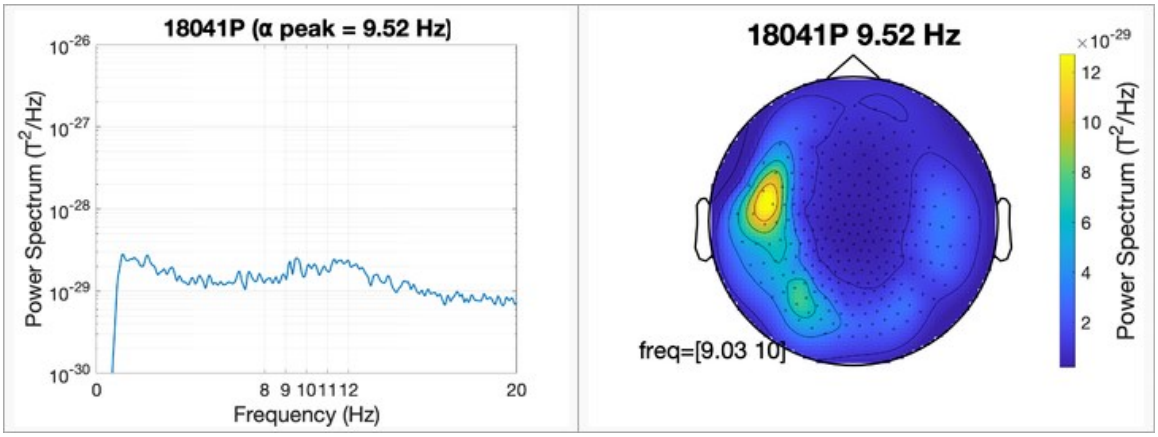

Figure 3.4. A tau wave in the temporal region.

3.4. Discussion

The findings shown in these studies matched previous findings, such as slowed PAF, decreased alpha power and peak amplitude in CP patients (Tran et al., 2004; Lim et al., 2016; De Vries et al., 2013). For the OMEGA and SFU data, significance in the alpha rhythm property changes was not found, and the null hypothesis was not rejected. However, the Crawford-Howell single-case test found significance in slowed PAF in the CP patient in eyes closed condition compared to the controls. The topography plots depicted the posterior alpha rhythm, the mu rhythm in the centro-parietal region (sensorimotor region) and the tau rhythm in the temporal lobe (auditory region). The stronger posterior alpha rhythm often covers the lesser tau rhythm, which is challenging to detect. The plot could show the tau rhythm due to the alpha rhythm not existing in the example.

3.4.1. Conclusion

Alpha rhythm property changes in CP were identified and matched previous findings in slowed PAF, decreased alpha power and peak amplitude. The analysis results showed no significance in the statistical tests, except the eyes closed condition in the Crawford-Howell single-case test, likely due to the small CP sample size limitation in the OMEGA and SFU data. Nevertheless, the results might motivate further explorations into brain oscillatory activity in CP, especially in using the MEG neuroimaging tool, as the primary neuroimaging tools used for the related studies up to now were EEG and MRI (Morton et al., 2016; Zebhauser et al., 2022).

Acknowledgement

Data used in the preparation of this work were obtained from the Open MEG Archive (OMEGA) (available at https://www.mcgill.ca/bic/neuroinformatics/omega) (Niso et al., 2016) and SFU. The author thanks Dr. Adonay Nunes for sharing a MEG preprocessing pipeline as a reference for the SFU data analysis.

Chapter 4.

Including Age in Chronic Pain MEG Analysis Using Support Vector Regression

The study in this chapter is in the process of submission for publication.

Henry Fu, Sam M. Doesburg and Teresa P. L. Cheung

Abstract

Introduction: Some previous aging and chronic pain (CP) studies using EEG/MEG exhibited similar slowed peak alpha frequency (PAF). The typical CP study design has selected age-matched, healthy controls compared to patients to reduce spurious results caused by aging. Instead of using age-matched controls, this exploratory study uses a support vector regression (SVR) model to include age in a CP MEG analysis.

Methods: This study used an open-access MEG database of 474 healthy controls and 22 CP participants aged 18 to 87. It first computed source space power spectral density for four alpha rhythm generation sites: frontal (frontal alpha), central (mu), temporal (tau), and parieto-occipital (posterior alpha) regions of interest (ROIs). It then used SVR to investigate the correlations between age and PAF, peak amplitude, and alpha power for controls in the four ROIs. A CP case study explored the alpha rhythm difference between CP participants and controls, using the correlations found and CP participants' age as input, then predicted the alpha rhythm property of controls at the same age as CP participants. This approach enabled non-age-matched controls in the study.

Results: K-sample Anderson-Darling tests showed significantly independent brain rhythms in the four ROIs with $P<0.001$. We observed the PAF slowing trends, and the PAF of female controls in the 18-27 age group was higher than male controls with significance, $P<0.025$ in three ROIs. Regression results showed PAF was negatively correlated with adult aging, with $R^2=0.147$ and $P=0.001$ in the mixed-sex parieto-occipital ROI. The CP case study showed that the CP participants had a slower PAF than the SVR-predicted controls in the posterior alpha generation site, though not significant in the Wilcoxon signed-rank test.

Discussion: Our analysis used alpha generation site ROIs, source space power, an extended alpha bandwidth of 6-14 Hz, 1 Hz individual alpha band power, and SVR. The use of SVR enabled the prediction of PAF across the lifespan of controls for comparison with CP participants. This novel method to create an aging model could be applied to other pathophysiological studies to mitigate the age-matched control requirement.

Keywords: aging; alpha rhythm; chronic pain (CP); magnetoencephalography (MEG); matched-control; peak alpha frequency (PAF); support vector regression (SVR)

4.1. Introduction

Brain rhythms are oscillation signals that can be measured using functional neuroimaging techniques like electroencephalography (EEG) and magnetoencephalography (MEG). EEG detects the changes of tiny electric currents on the scalp, and MEG spots the microscopic scale magnetic flux of the brain. EEG/MEG possesses excellent temporal resolution and is a non-invasive and direct neurophysiological measure, unlike functional magnetic resonance imaging (fMRI) and functional near-infrared spectroscopy (fNIRS). Therefore, EEG/MEG is ideal for recording brain rhythm activities in pathophysiological conditions, such as chronic pain (CP) (Fu et al., 2021).

Some previous CP studies using EEG/MEG have shown brain rhythm property changes mainly related to increased theta and decreased alpha power and slowed PAF (Witjes et al., 2021; Boord et al., 2008; De Vries et al., 2013; Lim et al., 2016; Sarnthein et al., 2006; Wydenkeller et al., 2009). Among these properties, the slowed PAF in CP was most consistent in previous studies, and here are some examples. Sarnthein et al. (2006) selected 15 neurogenic pain patients and 15 matched healthy controls. The EEG analysis showed increased spectral power in patients from the delta to the beta ranges (especially in 7-9 Hz) and a slowed PAF. De Vries et al. (2013) compared 16 chronic pancreatitis pain patients with matched controls in four brain regions in sensor space: frontal, central, parietal, and occipital, and found slowed PAF in the parietal and occipital lobes in their EEG analysis. Another study by Lim et al. (2016) showed that eighteen female fibromyalgia patients and eighteen matched healthy controls underwent a MEG

scanning for CP test. The analysis depicted that the patients had an increase in theta, beta, and gamma power and a slowing in PAF.

Some aging studies also showed a slowing of PAF with increasing age during adulthood. Chiang et al. (2011) examined a control group of 1,498 patients aged 6 to 86 years using EEG and found that PAF decreased with an increase in age in adults. Scally et al. (2018) recorded the eyes-closed resting state EEG of two age groups of 37 young adults and 32 older adults and replicated the finding of PAF slowing in the older adult group. Jabès et al. (2021) compared the EEG of two healthy groups of 21 adults aged 20-30 and 27 adults aged 65-75. The results showed PAF slowing and decreased alpha absolute and relative power in the older adult group.

CP can cause a slowed peak alpha frequency (PAF) (Sarnthein et al., 2006). However, adult aging also causes this phenomenon (Chiang et al., 2011). In finding significant signal differences between CP patients and healthy controls, previous works required age-matched patients and controls for analyses to avoid false statistical significance in comparisons. This is a limitation; any future clinical translation of such an approach in CP would require a consideration of patient age to disambiguate pathological oscillatory activity to that associated with healthy aging. An aging model to extend general future large database studies is desired. The model may also reduce the time, cost, and difficulty of recruiting suitable participants.

4.2. Methods

This study explores a method to include age in analyzing MEG parameters in pathophysiological conditions and verifies the method in a CP case study. This is a novel attempt to mitigate the age-matched patient and control requirement. This study focused on the alpha rhythm since the primary changes in rhythm properties in CP found were slowed PAF, increased theta, and decreased alpha power, where increased theta could be related to a shift of the alpha rhythm to a lower frequency. Also, the primary changes in rhythm properties in aging were slowed PAF and decreased alpha power. We sought to elucidate associations between alpha rhythm properties and adult aging in four alpha rhythm generation sites: frontal, central, temporal, and parieto-occipital regions of interest (ROIs). The rhythms within each ROI could show similar rhythm properties for the related pathophysiological conditions (Chiang et al., 2011; Jensen et al., 2013; Niedermeyer,

1997; Chatrian et al., 1959; Yokosawa et al., 2020). The use of ROIs enabled us to examine neural power spectra more systematically. A machine learning support vector regression (SVR) (Vapnik, 1995; Drucker et al., 1996) model was applied in a CP case study to verify the use of non-age-matched controls, and this approach could be extended to other pathophysiological studies.

4.2.1. Participants

This study used the Cambridge Centre for Ageing Neuroscience (CamCAN) Stage 2 database (Taylor et al., 2017) MRI and MEG datasets. The MRI datasets were Release 004 T1 weighted anatomical. The MEG resting state datasets were Release 005 with movement compensation and default space transformation. Participants recruited were between 18 and 87 of age, with 50 men and 50 women from each decade. Due to recruitment difficulties, only 27 men and 29 women were in the youngest decade. All participants were MEG scanned at rest with their eyes closed for 8 minutes and 40 seconds. The actual recording durations were found to vary. There were 619 participants with both MRI and MEG recordings.

The data in the CamCAN database were collected in the UK, where CP is prevalent and around one-third of adults suffer (GOV.UK, 2017). CP is common in causing frequent poor sleeping (Mathias et al., 2018; Finan et al., 2013; Bowers, 2011; Mann, 2010; Pacheco & Rehman, 2020). The CamCAN database did not directly reveal the CP information of the participants. However, one question in the MEG prescanning interview potentially inferred the participants' CP status. The question asked how often the participants had trouble sleeping in the past month due to pain. The choices were: (1) Not in the past month. (2) Less than once a week. (3) 1~2 times a week. (4) 3 or more times a week. (5) No answer.

For the purposes of demonstrating the utility of our algorithm, we have categorized participants who answered (1) in the question to be healthy controls with no CP and participants who answered (4) in the question to be CP participants. There are weaknesses in this inference, as there is no clinically complete evidence that the participants were CP patients. However, in the later part of this chapter, we demonstrated that our CP participants showed general brain rhythm characteristics similar to CP

patients. Data from the participants who replied (2), (3), or (5) were not used in the analysis.

The time difference between the interview and MEG scanning for the CP participants had a mean of 99.72 days, median = 63 days, and SD = 99.19 days. We removed two outliers, resulting in a mean = 75.83 days, median = 60 days, and SD = 49.59 days. As the interview date had only the year and month given, the 15th day of each month was assumed in the calculations.

We did not use the OMEGA and SFU data in Chapter 3 in this study because the data were collected using a different MEG system: CTF (CTF MEG, Coquitlam, Canada) with 275 axial gradiometers and a 2,400 Hz sampling rate. Also, the OMEGA data were collected in an eyes-open condition.

4.2.2. Equipment

The MRI tool was a Siemens TIM Trio 3T MRI scanner (Siemens Healthcare, Erlangen, Germany) with a 32 RF channel head coil. The MEG tool was a VectorView MEG system (Elekta Oy, Helsinki, Finland) with a sampling rate of 1,000 Hz, a 0.03 Hz high-pass filter, and a 330 Hz low-pass filter. Among the 306 MEG sensors, 204 were orthogonal planar gradiometers, and 102 were magnetometers. In addition, there were electrocardiogram (ECG), vertical electrooculogram (VEOG), and horizontal electrooculogram (HEOG) channels for detecting cardiac and ocular artifacts. Temporal signal space separation (Taulu & Simola, 2006) was used to remove noise from external sources. MaxFilter 2.2 software (Elekta Oy, Helsinki, Finland), using a correlation of 0.98 and a window of 10 s, was applied to notch-filter the 50 Hz power line noise and to detect and reconstruct bad channels.

4.2.3. Data Processing

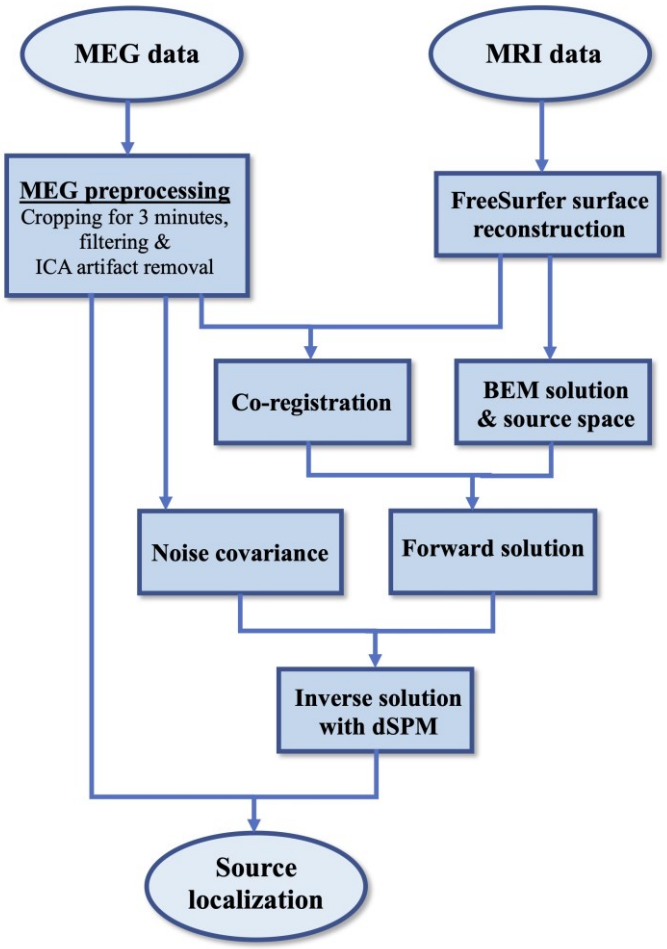

Figure 4.1. Source localization flow chart. MEG: Magnetoencephalography; MRI: magnetic resonance imaging; ICA: independent component analysis; BEM: boundary element model; dSPM: dynamic statistical parameter mapping.

Figure 4.1 shows the data processing and source localization procedure. The FreeSurfer (Fischl, 2012; Dale et al., 1999) tool was used to reconstruct the T1-weighted MRI anatomical from a 3-dimensional volume into a 2-dimensional cortical surface. The results were for later MEG-MRI co-registration, single-layer boundary element model (BEM) surface generation and source space use. Source localization required the cleaned MEG data, noise covariance, and the forward and inverse solutions. The analysis used the MNE-Python tool (Gramfort et al., 2013). A cropped 3-minute MEG signal was sufficient for our resting-state analysis and helped shorten the preprocessing and analysis computing time. The same data length used for the participants could ensure a similar

signal-to-noise ratio (SNR) in the analysis. The start time of the cropped recording was determined by the turn-on time of the Neuromag head position indicator (HPI) coils plus 10 seconds for stabilization, where the HPI turn-on time was recorded on the MEG's STI201 stimulation channel.

MEG magnetometer sensors are sensitive to environmental noise, so the analysis picked only the gradiometer channels. The MEG data provided by CamCAN was preprocessed – maxfiltered (Taulu & Kajola, 2005; Taulu & Simola, 2006) and already had the bad channels repaired and head movement compensated (Taylor et al., 2017). The bad channel reconstruction method was not indicated in Taylor et al.'s paper; interpolating the neighbourhood channels was the typical approach. The whole 3-minute cropped MEG signal was used in further data cleaning, and the data was not divided into epochs. A notch filter at 50 Hz and multiples at 100, 150, 200, 250, 300, and 350 Hz was used to remove power line noise and its harmonics; also, at 293, 307, 314, 321, and 328 Hz to remove the five HPI coil frequency noise. Also, a low-pass filter with a cutoff at 105 Hz was used to remove muscle artifacts in the 110-140 Hz range (Nunes & Bloy, 2023). Both filters were finite impulse response of zero-phase, two-pass to avoid temporal shifts, and with a hamming window for smoothing. The independent component analysis (ICA) process (Makeig et al., 1995) was used for ocular and cardiac artifact removal. It used a high-pass filter at 1 Hz cutoff to remove slow drifts and the Picard algorithm (Ablin et al., 2018) for fast convergence. Due to the high number of MEG channels, 40 ICA components were chosen to balance the computing time and to have enough components to isolate the artifacts. An automatic ICA process using the EOG and ECG channels was set up like that of Xifra-Porxas et al. (2021). Together, these steps effectively cleaned data from the delta to the gamma band range.

4.2.4. Co-registration

The MEG-MRI co-registrations were performed using a semi-automated approach. The first step was using the MNE-Python's "mne coreg" graphical user interface to manually identify the nasion, and left and right preauricular fiducial points on the MRI cortical surface. The second step was to use an automated script to fit the fiducials with the head shape points (HSP) and refine the process using the iterative closest points (ICP) algorithm (Besl & McKay, 1992). The final step involved omitting the bad head shape points with a distance greater than 10 mm and re-refining the co-registration with ICP.

4.2.5. Source Localization

Source localization is a process used to determine the positions of the signal sources in the brain. Figure 4.1 shows the process of using the co-registration results, BEM solution, and source space information to generate the forward model (Hamalainen & Sarvas, 1989). The noise covariance matrix was estimated using the empty-room recordings. The inverse solution was computed using the dynamic statistical parameter mapping (dSPM) method (Dale et al., 2000).

4.2.6. Source Space PSD

Table 4.1. Aparc labels corresponding to the four regions of interest (ROIs).

ROI	Aparc Labels
Frontal	frontal, pars
Central	central
Temporal	temporal, bankssts, fusiform, entorhinal, parahippocampal
Parieto-occipital	parietal, supramarginal, occipital, lingual, cuneus, pericalcarine

To estimate the source neural activities in the brain, source space power spectral density (PSD) was computed for the ROIs from 1 to 20 Hz using a 10-second, non-overlapped window with Hann taper smoothing. The 10-second window provided a PSD frequency resolution of 0.1 Hz. The ROIs were estimated based on the Aparc parcellation (Desikan et al., 2006). Table 4.1 shows the labels corresponding to the four ROIs. The average PSD was calculated from the grouped labels in each ROI. PSD was then smoothed by boxcar averaging, which helped reduce noise and improve SNR. A boxcar window of three points equivalent to a width of 0.3 Hz was used in the PSD data. This narrow window was chosen to minimize the chance of eliminating nearby peaks due to averaging. This process, however, lowered power amplitude at both ends of the 1-20 Hz spectrum, and the spectrum was cropped to 2-19 Hz to remove distortions. The source space PSD of every participant was plotted for visual inspection, and participants with abnormal PSD patterns, such as ringing as generated in filtering, were dropped.

4.2.7. Alpha Rhythm Properties

A fixed alpha bandwidth of 8-12 Hz (Foster et al., 2017; Scally et al., 2018) could not cover all the scenarios in this study, such as the slowing of alpha rhythms due to age and CP could shift PAF to 7 Hz or lower. The individual alpha bandwidth (Bazanova & Aftana, 2006) was a logical approach to consider, which was based on the upper and lower frequency points where amplitude suppression transited between eye-closed and eye-open conditions. Due to the availability of only eye-closed data in the CamCAN datasets, an extended fixed alpha bandwidth approach (Chiang et al., 2008; Moretti et al., 2011) was used in this study.

PAF, amplitude, and band power characterize the alpha rhythm. SciPy's signal function "find_peaks" was used to locate the maxima in the PSD. Based on the maxima, PAF and amplitude were determined for each participant individually. The absolute alpha band power calculation used a 1 Hz bandwidth (0.5 Hz on each side of PAF). High alpha was from PAF to PAF + 0.5 Hz, and low alpha was from PAF - 0.5 Hz to PAF. For instance, if a PAF was at 10.0 Hz, the high alpha was from 10.0 to 10.5 Hz, and the low alpha was from 9.5 to 10.0 Hz. This narrow bandwidth was chosen to minimize possible overlapping with other nearby peaks. Relative alpha power was computed by dividing the absolute alpha power by the sum of PSD at each frequency point from 2 to 19 Hz.

4.2.8. Statistical Analysis

The non-parametric K-sample Anderson-Darling test (Scholz & Stephens, 1987) was used to verify whether the samples in the four ROIs were from a single population without specifying the distribution type. A null hypothesis was set that the samples in the four ROIs were from the same distribution.

Boxplots were used for the age groups from 18-27 to 78-87 to show the spread of the data, median, mean, and outliers. Boxplots also showed the aging trend for the analyses, including mixed-sex, male, and female groups, since sex might affect the statistical analysis results (Ko et al., 2021). The analyses included PAF, absolute peak amplitude, relative peak amplitude, high and low alpha absolute, and relative power. Wilcoxon signed-rank and Mann-Whitney U tests were used to compare the boxplot

results. The former is the non-parametric equivalent of the paired t-test, and the latter is the non-parametric equivalent of the unpaired t-test.

SVR (described in Section 1.10.1) was used to study the correlation between the controls' alpha rhythm properties and aging. Then, alpha rhythm properties could be predicted using the regression at any specified age. Scikit-learn (Pedregosa et al., 2011) SVR based on the libsvm (Chang & Lin, 2011) implementation was used, and the analyses included in the boxplots above were repeated. Outliers were first removed from the data based on the quantile approach. The GridSearchCV function was used to determine the best SVR parameters for the regression fittings using the coefficient of determination (R^2) scoring. R^2 has a value from 0 to 1, which shows how well the regression model fits the data. Zero means a constant model, and one represents a perfect fit. R^2 also depicts effect size: small (R^2 = 0.01), medium (R^2 = 0.09), and large (R^2 = 0.25) (Cohen, 1988). The parameters to be determined were kernel (linear, polynomial, and RBF), regularization parameter (C) (1, 10, 100), the tube width (ε) (0.01, 0.1, 1), and the degree of the polynomial kernel (2, 3). The kernel coefficient (γ) was set to the default of the libsvm tool. Repeated K-Fold cross-validation was used to mitigate bias, with 5 splits and 10 repeats. The significance of the cross-validated score was evaluated using Scikit-learn's permutation_test_score function (Ojala & Garriga, 2009) with 1,000 permutations and significance level (α) = 0.01. The p-value returned specifies the probability that the cross-validated score would be obtained by chance. The null hypothesis was that age and the alpha rhythm properties had no statistically significant relationship.

4.2.9. Case Study

In this case study, we investigated if the CP participants exhibited the slowed PAF property, as in general CP patients (Sarnthein et al., 2006; De Vries et al., 2013; Lim et al., 2016). We used the SVR model to correlate the controls' PAF with age, then used the correlation and CP participants' age as input to predict the same age controls' PAF as output. The PAFs of controls and CP participants at the same age could then be compared; no real age-matched control was required.

Wilcoxon signed-rank test was used to compare the difference in PAF between the CP participants and controls. Two comparisons were made: CP participants with age and

sex-matched controls and CP participants with SVR-predicted controls. The comparisons were performed in each ROI individually.

4.3. Results

The participants who replied (2), (3), or (5) in the interview question were not used in the analysis. Also, some participants' data were found incomplete and then dropped. After data preprocessing, the number of controls was 474 (246 males and 228 females, mean = 53.90, SD = 18.29), and the number of CP participants was 22 (12 males and 10 females, mean = 64.03 years, SD = 15.64 years). Table 4.2 lists the number of controls and CP participants by age group.

Table 4.2. Number of controls and CP participants by age groups. SD: standard derivation.

Age Group	18-27	28-37	38-47	48-57	58-67	68-77	78-87	All
Control	38	76	81	76	73	66	64	474
Male Control	17	38	45	36	35	34	41	246
Female Control	21	38	36	40	38	32	23	228
Mean Age	23.92	32.96	43.41	52.73	63.16	72.54	81.43	53.90
SD of Age	3.12	3.26	2.91	2.98	2.82	2.99	2.67	18.29
CP participants	1	0	3	1	8	4	5	22
Male CP participants	1	0	1	1	5	3	1	12
Female CP participants	0	0	2	0	3	1	4	10
Mean Age	20.75	--	43.03	54.67	63.54	73.69	80.23	64.03
SD of Age	--	--	2.80	--	3.34	3.74	2.71	15.64

The grand average PSD plot of the four alpha-generation sites was used to determine an extended alpha bandwidth for the analysis. Figure 4.2 shows the grand average PSD of the participants in the four ROIs. Each participant's PSD was normalized by dividing by its mean power across all the frequency points from 2 to 19 Hz before averaging. The alpha rhythm in the parieto-occipital ROI had the highest amplitude, which matched previous findings (Chiang et al., 2011), and the frontal ROI had the weakest peak amplitude among the four ROIs.

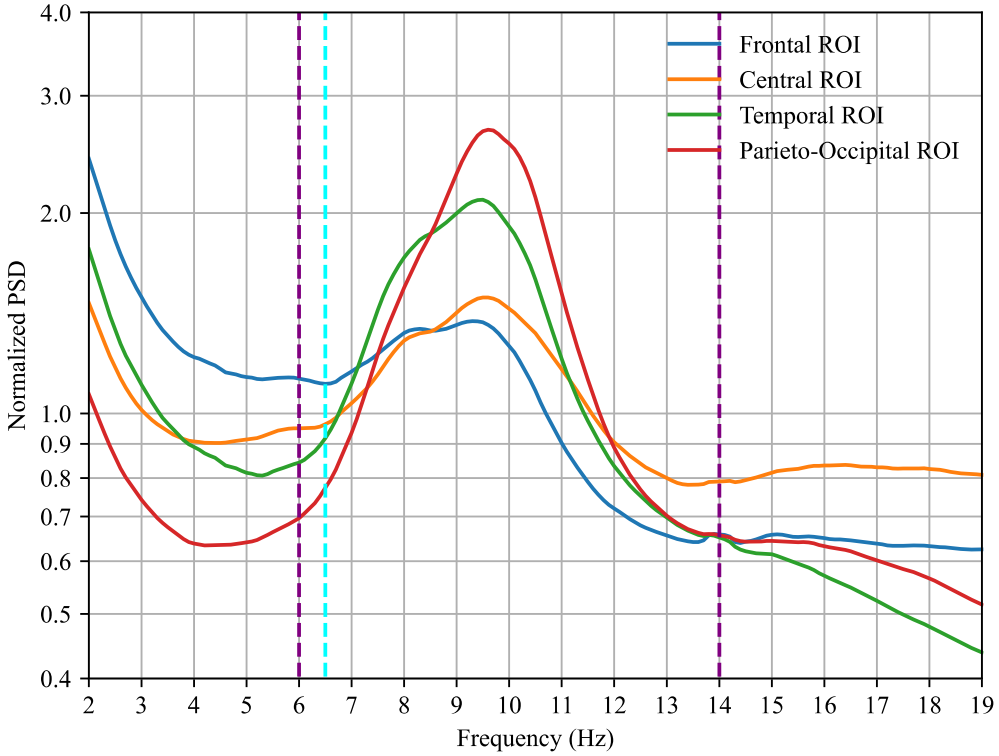

Figure 4.2. Grand average of normalized source space power spectral density (PSD) of controls (N = 474) in the four regions of interest (ROIs). The two purple vertical dashed lines show the lower and upper boundaries of the extended alpha bandwidth (6-14 Hz). The cyan vertical dashed line shows the lower boundaries of the frontal alpha bandwidth.

By inspecting the alpha rhythm widths in the figure, the bandwidth of 6-14 Hz (Scally et al., 2018) was determined for finding PAF in the ROIs, 2 Hz in extension to the conventional alpha bandwidth of 8-12 Hz on the lower and upper ends. An exception was the frontal ROI; the figure shows the left trough of the frontal alpha rhythm was at 6.5 Hz, and a 6.5-14 Hz bandwidth was used. Since the frontal ROI power was much weaker than the others, a more precise left boundary of the frontal range had to be specified to reduce spurious results caused by misrecognizing the theta power as the alpha peak by SciPy's find_peaks function. The prominence parameter of find_peaks was set to 0.15 by inspecting the grand average frontal peak amplitude. If an alpha rhythm peak prominence was less than this threshold or the peak was outside the extended alpha range, it was assumed that no peak was found. Participants with no dominant peak found in an ROI were not used in the plot and analysis of that ROI. As the find_peaks function was applied

to the four ROIs individually, the number of participants with an alpha peak found differed in each ROI. Table 4.3 shows the number of controls and CP participants with an alpha peak in the final sample.

Table 4.3. Number of controls and CP participants in the final sample with peak alpha frequency (PAF) found in each region of interest (ROI). N: number of participants; M: male; F: female; SD: standard derivation.

ROI	Participant Data	Control	CP participants
Frontal	N	424 (220M/204F)	21 (11M/10F)
	Mean Age	53.47	63.94
	SD Age	18.61	16.02
	Mean PAF	9.23	8.97
	SD of PAF	1.15	0.96
Central	N	435 (229M/206F)	21 (11M/10F)
	Mean Age	53.40	63.94
	SD Age	18.61	16.02
	Mean PAF	9.55	9.43
	SD of PAF	1.34	1.33
Temporal	N	467 (245M/222F)	21 (12M/9F)
	Mean Age	53.95	64.19
	SD Age	18.34	16.01
	Mean PAF	9.31	9.15
	SD of PAF	1.13	0.98
Parieto-occipital	N	468 (245M/223F)	21 (11M/10F)
	Mean Age	53.76	63.94
	SD Age	18.34	16.02
	Mean PAF	9.61	9.26
	SD of PAF	1.07	0.90

4.3.1. K-Sample Anderson-Darling Test

The K-sample Anderson-Darling test was used to check if the data in the ROIs were from the same distribution regarding PAF, absolute peak amplitude, relative peak amplitude, high alpha absolute power, low alpha absolute power, high alpha relative power, and low alpha relative power. A P-value < 0.001 was obtained in most tests, so the alpha rhythm properties significantly differed in the four ROIs. The null hypothesis that all the samples in the four ROIs were from the same distribution was rejected.

Table 4.4 shows the P-values of the statistical results of the four regions and the two-region combinations. Namely, frontal and central ROIs, frontal and temporal ROIs, frontal and parieto-occipital ROIs, central and temporal ROIs, central and parieto-occipital ROIs, and temporal and parieto-occipital ROIs. The significance levels (α) required to reject the null hypothesis was Bonferroni corrected by dividing the two-tailed α of 0.025 by six comparisons and then α = 0.004. The only case the null hypothesis failed to reject was the frontal and temporal PAF comparison. This evidence showed that choosing the four ROIs in this study helped the understanding of alpha rhythm variations in different brain areas related to human aging.

Table 4.4. P-values of the K-sample Anderson-Darling comparisons between the different regions of interest (ROIs). All: all four ROIs, f-c: frontal and central ROIs, f-t: frontal and temporal ROIs, f-po: frontal and parieto-occipital ROIs, c-t: central and temporal ROIs, c-po: central and parieto-occipital ROIs, t-po: temporal and parieto-occipital ROIs. Level of Significance (α) = 0.004 was Bonferroni corrected.

Alpha Rhythm Property	ROI Comparison						
	All	f-c	f-t	f-po	c-t	c-po	t-po
Peak Alpha Frequency	< 0.001	< 0.001	> 0.250	< 0.001	0.001	0.003	< 0.001
Absolute Peak Amplitude	< 0.001	< 0.001	< 0.001	< 0.001	< 0.001	< 0.001	< 0.001
Relative Peak Amplitude	< 0.001	< 0.001	< 0.001	< 0.001	< 0.001	< 0.001	< 0.001
High Alpha Absolute Power	< 0.001	< 0.001	< 0.001	< 0.001	< 0.001	< 0.001	< 0.001
Low Alpha Absolute Power	< 0.001	< 0.001	< 0.001	< 0.001	< 0.001	< 0.001	< 0.001
High Alpha Relative Power	< 0.001	< 0.001	< 0.001	< 0.001	< 0.001	< 0.001	< 0.001
Low Alpha Relative Power	< 0.001	< 0.001	< 0.001	< 0.001	< 0.001	< 0.001	< 0.001

4.3.2. Boxplots

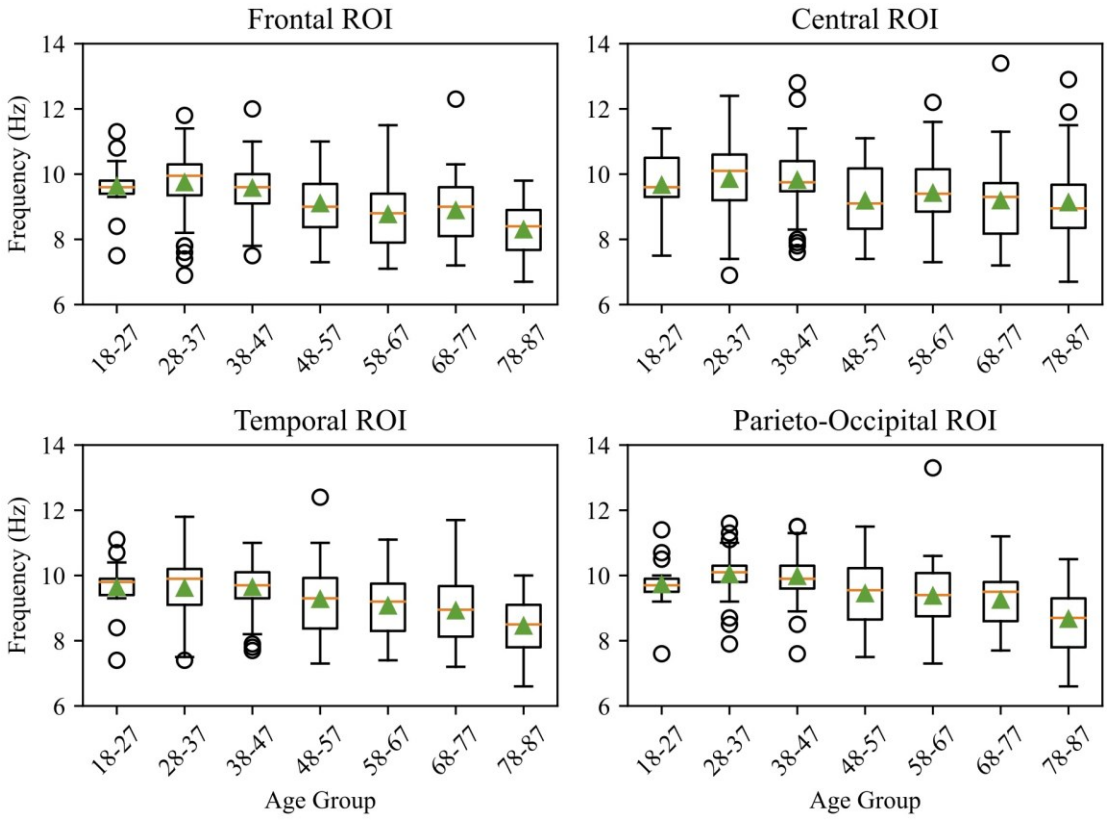

Figure 4.3. Boxplots of PAF versus male control age group. The triangle marker shows the mean in each age group, and the orange line shows the median.

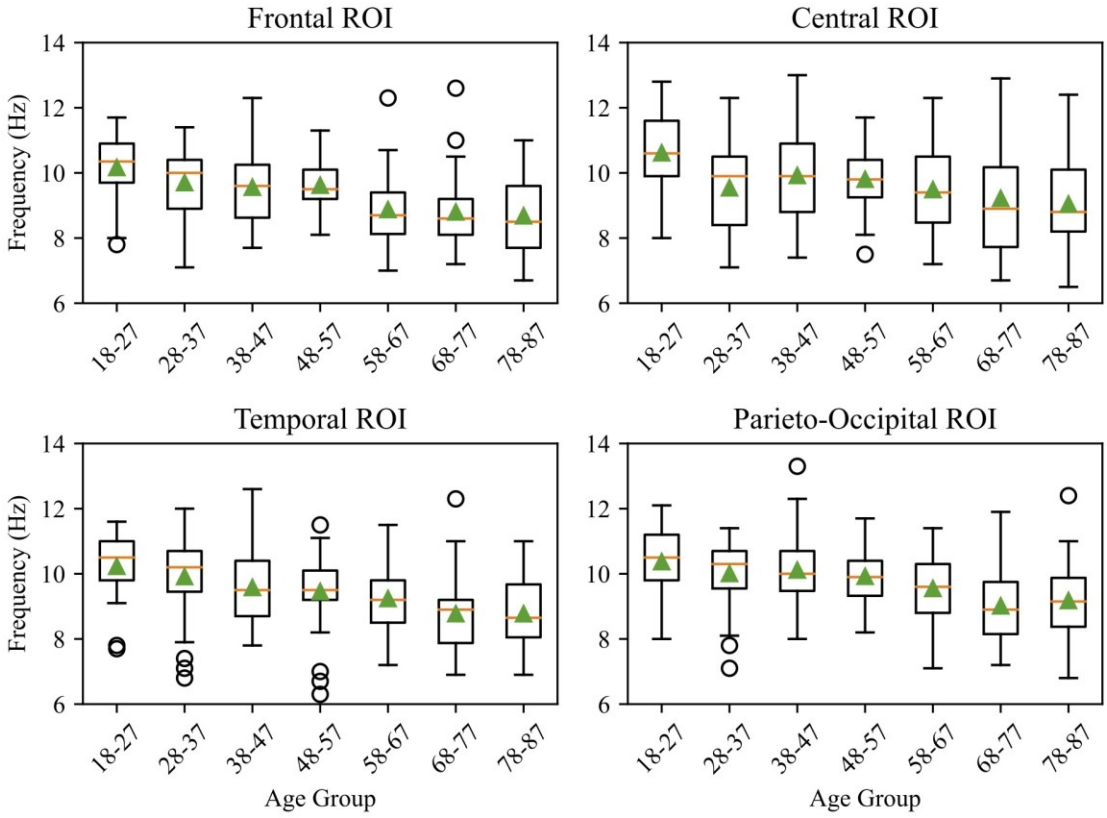

Figure 4.4. Boxplots of PAF versus female control age group. The triangle marker shows the mean in each age group, and the orange line shows the median.

Figures Figure 4.3 and Figure 4.4 show the male and female control groups' PAF boxplots in the four ROIs. The x-axis is the age group. The y-axis is the frequency in the extended alpha band. The orange line in each box shows an age group's median or the 50th percentile. A box's top and bottom lines are the 75th and 25th percentiles. The top and bottom whiskers are the 100^{th} and 0^{th} percentiles, excluding outliers. The circles show the outliers, and the green triangle shows the mean. The plots show a PAF slowing trend, though the central ROI looked less regular. These results matched previous findings in slowed PAF with aging (Chiang et al., 2011; Scally et al., 2018; Jabès et al., 2021). By observation, the female controls showed a higher mean PAF in the youngest age group in all ROIs. To verify if sex has any effect on the alpha rhythm (Matthis et al., 1980; Benninger et al., 1984; Díaz De León et al., 1988; Harmony et al., 1990; Chiang et al., 2011; Ko et al., 2021), Table 4.5A compared the PAF of the male and female controls in the 18-27 age group using the Mann-Whitney U test, with significance found in the central, temporal, and parietal-occipital ROIs, $P<0.025$ and level of significance (α) = 0.025 for the

two-tailed tests. Bonferroni correction was not required. Table 4.5B compared the mean PAF of the male and female controls in all age groups using the Wilcoxon signed-rank test. No significant difference was found.

Table 4.5. (A) Comparison of the PAF of the male and female controls in the 18-27 age group. (B) Comparison of the mean PAF of the male and female controls in all age groups. Level of Significance (α) = 0.025 for the two-tailed tests. Bonferroni correction was not required.

Male vs. female controls: PAF of the 18-27 age group (Mann-Whitey U tests)				
ROI	Frontal	Central	Temporal	Parietal-occipital
Z	-1.987	-2.616	-2.251	-2.529
P-value	0.047	0.009	0.024	0.011
Male vs. female controls: mean PAF of all age groups (Wilcoxon signed-rank tests)				
ROI	Frontal	Central	Temporal	Parietal-occipital
Z	-1.352	-1.014	-1.859	-1.521
P-value	0.176	0.310	0.063	0.128

For other boxplots not shown here (refer to Appendix D for all the boxplots), the absolute amplitude and absolute power plots showed much irregularity, and no apparent trend in aging was observed. For the relative amplitude and relative power plots, it seemed to be a slight trend of amplitude and power decrease in aging in the central and parietal-occipital ROIs, but less evident and smooth than the PAF trend.

4.3.3. Support Vector Regression

Table 4.6 shows the GridSearchCV exhaustive search results with K-fold cross-validation of 5 splits and 10 repeats. The results included the best kernel and parameters found (C: regularization parameter; ε: tube width, and degree of the polynomial kernel), R^2, and P-value. The P-values were obtained using permutation tests with 1,000 permutations and a significance level α = 0.01 (Ojala & Garriga, 2009). Bolded R^2 depicts a medium effect size. SVR was applied separately to the mixed-sex, male, and female controls, and age was the only input feature. The very low P-values confirmed the significance of the results. The PAF of the frontal, temporal, and parietal-occipital ROIs showed R^2 with medium effect size for the mixed-sex, male, and female controls, except the parietal-occipital PAF of the female controls. Besides PAF, the only other alpha rhythm property with $R^2>0$ was mixed-sex relative amplitude in the parieto-occipital ROI. As

significant relationships were found between PAF and aging, the second null hypothesis was rejected.

Table 4.6. Support vector regression (SVR) fittings of alpha rhythm properties versus age. The table shows the grid search results of the best kernel and parameters, coefficient of determination (R^2), and p-value, with repeated K-fold cross-validation of 5 splits and 10 repeats. The p-values were obtained using permutation tests, with significance level $\alpha = 0.01$. Bolded R^2 depicts a medium effect size. PO: parieto-occipital; C: regularization parameter; ε: tube width.

Control	Alpha Rhythm Property	C	ε	Kernel	Degree of the Polynomial	R^2	P-value
Mixed-sex	Frontal PAF	1	1	Linear		**0.155**	0.001
Mixed-sex	Central PAF	100	0.1	Linear		0.025	0.001
Mixed-sex	Temporal PAF	100	1	Polynomial	2	**0.133**	0.001
Mixed-sex	PO PAF	10	0.1	Polynomial	2	**0.147**	0.001
Male	Frontal PAF	1	0.1	Linear		**0.163**	0.001
Male	Central PAF	1	0.01	Linear		0.018	0.002
Male	Temporal PAF	1	0.1	Polynomial	3	**0.126**	0.001
Male	PO PAF	100	0.1	Polynomial	3	**0.156**	0.001
Female	Frontal PAF	100	1	Linear		**0.090**	0.001
Female	Central PAF	100	1	Polynomial	2	0.023	0.002
Female	Temporal PAF	100	1	Linear		**0.095**	0.001
Female	PO PAF	100	1	Polynomial	2	0.089	0.001
Mixed-sex	PO relative amplitude	1	0.01	Linear		0.004	0.001

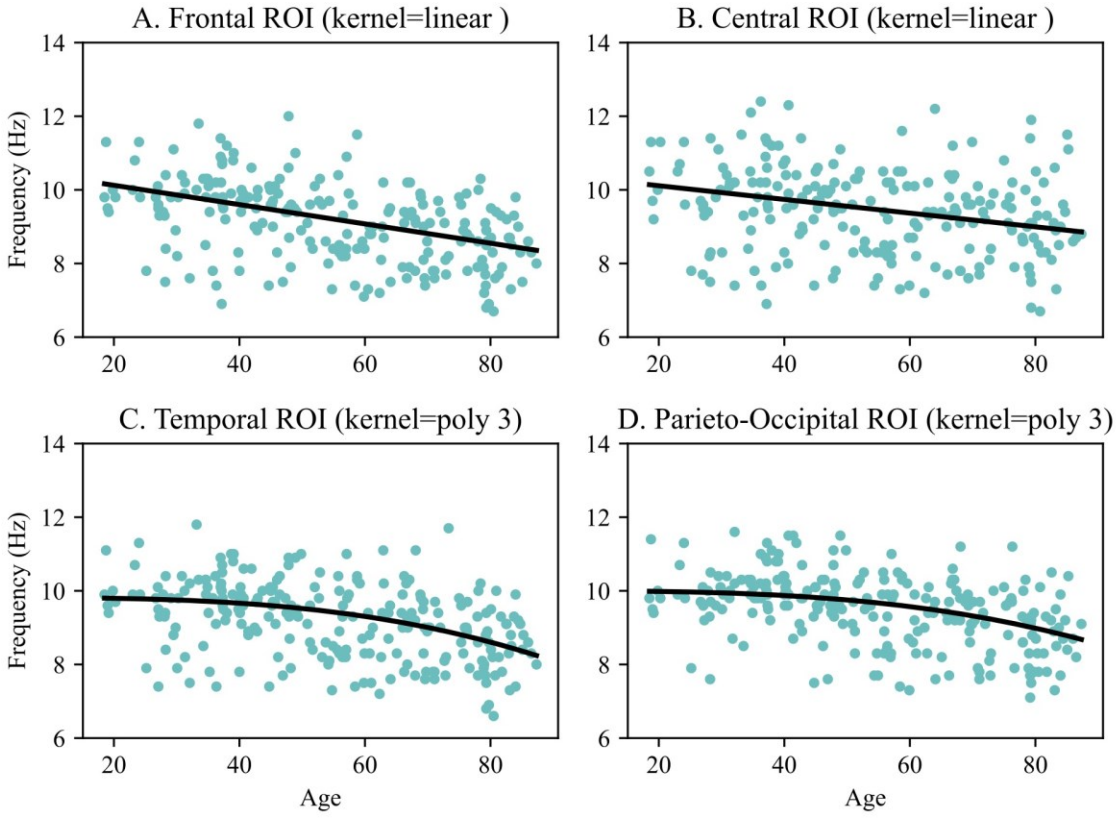

Figure 4.5. Support vector regression (SVR) of PAF versus age of the male controls. Cyan circles are PAF data points. The black line is the regression model (hyperplane).

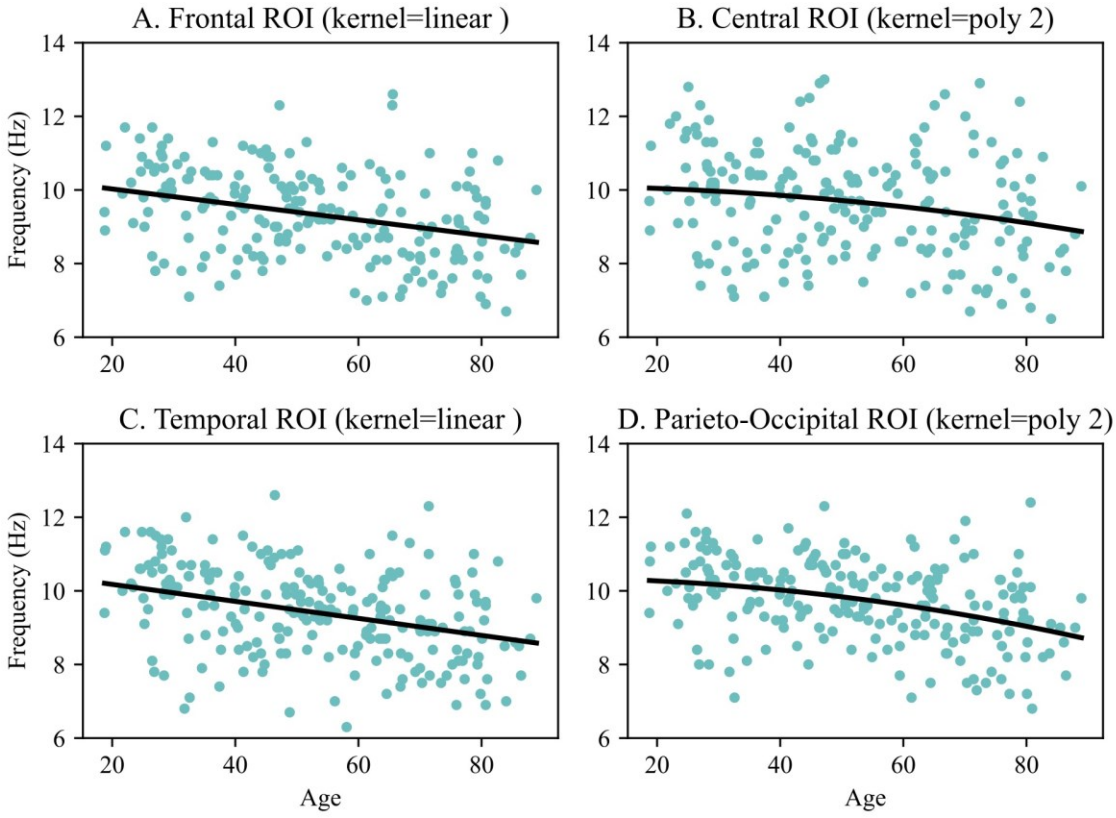

Figure 4.6. Support vector regression (SVR) of PAF versus age of the female controls. Cyan circles are PAF data points. The black line is the regression model (hyperplane).

Figure 4.5 &Figure 4.6 show SVR fittings of PAF versus age of the male and female controls, respectively. The figures indicate a downshift of PAF in all four ROIs with slightly different slopes and curve shapes. Both male and female controls had similar kernels chosen in the frontal (linear) and parieto-occipital (degree 3 and 2 polynomials) ROIs and different in the central (linear and degree 2 polynomial) and temporal (degree 3 polynomial and linear) ROIs.

4.3.4. Case study results

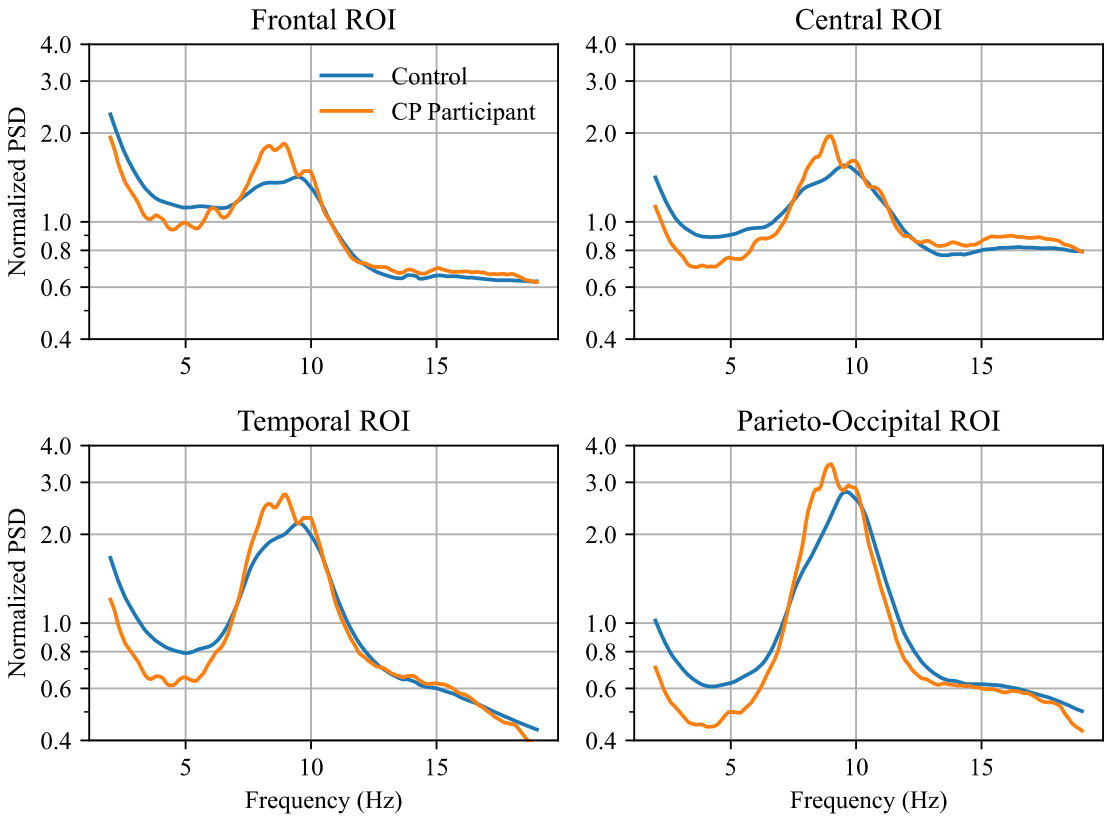

Figure 4.7. Grand average of normalized source space power spectral density (PSD) of controls and CP participants in the four regions of interest (ROIs). $N_{control}$ = 474, $N_{CP\ participants}$ = 22.

Figure 4.7 shows the grand averaged PSD plots in four ROIs of the controls (N = 474, 246 males and 228 females, mean = 53.90, SD = 18.29) and the CP participants (N = 22, 12 males and 10 females, mean age = 64.03, SD = 15.64) (Table 4.2). By observation, the plots show the typical slowed PAF of CP patients (Sarnthein et al., 2006; Boord et al., 2008; Lim et al., 2016) in all ROIs without including age.

Table 4.7 shows the mean PAF of the mixed-sex controls and CP participants. The CP participants had slower PAFs than the controls in all four ROIs. As the controls and CP participants had different mean ages, SVR models were applied to predict the controls' PAF using the CP participants' mean age as inputs. Compared with the SVR-predicted controls, the CP participants showed a slowed PAF only in the parieto-occipital ROI with

a difference of 0.20 Hz. The 2.16% difference in the parieto-occipital ROI was the highest in all four ROIs, compared to 0.00 to 0.55%. The results implied that the mean PAFs of the CP participants were about the same as the controls' normal aging in the frontal, central, and temporal ROIs but slower in the parieto-occipital ROI.

Table 4.7. Peak alpha frequency (PAF) prediction for controls using SVR. The rightmost column shows the SVR-predicted controls obtained by using CP participants' mean age as input. Bolded numbers are the mean PAF of CP participants and PAF of SVR-predicted controls. ROI: region of interest; PAF: peak alpha frequency; N: number of participants.

ROI	Participant Data	Control	CP participant	SVR-Predicted Control
Frontal	N	424	21	424
	Mean Age	53.47	63.94	63.94
	Mean PAF	9.23	**8.97**	**8.97 (±0.00%)**
Central	N	435	21	435
	Mean Age	53.40	63.94	63.94
	Mean PAF	9.55	**9.43**	**9.39 (-0.42%)**
Temporal	N	467	21	467.0
	Mean Age	53.95	64.19	64.2
	Mean PAF	9.31	**9.15**	**9.10 (-0.55%)**
Parieto-occipital	N	468	21	468
	Mean Age	53.76	63.94	63.936
	Mean PAF	9.61	**9.26**	**9.46 (+2.16%)**

For verification purposes, the CP participants were compared with sex and age-matched controls using the Wilcoxon signed-rank test (Table 4.8), with a significance level (α) = 0.025 for the two-tailed tests, and Bonferroni correction was not required. No significance was found in the four ROIs. Table 4.8 also compares PAF between CP participants and SVR-predicted controls. Controls' PAF was predicted using the CP participants' age. Also, no significance was found in the Wilcoxon signed-rank test. However, the P-value improved using SVR-predicted controls in the parieto-occipital ROI.

Table 4.8. Wilcoxon signed-rank tests of CP participants versus sex and age-matched controls and SVR-predicted controls. Level of Significance (α) = 0.025 for the two-tailed tests. Bonferroni correction was not required.

ROI	CP participant	Matched Control		SVR-Predicted Control	
		Z	P-value	Z	P-value
Frontal	21	-0.557	0.578	-0.122	0.903
Central	21	-0.616	0.538	-0.191	0.848
Temporal	21	-0.365	0.715	-0.400	0.689
Parieto-Occipital	21	-0.435	0.664	-0.643	0.520

4.4. Discussion

We proposed a novel method for including age in pathophysiological studies. The method uses SVR to explore the correlations between alpha rhythm properties and age in EEG/MEG source space PSD regarding the four alpha generation ROIs. The method was tested in a CP case study, and it was found that the CP participants exhibited a slowed PAF property in the parietal-occipital ROI, similar to that of general CP patients. The method could be used in other pathophysiological studies to mitigate the limitation of age-matched control requirements.

This study yielded several primary findings using the novel method. First, the slowed PAF was the primary alpha rhythm property related to aging, especially in the frontal, temporal, and parieto-occipital ROIs, as found in the boxplots and SVR tests (Table 4.6). Second, in the boxplots, female controls showed higher PAF than male controls in the 18-27 age group, with significance in the central, temporal, and parieto-occipital ROIs. Some previous works also compared sex differences in the alpha rhythm but mostly in children (Matthis et al., 1980; Benninger et al., 1984; Díaz De León et al., 1988; Harmony et al., 1990; Chiang et al., 2011; Ko et al., 2021). Third, the boxplots show that male controls' PAF slowing started from the 28-37 age group, but for female controls, it started from the 18-27 age group. Similar results but at different ages were previously reported (Köpruner et al., 1984; Chiang et al., 2011; Aurlien et al., 2004). Fourth, as shown in the case study, the slowed PAF of the CP participants was in the parieto-occipital ROI. A previous study (De Vries et al., 2013) also reported a similar finding using EEG and sensor space.

The SVR results showed that the frontal, temporal, and parieto-occipital PAF decreased with age with a medium effect size (Table 4.6). They could be further explored as a biomarker for aging. An individual fixed bandwidth of 1 Hz based on PAF was used to compute the alpha band power. This helped to avoid misleading alpha power change due to the alpha rhythm being shifted off a fixed alpha bandwidth and also to avoid overlapping nearby peaks.

The higher PAF of the female than the male controls in the 18-27 age group and the PAF slowing of male controls starting from the 28-37 group depicted unique properties of the alpha rhythm. Previous studies showed a similar effect at age 20 (Köpruner et al., 1984; Chiang et al., 2011) or age 45 (Aurlien et al., 2004). Due to the smaller sample size in the 18-27 age group than the other age groups, these effects have yet to be verified. In this study, SVR was fitted using hundreds of controls. The regression fitting might become less effective for a smaller sample, for instance, less than 25 participants (Jenkins & Quintana-Ascencio, 2020).

The case study showed that one could use SVR to predict rhythm properties corresponding to age, such that non-age-matched controls can be used in pathophysiological studies. Using SVR to predict features may have the advantage of more consistent results. The improved P-values in the Wilcoxon signed-rank test using SVR-predicted controls were likely due to the more consistent PAF values from the regression (Table 4.8).

PAF was reported to be positively related to thalamic and salience network (SN) activity (McLain et al., 2022). SN acts as a switch in information processing of the other brain networks and comprises the ventral anterior insula and anterior cingulate cortices (Seeley, 2019). The thalamus receives pain signals from the spinal cord and relays the signals to the somatosensory cortex, the cingulate, and the insula (Baller & Ross, 2017). This relationship infers that PAF may be associated with pain (McLain et al., 2022). PAF may be a biomarker reflecting changes in the neurophysiological properties of the brain and may reflect the performance of information sampling and processing of cortical neurons (Mierau et al., 2017). De Vries et al. (2013) showed that slowed PAF was related to CP, mainly in the parieto-occipital region, using EEG and sensor space. The case study showed a similar result: with age included, the CP participants showed slowed PAF only in the parieto-occipital ROI.

The case study has a limitation to be considered in interpreting the results since the CP participant data sample size of 22 was relatively low. The Wilcoxon signed-rank test results (Table 4.8) showed no significant difference between CP participants and sex and age-matched controls, likely because the CP participants had an average delay of more than three months between the interview and MEG scans. The conditions of some participants could have varied within this period. The non-significant results could also be because even normal and age-matched controls could exhibit a PAF standard deviation of about 1 Hz (Klimesch, 1996). When compared with SVR-predicted controls, P-values improved in the parieto-occipital ROI. This might imply that the SVR method could provide more consistent PAF values than sex and age-matched controls.

4.4.1. Conclusion

The findings suggest that using multiple ROIs in the alpha rhythm versus age correlation analyses was effective, with P-values < 0.001 in comparing the ROIs. The trend of PAF changes with age was identified in the ROIs and with medium effect sizes in SVR fittings. The slowed PAF started from the 28-37 age group in the male controls is similar to previous findings. The case study demonstrated the techniques to include age in a CP study using SVR-predicted controls. The PAF versus age regression results can be represented in a table format for a quick lookup, reducing computing time in reusing the data and SVR models. The proposed novel method could create an aging model for pathophysiological studies. This novel method of including age in CP studies may guide further studies to explore (1) including age in other pathophysiological studies, such as dementia, and (2) using other machine learning approaches, like CNNs, to achieve the best accuracy. To our knowledge, our group is the first to use SVR to explore the correlation between alpha rhythm properties and age in MEG source space PSD regarding the four alpha generation ROIs. We are also the first to use SVR to predict PAF with age for controls in a pain analysis. The novel method provides a way to include age in CP or other neurophysiological analyses.

Acknowledgements

This research was partly enabled by support provided by the Digital Research Alliance of Canada (www.alliancecan.ca). Data used in the preparation of this work were

obtained from the CamCAN repository (https://www.mrc-cbu.cam.ac.uk/datasets/camcan/) (Taylor et al., 2017; Shafto et al., 2014).

Conflict of Interest

The authors declare that the research was conducted in the absence of any commercial or financial relationships that could be construed as a potential conflict of interest.

Chapter 5.

Virtual Reality–Guided Meditation for Chronic Pain in Patients with Cancer: Exploratory Analysis of Electroencephalograph Activity

The study in this chapter corresponds to the publication:

Fu, H., Garrett, B., Tao, G., Cordingley, E., Ofoghi, Z., Taverner, T., Sun, C., & Cheung, T. (2021). Virtual Reality–Guided Meditation for Chronic Pain in Patients with Cancer: Exploratory Analysis of Electroencephalograph Activity. JMIR Biomedical Engineering, 6(2), e26332. https://doi.org/10.2196/26332

Abstract

Mindfulness-based stress reduction has demonstrated some efficacy for chronic pain (CP) management. More recently, virtual reality (VR)–guided meditation has been used to assist mindfulness-based stress reduction. Although studies have also found electroencephalograph (EEG) changes in the brain during mindfulness meditation practices, such changes have not been demonstrated during VR-guided meditation.

This exploratory study is designed to explore the potential for recording and analyzing EEG during VR experiences in terms of the power of EEG waveforms, topographic mapping, and coherence. We examine how these measures changed during a VR-guided meditation experience in participants with cancer-related CP.

A total of 10 adult patients with chronic cancer pain underwent a VR-guided meditation experience while EEG signals were recorded during the session using a BioSemi ActiveTwo system (64 channels, standard 10-20 configuration). The EEG recording session consisted of an 8-minute resting condition (pre), a 30-minute sequence of 3 VR-guided meditation conditions (med), and a final rest condition (post). Power spectral density (PSD) was compared between each condition using a cluster-based permutation test and across conditions using multivariate analysis of variance. A topographic analysis, including coherence exploration, was performed. In addition, an exploratory repeated measures correlation was used to examine possible associations between pain scores and EEG signal power.

The predominant pattern was for increased β and γ bandwidth power in the meditation condition (P<.025), compared with both the baseline and postexperience conditions. Increased power in the δ bandwidth was evident, although not statistically significant. The pre versus post comparison also showed changes in the θ and α bands (P=.02) located around the frontal, central, and parietal cortices. Across conditions, multivariate analysis of variance tests identified 4 clusters with significant (P<.05) PSD differences in the δ, θ, β, and γ bands located around the frontal, central, and parietal cortices. Topographically, 5 peak channels were identified: AF7, FP2, FC1, CP5, and P5, and verified the changes in power in the different brain regions. Coherence changes were observed primarily between the frontal, parietal, and occipital regions in the θ, α, and γ bands (P<.0025). No significant associations were observed between pain scores and EEG PSD.

This study demonstrates the feasibility of EEG recording in exploring neurophysiological changes in brain activity during VR-guided meditation and its effect on pain reduction. These findings suggest that distinct altered neurophysiological brain signals are detectable during VR-guided meditation. However, these changes were not necessarily associated with pain. These exploratory findings may guide further studies to investigate the highlighted regions and EEG bands with respect to VR-guided meditation.

Trial Registration: ClinicalTrials.gov NCT00102401; http://clinicaltrials.gov/ct2/show/NCT00102401

Keywords: virtual reality (VR); guided meditation; neurophysiology; electroencephalograph (EEG)

5.1. Introduction

5.1.1. Background

Chronic pain (CP) is a common condition occurring in 1 in 5 Canadians (Chronic pain in Canada, 2019), and it has limited practical treatment approaches. Mindfulness-based stress reduction (MBSR) has shown some evidence of efficacy in this area (Kabat-Zinn, 2003; Rosenzweig et al., 2010) and has also been used to treat other clinical conditions, such as migraine, depression, addiction, and substance misuse (Kabat-Zinn, 2003; Lomas et al., 2015).

Mindfulness meditation encompasses a range of mental exercises that share a common focus on regulating attention and awareness to improve well-being (Kabat-Zinn, 2003; Rosenzweig et al., 2010; Lomas et al., 2015). It is described as the quality of being completely engaged in the present moment, free from distractions and judgments, and being aware of bodily sensations, thoughts, and feelings without getting caught up by them, and it is used as a therapeutic technique in MBSR (Hanson & Mendius, 2009; Nyklíček et al., 2014). These practices involve mental training that allows practitioners to develop their minds in specific ways to help them deal with stress and anxiety (Lee et al., 2018; Schoenberg & Vago, 2019). Although the clinical benefits remain somewhat controversial, it is generally viewed as a beneficial practice for mental well-being, stress reduction, and pain management (Farias & Wikholm, 2016; Keng et al., 2011; Seay et al., 2002).

A recent trend in MBSR practice has been the use of immersive virtual reality (VR) to help participants focus on meditative exercise (Botella et al., 2013; Erlacher & Chapin, 2010; Gromala, 2015; Navarro-Haro, 2019; Venuturupalli et al. 2019). However, to date, neurological studies have not been performed with VR-guided meditation practices. Therefore, this exploratory study sought to identify any identifiable neurological effects of VR-guided meditation practices using electroencephalographs (EEGs).

5.1.2. Neurological Mindfulness Studies

Subjective reports of the benefits of mindfulness meditation have prompted investigations into the potential corresponding neurophysiological states. Exploration of fluctuations in brain wave voltage amplitude (power) topography and coherence (associated areas of activity) using EEG variations in neural activity assessed with functional magnetic resonance imaging and cortical evoked responses to visual and auditory stimuli that reflect the impact of meditation on attention (Lomas et al., 2015; Cahn & Polich, 2006; Davidson & Lutz, 2008; Ivanovski & Malhi, 2007; Panjwani et al., 2000; Heeger & Ress, 2002; Chiesa & Serretti, 2010; Magalhaes et al., 2018; Mishra et al., 2017; Froeliger et al., 2012; Goldin et al., 2013). However, findings remain speculative. EEG studies have previously reported modulation in α, θ, and γ band frequencies, generally with increased power and coherence during mediation (Lomas et al., 2015; Lee et al., 2018; Cahn & Polich, 2006; Delmonte, 1984). Some studies theoretically conjectured how meditative states relate to EEG bandwidths. For example, Travis and Shear (Travis &

Shear, 2010) suggested that focused attention (sustained attention is focused on a given object) increases γ band power, open monitoring (nonreactive monitoring of an ongoing experience) increases θ, and an automatic-self-transcending stage (transcending the procedures of the meditation) increases α (Travis & Shear, 2010). Nevertheless, a consensus on what we currently know about how EEG forms correlate with meditation or how this may map onto stages of mental development or specific cognitive skills is yet to be reached (Lee et al., 2018; Schoenberg & Vago, 2019).

The α frequency band lies between 8 and 12 Hz and is predominantly located in the occipital cortex. α waves are present in deep relaxation and sleep, usually when the eyes are closed. θ waves are characterized by oscillations in the 4-8 Hz band found in both cortical and subcortical structures. Increases in θ have been described during a variety of learning and recognition tasks, light sleep (including the rapid-eye-movement dream state), and deep meditation. θ and α power changes have been reported to increase in a number of meditation studies (Lomas et al., 2015; Cahn & Polich, 2006; Ivanovski & Malhi, 2007; Dunn et al., 1999; Fell et al., 2010; Lagopoulos et al., 2009). Moreover, γ is a higher frequency range generally regarded as between 30 and 50 Hz, although the range reported has varied substantially between 20 and 200 Hz across different studies (Fell et al., 2010). This initial research suggests that γ is associated with a number of sensory and cognitive high-level information processing functions, such as semantic insights, learning, and neural plasticity. Peak γ frequencies around 40 Hz in bilateral hemispheres have only been observed in highly practiced meditators (Cahn & Polich, 2006; Fell et al., 2010). In addition, a posterior increase in γ activity may be related to enhanced perceptual clarity reported in some open monitoring (focusing on awareness itself) meditative processes (Lee et al., 2018; Cahn & Polich, 2006; Fell et al., 2010).

5.1.3. VR-Assisted Mindfulness

VR is rapidly developing as a new form of media and uses computer-generated audio-visual displays and hand controller user interfaces to produce a sense of immersion in a digital 3D environment. Instead of watching an image on a typical computer or video display, VR technologies provide an increased sense of presence by engaging the senses (sight, sound, and touch) in real-time stereoscopic audio-visual media where users can move around and explore the environment as if they were there.

5.1.4. VR in Pain Management

One of the most common health care applications of VR is its use in pain management. Several studies have explored the value of MBSR in CP management, although the reported effect sizes for this technique have been typically mild to moderate, and regular adherence with meditative practice is problematic (Rosenzweig et al., 2010; Rosenzweig, 1995; Johnson et al., 2005). It has been suggested that combining mindfulness meditation within a VR intervention may help support acceptance and adherence to practice while having a synergistic effect on pain reduction through immersive VR distraction (Garrett et al., 2018; Jin et al., 2016; Shaw et al., 2007). This remains an active area of research, as adjunctive VR strategies have been used successfully in the treatment of acute pain (Garrett et al., 2014; Maani et al., 2011; Scapin et al., 2018; Schmitt et al., 2011; Wolitzky et al., 2005) and more recently have also been explored with CP (Botella et al., 2013; Jin et al., 2016; Garrett et al., 2017; Li et al., 2007). The theoretical rationale behind why VR may enhance mindfulness skills is that VR provides the user with cognitive displacement by actively engaging in a coping activity that provides a profound sense of through presence in another world. Cognitive distraction is a common strategy in pain control and relies on creating competition for cognitive resources, that is, attention to a novel spatial orientation, and engaging within it reduces the perception of pain (Eccleston, 1995; Johnson, 2005; Garrett et al., 2018). Therefore, immersive VR interventions using stereoscopic head-mounted displays (HMDs) have been proposed as powerful tools for providing visual, audio, cognitive, and emotional engagement (Dascal et al., 2017; Li et al., 2011; Malloy & Milling, 2010). In MBSR, VR experiences are typically accomplished using computer-simulated environments, stereoscopic headsets, and motion tracking to support a more immersive meditative experience. This was the approach taken in this study, and an EEG analysis was selected as a practical technique to assess neurophysiological activity while experiencing VR.

5.1.5. Objectives

Overall, this inductive exploratory study sought to assess how EEG power of waveforms, their topographic mapping, and coherence measures altered in 3 main states during a VR-guided meditation experience in patients with cancer-related CP: at baseline (pre), during VR-guided meditation (med), and after VR-guided meditation (post). Moreover, we explored whether their pain level was associated with waveform power

measures. We were particularly interested in the power, topography, and coherence of α, γ, and θ wave activity, and possible synchrony with VR activity, as other researchers have reported changes in these 3 waveforms with MBSR activities. Therefore, we were interested in determining whether prior findings were consistent with those observed during a VR experience. Specifically, the questions we sought to address in this study were as follows:

1. Were there any observable or significant changes between pre and during VR-guided meditation experiences and between pre and post VR-guided meditation experiences with the power, topographic changes, or EEG coherence in specific waveforms?

2. Was there any evidence that changes in the pain experienced by participants during a VR-guided meditation activity were associated with observable EEG changes?

5.2. Methods

5.2.1. Approach

An exploratory, single-subject design study was undertaken to compare EEG activity and pain levels before, during, and after VR-based meditation practice. This study was reviewed and approved by the University of British Columbia Clinical Research Ethics Board.

5.2.2. Recruitment

A convenience sample of 10 participants was used and recruited from those in an existing randomized controlled trial (RCT; ClinicalTrials.gov: NCT 02995434) where patients with cancer were using VR as an adjunctive therapy to help manage their CP (Textbox 1). These participants were completing or had completed cancer treatment and experienced a range of cancer-related pain, including neuropathy, fibromyalgia, postsurgical pain, or an exacerbation of pre-existing pain.

Randomized controlled trial eligibility criteria.

Eligibility Criteria

- Aged ≥16 years, with a past or current diagnosis of cancer
- Prior or ongoing cancer treatment
- A chronic pain diagnosis (ongoing daily pain for ≥3 months, with a Neuropathic Pain Rating Scale of ≥4)
- Able to understand English (read and write)
- Normal stereoscopic vision
- Able to move their head up, down, left, and right and able to wear a virtual reality head-mounted display
- Sufficient fine motor control in one hand to use a game controller
- Have space at home for a computer and monitor

Textbox 1. Randomized controlled trial eligibility criteria.

Participants were purposively recruited, focusing on recruiting those from the RCT cohort who had previously responded well to a VR-based meditation experience, with a self-reported reduction of a Visual Analog Scale for Pain ≥1. They were invited to participate in a single 2-hour VR-guided meditation experience, with EEG recorded in their home or at the university, and were offered a Can $100 (US $83) honorarium and expenses for taking part. As an exploratory study designed to establish methods and feasibility using a limited convenience sample, with an unknown effect size, the power to inform the sample size was not calculated a priori. This is acceptable for this type of inductive study (Johanson & Brooks, 2009).

5.2.3. Equipment

EEG signals were recorded during the session using a BioSemi ActiveTwo system (BioSemi) with 64 channels in a standard 10-20 configuration. This system uses a head cap system with pin active silver chloride electrodes. The EEG ground (labeled DRL [Driven Right Leg]) on the Biosemi system was placed between POz and PO4, and the

EEG reference (labeled CMS [Command Mode Sense]) was placed between POz and PO3. The antialiasing filter was a fixed first-order analog filter with −3 dB at 3.6 kHz, and the low-pass filter was a fifth-order cascaded integrator-comb digital filter with −3 dB at one-fifth the sample rate. A powerline notch filter was not applied because the system used active electrodes, a battery power supply, and optic fiber, greatly reducing noise from the powerline. Each channel consisted of a 24-bit analog-to-digital converter. Recordings were made at 1024 Hz (although one was recorded at 2048 Hz) using ActiView software (Biosemi Instrumentation).

An HTC Vive VR system (HTC) with a Deluxe Audio Strap fitted over the top of the EEG cap was used. This system features a 2160×1200 resolution, 90 Hz refresh rate, and 110° field of view. Positional tracking from 2 infrared cameras enabled 5-degrees-of-freedom motion tracking of the headset and hand controllers. Integrated stereo headphones supported 3D audio immersions. During the initial pilot testing, this system was found to work effectively. Minor noise was evident in the EEG from the VR system on rare occasions, but we were able to remove most of this noise by careful repositioning of the equipment.

For meditation practice, a commercially available Guided Meditation VR application (Cubicle Ninjas) was used. As each meditation was only 10 minutes in this app, we selected a single sequence of 3 unique meditations, Zen 2-4, to form a 30-minute block of meditation. In the guided meditation experience, users were situated in the Lost Woods virtual environment with the Calm music selected. They were able to explore a calm, forest 3D environment with running water features with soft chirping bird and gentle wind sounds. Using a controller, participants could move to different positions in the forest to explore or find a particular viewpoint they liked and found most conducive to their meditation. A narrative provided audio guidance on the meditative practice. This environment was selected to maximize the similarity with the participants' prior VR experiences in the RCT.

Both EEG recording and the VR system were run on a Dell G7 17 7790 gaming laptop (Intel Core i7-8750H, 16 GB DDR4, RTX 2060) placed in front of the participant. During recording, the laptop screen was arranged to display the ActiView software and a mirror window of the Guided Meditation VR application experience, showing the participant's perspective in the VR HMD. In addition, a Windows 10 (Microsoft) camera

app was used to record the video. This arrangement was recorded using Snagit (Techsmith) screen capture software to accommodate the time synchronization of EEG and recordings of participants' physical movements (Figure 5.1).

Figure 5.1. Electroencephalograph recording during a virtual reality experience.

5.2.4. Procedures

Participants were seated in front of the laptop, and the laptop webcam was framed to capture the participants' head, arms, and upper body. Before putting on the EEG head cap, participants were familiarized with the VR app, its controls, and how to navigate and select meditations. The Cz, inion, and left and right preauricular locations were marked using standard EEG landmarking methods. These locations were used to align the EEG head cap on the participant. The electrode paste was then applied, and the electrode contacts were adjusted until the electrode offsets were less than 50 μV. The VR HMD was then placed in position over the EEG head cap, and the experience commenced.

The overall structure of data collection used an 8-minute resting condition, followed by the 30-minute sequence of meditations and followed by another 8-minute rest condition (Figure 5.2). The 8-minute period was considered a balance between being shorter to reduce strain and being longer for more data; this period has been used in EEG studies in a variety of fields for baselines (Boonstra et al., 2016; Konicar et al., 2021; Sikka et al., 2019).

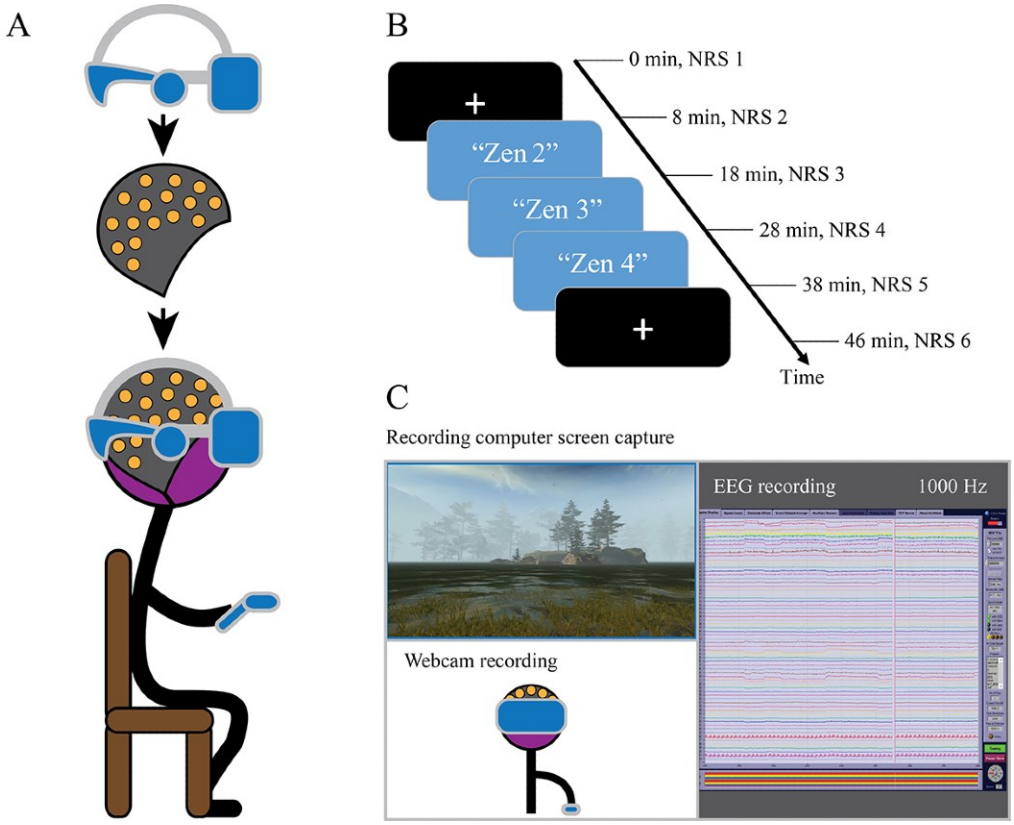

Figure 5.2. (A) Diagram of equipment setup. (B) Timeline of recording, including rest and meditation conditions. (C) Diagram of desktop view. EEG: electroencephalograph; NRS: numerical rating scale.

During the rest conditions, the participants were asked to rest quietly and observe a small white crosshair displayed on a black background in the VR HMD. Participants were instructed to keep their eyes open while blinking naturally, to keep their eyes on the crosshair, and to stay still while not thinking about anything. During the meditation practice, participants were instructed to engage with the guided meditation and look around or move around the virtual environment as they liked, to find an enjoyable perspective. Each guided meditation experience lasted 10 minutes, and participants were instructed to begin the next one immediately after the intervening rest condition. Pain was assessed before and

after the first rest condition, after each 10-minute guided meditation, and after the second rest condition. Participants were asked to verbally rate their pain from 0 to 10 on the simple numerical rating scale (NRS) (Williamson & Hoggart, 2005).

5.2.5. Analysis

Data Preprocessing

The recording sessions of the resting condition, the 3 guided meditation conditions, and the final resting condition were referred to as the Pre, Med1, Med2, Med3, and Post, respectively, for the analysis. These 5 conditions were extracted based on the time stamps acquired from the EEG video recordings.

Figure 5.3 illustrates the EEG data preprocessing steps. The raw EEG data in the Biosemi format were imported and preprocessed using FieldTrip software (Donders Institute for Brain, Cognition and Behaviour) (Oostenveld et al., 2011). As the bandwidth of interest was less than 50 Hz, the data were downsampled to 512 Hz to reduce computing time in later processes. To prepare for downsampling, an antialiasing sixth-order low-pass Butterworth two-pass filter set to 70 Hz was first applied to the data. The primary 64 EEG channels were then re-referenced to the averaged left and right mastoid electrodes (T7 and T8). This re-referencing process effectively eliminated the noise introduced from the original reference electrodes. After this process, the reference electrodes T7 and T8 were eliminated from the data, and only 62 channels were retained.

In addition, a sixth-order high-pass Butterworth two-pass filter with a cut-off at 1 Hz was used to remove slow drifts and to prepare the data for independent component analysis (ICA) (Makeig et al., 1995). The data were further notch-filtered to remove any powerline noise and harmonics, with cut-offs set at 60, 120, and 180 Hz. Bad channels were identified during the EEG recording process using an EEG data browser and rejected.

These data for each condition were further segmented into nonoverlapping epochs of 2 seconds in length to enable signal averaging in the frequency domains (Levy, 1987). A data cleaning process was then performed using the FieldTrip automatic artifact removal feature, which is based on a Z-transformation and the setting of a threshold to reject bad epochs. This artifact removal result was found to be unsatisfactory, so a manual cleaning

process was then performed. Segments with participant movement observed in the videos were identified, and any residual bad segments and channels were rejected. These steps effectively eliminated the artifacts caused by head and body movements.

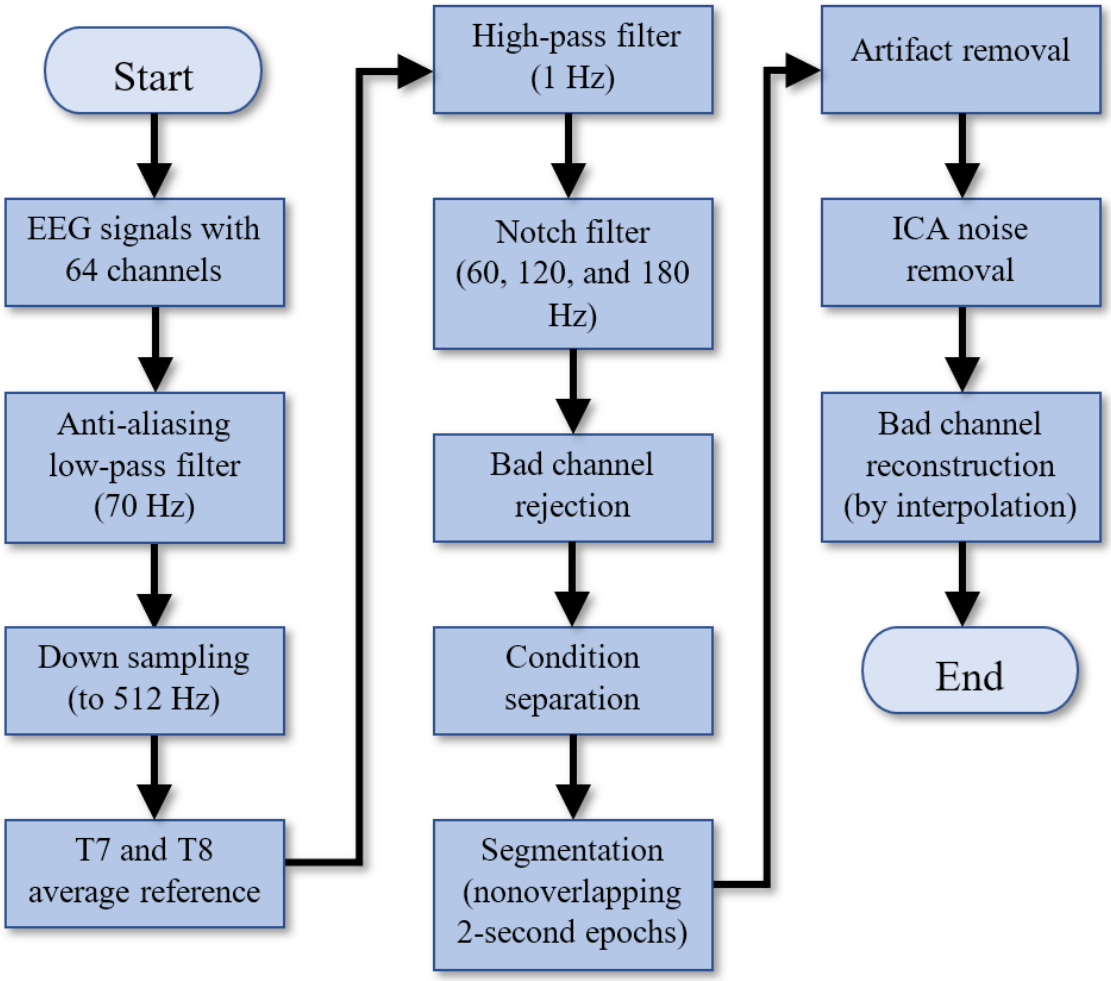

Figure 5.3. Electroencephalograph data preprocessing chart. EEG: electroencephalograph; ICA: independent component analysis.

Any remaining artifacts caused by eye blinks, eye movements, and external noise were eliminated from the data using ICA. These manual artifact removal and ICA processes were repeated 3 times during the cleaning process to ensure that all movement-based artifacts had been captured. Finally, bad channels were repaired (Bigdely-Shamlo et al., 2015) using the established practice of spline interpolation of the neighborhood channels on the bad channels (Perrin et al., 1989).

Power Spectral Density Analysis

The power spectral density (PSD) (Johnson et al., 1969) was computed for the conditions using a fast Fourier transform method (Cooley & Tukey, 1965). Hanning taper smoothing was applied to reduce spectral leakage owing to the discontinuity of the signal at the start and end points of the epochs. To improve the signal-to-noise ratio, the average PSD of the epochs was used. The PSD was further normalized by dividing the average power across all the frequency bins in each channel. The frequency range in the analysis was set to 2-50 Hz, which effectively covers the waveforms commonly used in EEG analysis. The PSD results of the premeditation experiences, during meditation experiences, and postmeditation experiences were then plotted and shown as pre, med, and post conditions, respectively. For med, the average PSD of the meditation conditions was computed using the average of the 3 meditation conditions (Med1, Med2, and Med3). For a graphical overview, a band power box and whisker plot were created. The plot revealed the signal power over the typical EEG frequency bands: 2-4 Hz (δ), 4-8 Hz (θ), 8-12 Hz (α), 12-30 Hz (β), and 30-50 Hz (γ) (Nayak & Anilkumar, 2020). The lower boundary of 2 Hz was set to avoid any distortion introduced by the high-pass filter at 1 Hz. The upper boundary of 50 Hz was selected to avoid the heavy power-level drop due to the use of a 60 Hz notch filter. In addition, 50 Hz was considered a reasonable cut-off between the high and low γ ranges.

Topographic and Coherence Analysis

To explore the spatial properties of the signals on each EEG channel, a topographic mapping of the PSD was plotted according to the traditional frequency ranges. The PSD was plotted using a heat map visualization technique to display the magnitude of the PSD with a 2D color representation. An interpolation based on the MATLAB 4 grid data method was used to smooth the topography, where a surface was fitted to the scattered data points using a biharmonic spline interpolation (Sandwell, 2012). This PSD plot was used to graphically illustrate the spatial properties associated with the pre, med, and post experiences.

A coherence analysis (Classen, 1998) was performed to visualize the functional connectivity between the electrodes as an indication of the brain areas that may be functionally integrated. Coherence of the pre, med, and post conditions were plotted for the frequency bands. A value between 0 and 1 was displayed for each channel pair. A

value of 1 indicates full synchronization between the channel pair, and a value of 0 reveals that the channel pair does not work in the synchronized condition. The significance of the coherence difference between the conditions was computed using the two-tailed Student t test and then plotted.

Pain

Pain experience was measured using the NRS. Pain scores were collected from the patients as an initial baseline at the start, and after each condition, to explore any correlation between pain levels and any PSD changes identified during the meditative experience.

Statistical Analysis

For the PSD and coherence analysis, the null hypothesis set for inferential statistical analysis was that the probability distribution of the condition-specific averages for PSD and coherence would be identical for all conditions.

As a cluster-based permutation test (Maris & Oostenveld, 2007) can be used to effectively resolve multiple comparisons in EEG signal statistical analysis, this test was used in this study to examine the overall PSD differences between the pre-med, med-post, and pre-post conditions by identifying the clusters of electrodes with significant changes. The tests were conducted using the Monte Carlo method, with 128 permutations, two tails, and α=.025 (negative and positive tails together equal .05). In addition, for comparison of all 3 conditions together, a multivariate analysis of variance (MANOVA) was used, with 2048 permutations, one tail, and α level set to .05.

The effect size was calculated after the cluster-based permutation test. First, a bounded rectangular area spanning each cluster was identified. This rectangular area was bounded by the frequency window of the cluster and all the channels in that cluster. The PSD in this area was then averaged. The maximum Cohen d effect size was then computed using FieldTrip for each of the conditions. The effect size was not computed for the MANOVA because it requires the specification of 2 mean groups for comparison. Generally, a Cohen d effect size around 0.2 is considered small and around 0.8 and higher is considered large to very large (Cohen, 1988; Sawilowsky, 2009). Finally, peak channel tests were performed to verify the PSD changes, and post hoc power analyses using

G*Power (Faul et al., 2007) were performed to indicate statistical power based on the effect sizes observed in the sample.

For the coherence analysis, the Student t test was used to examine significant coherence differences between the conditions. Parameters were set to two-tailed, paired samples, and α=.05, with a 10% false discovery rate (FDR) adjustment set (Benjamini & Hochberg, 2018).

To explore the associations between pain scores and PSD, repeated measures correlation (Bakdash & Marusich, 2017) was conducted. Some peak PSD channels identified with a high significance of PSD change from the cluster topoplot were input for each condition as the repeated independent variable, and the NRS pain score was input as the dependent variable.

5.3. Results

5.3.1. Overview

A total of 10 participants were recruited (Table 5.1). As we went through the data cleaning process, the data from 1 participant (S05) were found to be excessively noisy, and on video review, 2 other participants (S08 and S09) were found not to be following the procedures. Hence, their results were excluded, and a sample size of 7 was used in the final analysis.

Table 5.1. Participant demographics.

Subject	Age (years)	Sex	Cancer history
S01	59	Female	Abdominal tumors
S02	66	Male	Non-Hodgkin lymphoma
S03	37	Male	Non-Hodgkin lymphoma
S04	58	Female	Breast cancer
S06	47	Female	Chondrosarcoma
S07	50	Female	Colon cancer
S10	64	Male	Prostate cancer

5.3.2. PSD Analysis

Figure 5.4 illustrates the average of the power spectrum of the 3 conditions to provide a general overview of the power spectrum in the data, whereas Figure 5.5 shows the box and whisker plot of band power of the pre, med, and post conditions in the 5 traditional frequency ranges. From these figures, the differences in power in the frequency bands between the conditions were identified. The post condition power level had the lowest median and mean values in the δ range. The med condition changed from the lowest median and mean values in θ and α to the highest median and mean values in β and γ.

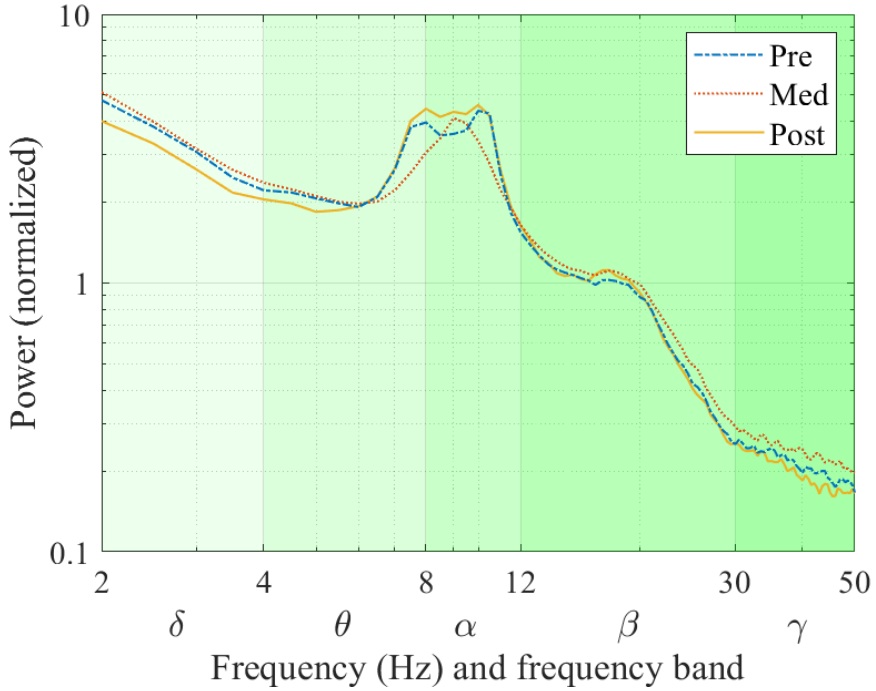

Figure 5.4. Grand average power spectrum.

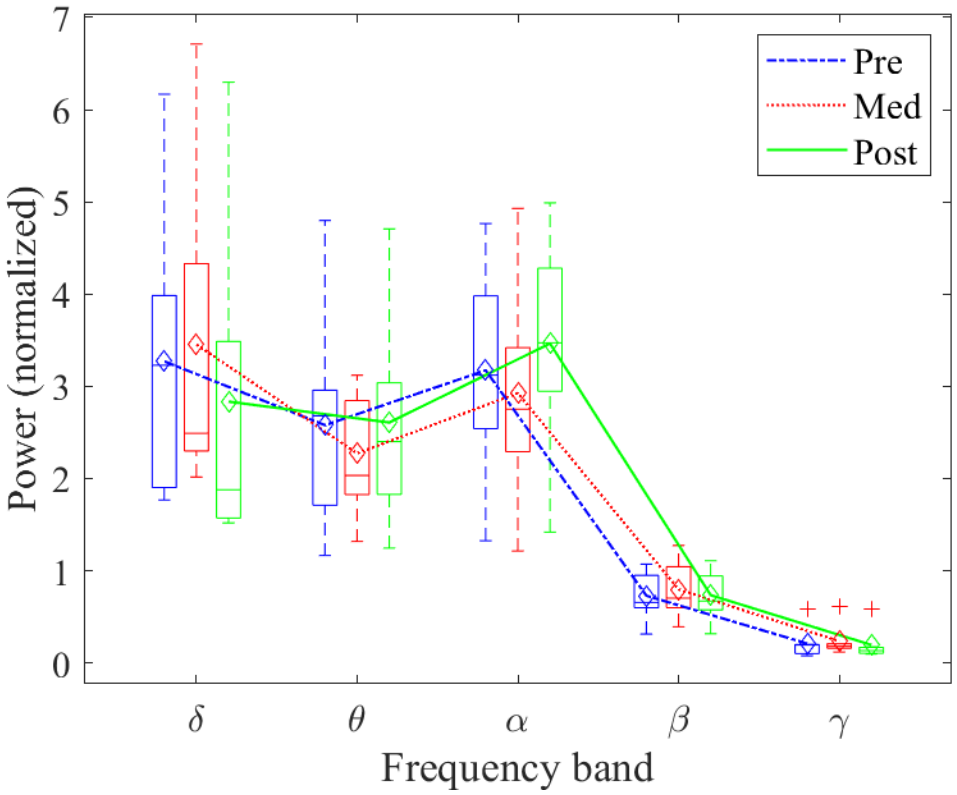

Figure 5.5. Power level changes between the pre, med, and post conditions in different frequency ranges. Boxplot shows the median and range of power level of the participants. Line plot shows the changes in mean power.

The topographic distribution of the PSD is shown in Figure 5.6. Differences in pre, med, and post conditions are shown spatially in all bands and in different brain regions. Changes in the power levels during meditation were observed in all frequency bands. In δ, an increase in power level in the central occipital region was observed, and a drop of power in the frontal-central region was observed in the post condition. In θ, there was a drop in the power level in the frontal cortex. In α, a decrease in power level in the central parietal region was noted. In the β band, an increase in power level was found in the bilateral central and prefrontal regions during meditation. In γ, an increase in power level was noted in the left frontal (LF) and right frontal (RF) regions, and a slight increase in the central parietal region was observed.

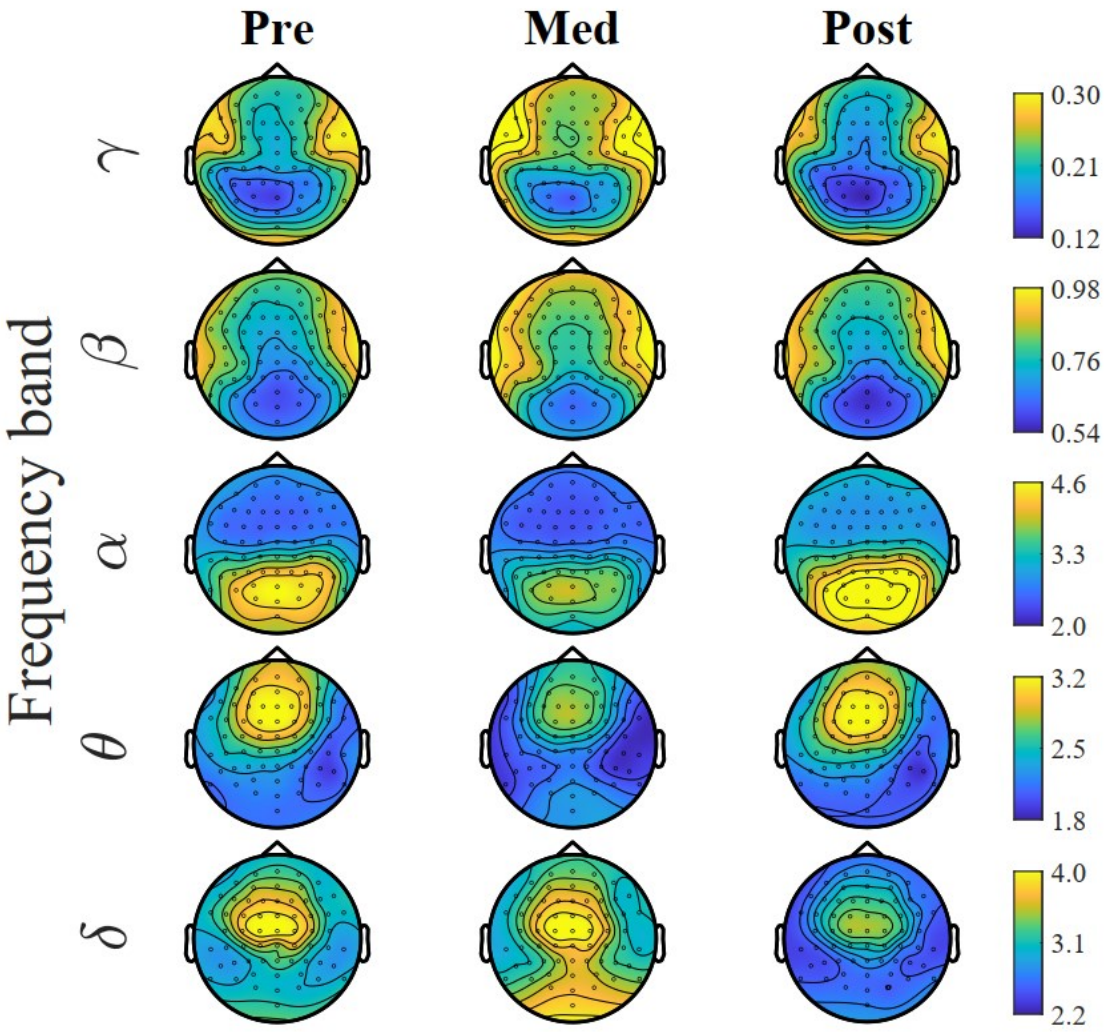

Figure 5.6. **Topography of power spectrum shown in different frequency ranges. Different color scales are used for the frequency ranges to reveal the details in the central areas.**

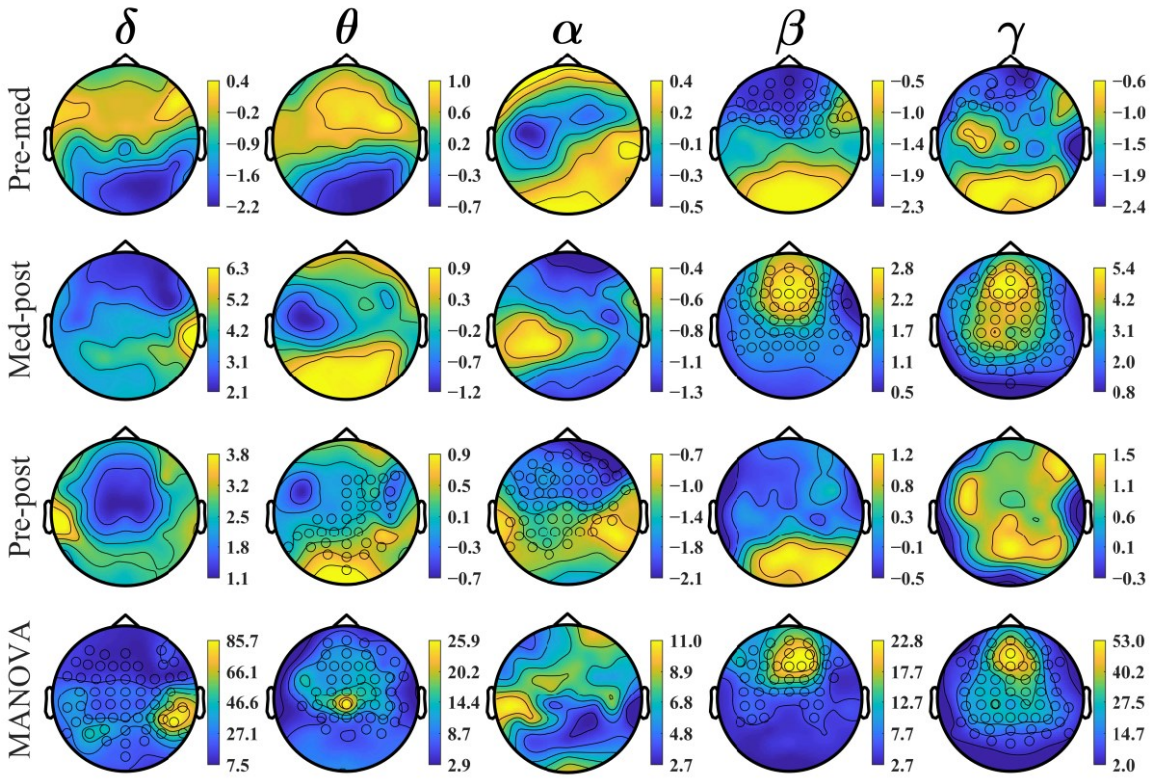

Figure 5.7. Power spectrum analysis using the cluster-based permutation test. Clusters of electrodes found with significant changes in power are marked with a circle marker at the electrodes. The color bars show the permutation test t-value level. MANOVA: multivariate analysis of variance.

Error! Reference source not found. shows the topoplot of the two-tailed cluster-based permutation test results. The conditions were compared in the test, including two-tailed pre versus med, med versus post, and pre versus post and a one-tailed MANOVA for all 3 conditions together. The clusters of electrodes with significant differences found in PSD changes were marked with a circle marker at the electrodes. The color bars indicate the t values computed from the test. For the pre versus med comparison, a cluster with a significance of P=.02 was found in the range of 24.5-31 Hz (high β and low γ) in the frontal cortex. For the med versus post comparison, significance was found in the β and γ ranges. A cluster with a significance of P=.001 was found in the range of 37-50 Hz (γ), and the cluster covered most brain regions; a cluster with a P value of .008 was found in the range of 23-36 Hz (high β and low γ) in the frontal and central cortices. For the pre versus post condition comparison, a cluster with P=.02 was obtained in the frontal, central, and parietal regions in the range of 8-9.5 Hz (high θ and low α). The MANOVA cluster-

based permutation test for all the pre, med, and post conditions returned 4 clusters with P≤.05, where the test was one-tailed. The first cluster found has P=.002 in the range of 37.5-50 Hz (γ) in the frontal, central, and parietal cortices. The second cluster with P=.03 was found in the range of 31-36 Hz (low γ) in the frontal and central cortices. The third cluster with P=.03 was found in the range of 2-5 Hz (δ and low θ) in the frontal, central, and parietal cortices. The last cluster with P=.04 was found in the range of 24-30 Hz (high β) in the frontal and central cortices. Table 5.2 shows the test results for all the clusters of significance. The very large effect size indicated that the permutation tests were effective in rejecting the null hypothesis.

Table 5.2. Cluster-based permutation test results. All clusters with P≤.025 are shown for the first 3 tests, and clusters with P≤.05 are shown for the multivariate analysis of variance test.

Comparison and cluster	P value	Effect size
Pre-med		
1	.02	1.252
Med-post		
1	.001	3.190
2	.008	1.318
Pre-post		
1	.02	1.504
MANOVA[a]		
1	.002	—[b]
2	.03	—
3	.03	—
4	.04	—

[a]MANOVA: multivariate analysis of variance.
[b]Not calculated as it required to specify which 2 conditions to compare.

By inspecting the topoplots (Figure 5.6 and **Error! Reference source not found.**), 5 peak channels with noticeable changes in the power levels between the conditions were selected for additional analysis and for better understanding the observed power level changes. The peak channels selected were AF7 and Fp2 in the prefrontal region, FC1 in the frontal region, CP5 in the left central (LC) region, and P5 in the left parietal (LP) region. Two-tailed, paired-sample t tests were performed to examine the overall PSD changes in different conditions. These tests were conducted on the pre and med, med and post, and pre and post conditions. The resulting P values were reported with an FDR adjusted to

10%. The t test results were plotted graphically for ease of interpretation. For each of the peak channels, a combined plot of the results of the 3 conditions was used.

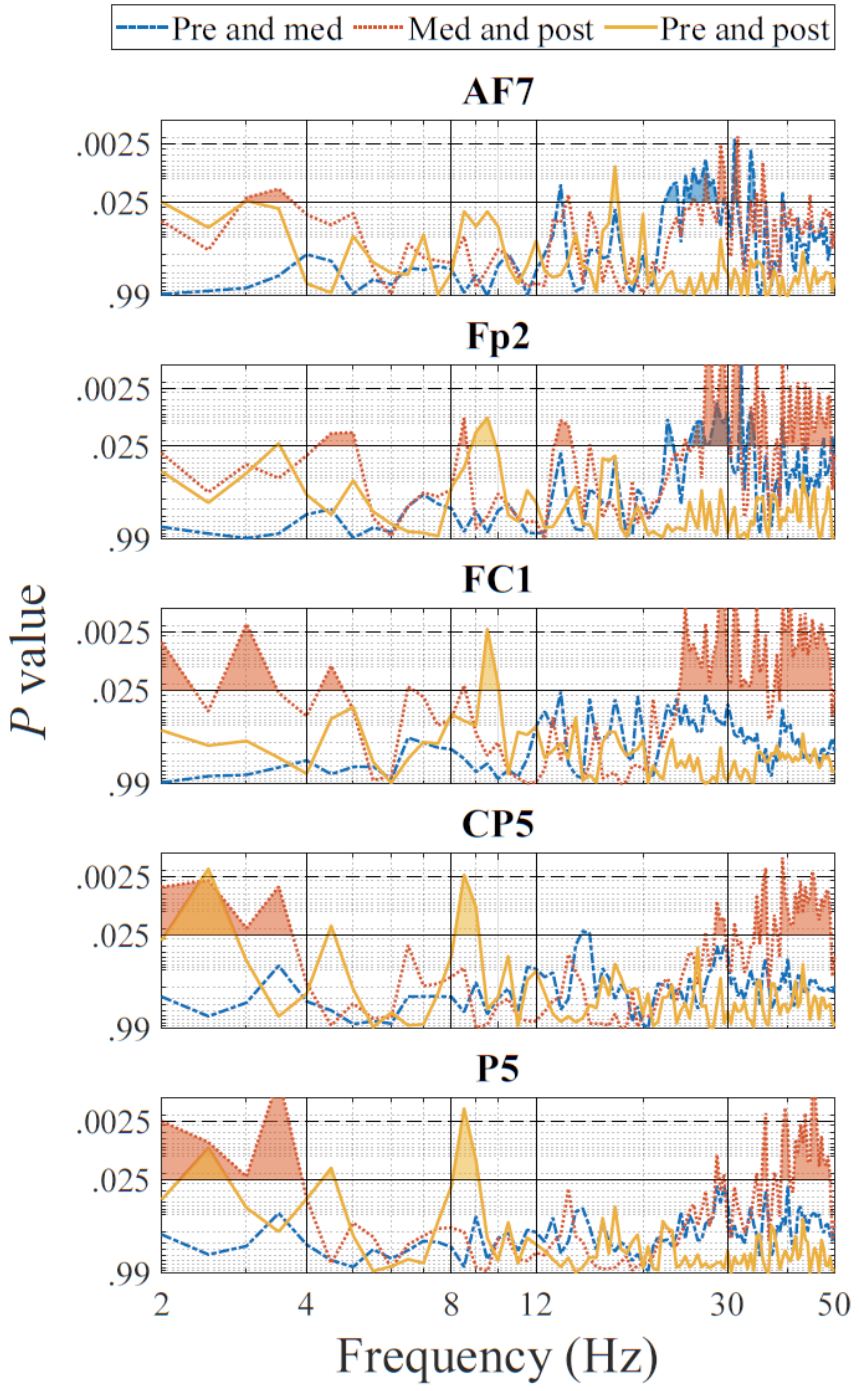

Figure 5.8. **Graphical depiction of P values of changes in power spectral density between conditions for the selected channels. Shading indicates significance found at the .025 level, and shading above the dashed line indicates the adjusted significance at the .0025 level (with the false discovery rate set to 10%).**

Figure 5.8 shows the P values obtained in a graphical form for the comparison of the 3 conditions. The upper shaded areas represent P≤.025. The shaded areas above the dashed line represent the adjusted significance with P≤.0025.

A statistical power analysis was also performed to verify the probability of detecting a true effect in the t tests. Table 5.3 shows the maximum effect size value and the respective frequency point found for each channel and for each comparison. Table 5.4 shows the statistical power based on the effect sizes listed in Table 5.3. It is shown that the t test results have a high power ≥0.7302 even when using the adjusted α value of .005.

Table 5.3. The maximum channel effect size and the frequency at which it was located.

Channel	Pre-med		Med-post		Pre-post	
	Max effect size	Frequency (Hz)	Max effect size	Frequency (Hz)	Max effect size	Frequency (Hz)
AF7	**1.9542**[a]	**31**	**1.9946**	**31.5**	1.5613	17.5
Fp2	**2.3861**	**32**	**3.7903**	**31.5**	1.4682	9.5
FC1	1.1037	13.5	**2.9888**	**29**	**1.9221**	**9.5**
CP5	1.1651	15	**2.1765**	**39**	**1.9937**	**2.5**
P5	1.0514	40	**2.6077**	**3.5**	**2.0736**	**8.5**

[a]Bolded values indicate where P≤.0025 was found for that frequency value.

Table 5.4. Power analysis for the effect size found.

Channel	Pre-med, α=.005	Med-post, α=.005	Pre-post, α=.005
AF7	**0.7472**[a]	**0.7676**	0.5073
Fp2	**0.9125**	**0.9998**	0.4450
FC1	0.2225	**0.9890**	**0.7302**
CP5	0.2556	**0.8470**	**0.7672**
P5	0.1962	**0.9558**	**0.8047**

[a]Bolded values indicate where P≤.0025 was achieved.

5.3.3. Topographic and Coherence Analysis

Figure 5.9 demonstrates the coherence detected in the α band during meditation. The functional connectivity level is represented by a red to blue color scale. The red color with a value close to 1 indicates that a channel pair is highly synchronized in the signal transfer. The blue color with a value close to 0 indicates that the channel pair is working independently.

Figure 5.10 shows the significant difference in coherence for the comparison of the med and post conditions in the α band. Channel pairs with P≤.025 are highlighted in green. Those with P≤.0025 (FDR adjusted) are highlighted in yellow. For clarity, the EEG channels were divided into regions according to their respective locations in the brain, namely, LF, LC, LP, left occipital, central parietal and occipital, RF, right central, right parietal and right occipital. Table 5.5 summarizes the results of a series of plots, as shown in Figure 5.10, for all the bands and all 3 comparisons. The table shows the significant coherence changes with P≤.0025 between the brain regions, where 1 denotes the pre and med comparison, 2 denotes the med and post comparison, and 3 denotes the pre and post comparison. The frequency band of the region pair at which a significance was found is shown with the Greek letter of the band. The number inside parentheses indicates the number of significant channel pairs in the frequency band.

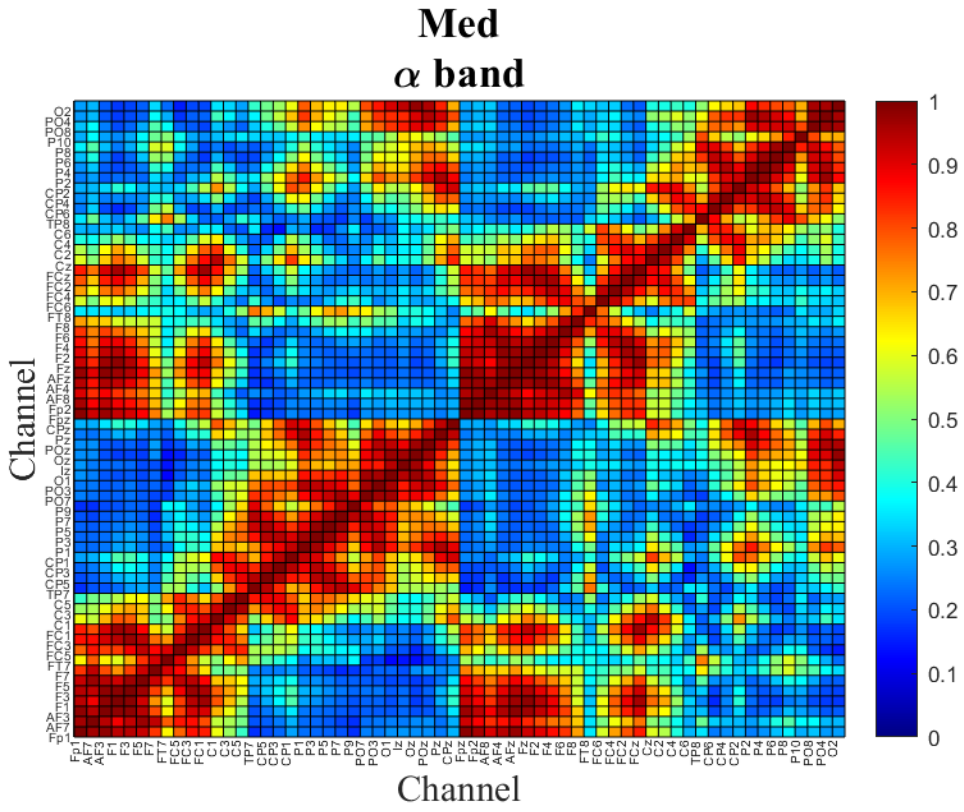

Figure 5.9. Coherence between the electroencephalograph channels during the virtual reality–guided meditation and in the α frequency range.

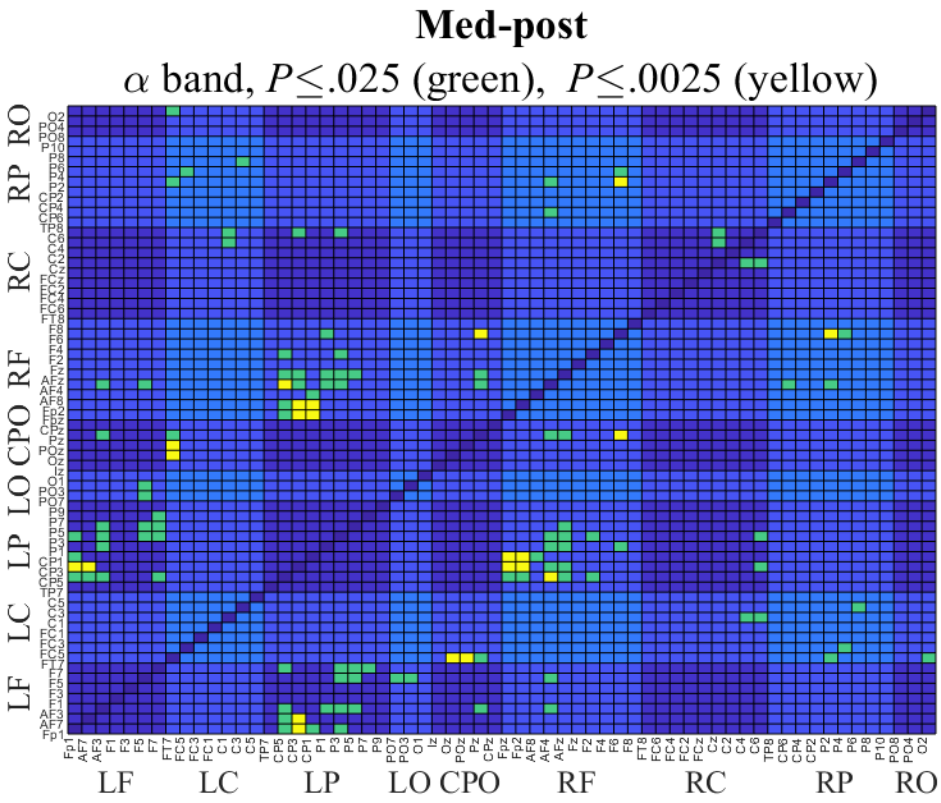

Figure 5.10. Channel pairs with significant coherence difference between the meditation and post meditation conditions in the α band. t test was used in the analysis, and channel pairs with a P≤.025 are highlighted in green, and channel pairs with a P≤.0025 (with the false discovery rate set to 10%) are highlighted in yellow. CPO: central parietal and occipital; LC: left central; LF: left frontal; LO: left occipital; LP: left parietal; RC: right central; RF: right frontal; RO: right occipital; RP: right parietal.

As shown in Table 5.5, significant changes were mostly found between the frontal and parietal regions, namely, RF-LP (11 channel pairs) and LF-LP (4 channel pairs). In addition, the most active regions were LP (related to 17 channel pairs), RF (15 channel pairs), LF (7 channel pairs), right parietal (7 channel pairs), and central parietal and occipital (7 channel pairs). For the 3 comparisons overall, significant changes were mostly found between the frontal and parietal and occipital regions, particularly in the θ, α, and β bands in the med-post comparison. For the pre-med comparison, the frontal-parietal region-pair coherence changes were observed in the γ band. For the pre-post comparison, the frontal-parietal and occipital region-pair coherence changes were observed in the δ, α, and β bands. Table 5.6 shows the effect sizes of the 2 regions of interest, namely, RF-

LP and LF-LP. Some large to very large effect sizes (≥0.8) were found in the δ, θ, α, and γ bands.

Table 5.5. False discovery rate–adjusted significant coherence changes found in the region pairs for the 3 comparisons: 1: pre versus med, 2: med versus post, and 3: pre versus post.

Region	LF[a]	LC[b]	LP[c]	LO[d]	CPO[e]	RF[f]	RC[g]	RP[h]	RO[i]
RO	3: δ[j]	3: θ	—[k]	—	—	—	—	—	✓[l]
RP	—	—	2: δ(2)[m]	2: δ	2: δ	2: α; 3: β	1: θ	✓	—
RC	—	—	—	—	—	1: β	3: α (✓)	—	—
RF	—	—	1: γ(2); 2: θ(2), α(5); 3: δ(2)	—	2: α	✓	—	—	—
CPO	3: δ α	1: α; 2: α(2)	—	—	✓	—	—	—	—
LO	—	—	—	✓	—	—	—	—	—
LP	2: θ, α(2), β	—	✓	—	—	—	—	—	—
LC	—	✓	—	—	—	—	—	—	—
LF	✓	—	—	—	—	—	—	—	—

[a]LF: left frontal.
[b]LC: left central.
[c]LP: left parietal.
[d]LO: left occipital.
[e]CPO: central parietal and occipital.
[f]RF: right frontal.
[g]RC: right central.
[h]RP: right parietal.
[i]RO: right occipital.
[j]Greek letter indicates the frequency band of the region pair with significant change.
[k]The empty cells in the upper left of the check mark diagonal show no significant channel pair was found. The cells in the lower right of the check mark diagonal are not used, as they are just mirrored duplicates of the cells in the upper left of the check mark diagonal.
[l]The checkmark indicates a region connects to the same region in the region pair.
[m]Number within parentheses indicates the number of channel pairs with significant changes in that frequency band. If there is only 1 channel pair, the number is not shown.

Table 5.6. Effect sizes of the 2 region pairs of interest: right frontal-left parietal and left frontal-left parietal.

Band	Region-pair RF-LP[a] average, effect size			Region-pair LF-LP[b] average, effect size		
	Pre-med	Med-post	Pre-post	Pre-med	Med-post	Pre-post
δ	0.2873	0.7545	**0.8511**[c]	0.1636	0.4461	0.2862
θ	0.5568	0.7738	0.1496	0.7464	**0.8234**	0.1610
α	0.5855	**1.3032**	**0.8593**	0.7742	**1.7736**	**1.0655**
β	0.4643	0.6142	0.2211	0.2759	0.5135	0.1294
γ	0.3482	**1.0220**	0.2218	0.3032	0.5880	0.1633

[a]RF-LP: right frontal-left parietal.
[b]LF-LP: left frontal-left parietal.
[c]Bolded values indicate large and very large effect sizes.

Table 5.7 shows the NRS pain scores collected immediately after the pre, Med1, Med2, Med3, and post conditions. A repeated measures correlation analysis was performed on some selected peak channels and clusters. In the test, no significant relationship between the collected pain scores and PSD was found.

Table 5.7. Numerical rating scale scores collected after each condition.

Participant	NRS[a] score				
	Pre	Med1	Med2	Med3	Post
S01	4	2	2	2	1
S02	4	3	0	0	1
S03	7	4	7	5	3
S04	6	5	4	4	3
S06	5	6	5	4	5
S07	3	5	4	2.5	4
S10	3	3	2	2	2

[a]NRS: numerical rating scale.

5.4. Discussion

5.4.1. Principal Findings

Overview

In answer to the primary research question, there were significant changes in EEG power and coherence among three conditions (pre, VR-guided meditation, and post). Therefore, the null hypothesis of no difference was rejected.

The visual inspection of the global normalized power spectrum analyses revealed various changes in all bandwidths. The predominant pattern was for increased δ, β, and γ bandwidth power in the meditation condition, compared with both the pre and post conditions. In the θ and α bandwidths, the changes in power were more varied within the 3 conditions.

Pre-Medication Versus VR-Guided Meditation

Visual inspection of the topographic distribution showed 2 main patterns comparing meditation with the prior resting condition. The first was an increase in power of δ (mainly in the central and occipital areas), β (mainly in the bilateral prefrontal areas), and γ (mainly in the frontal and bilateral prefrontal areas) during VR-guided meditation.

The second pattern that emerged from the visual topography map was decreased low-frequency range power of the θ (mainly in frontal areas) and α (mainly in occipital and parietal areas) bandwidths in the med condition compared with the pre condition. However, these visually observed changes were not significant in the permutation test.

Among the significant changes identified, the permutation test showed that a cluster of increased signals occurring across the high β and low γ range (24.5-31 Hz) in frontal areas was significantly different in the pre condition than in the med condition. In addition, comparison of single selective channels between conditions showed a significant difference in this bandwidth in the frontal areas recorded from AF7 and FP2.

β waves generally replace α waves when participants open their eyes, and in the motor cortex, β waves are associated with muscle motor activity (Johnson et al., 1969; Nayak & Anilkumar, 2020). They are normally most prominent in the frontal and central head regions and attenuate posteriorly. This may have been the case for the increase observed here. β activity is also commonly associated with drowsiness, stage nonrapid eye movement 1 sleep, and subsequently decreases in deeper sleep, and β activity is not affected by eye opening (Nayak & Anilkumar, 2020). Interestingly, sedative medications are also known to increase the amplitude and quantity of β activity (Louis & Frey, 2016). This finding suggests that an increase in the power of the β range might potentially be useful as a neurophysiological correlate of VR-guided meditation. Nevertheless, findings regarding changes in the β band with meditation have been inconsistent. Several studies have reported no significant changes associated with meditation in the β range (Lomas et

al., 2015; Lagopoulos et al., 2009). However, an increase in β and θ band power was reported in one study after a longer period of 6 weeks of meditation compared with baseline (Ahani et al., 2014). It is possible that the changes in β power in the meditation condition compared with the premeditation condition here may be more specific to the use of VR-guided meditation and the visual activity involved, but further work is required to explore this.

In contrast, the activity of the γ band has been reported to be associated with activation of the default mode network (Berkovich-Ohana et al., 2012). The default mode network is most frequently detected during the resting conditions and reflects the neural activity of different brain areas, such as the cingulate cortex, hippocampus, medial frontal lobes, inferior parietal lobes, and temporal lobes. It is thought to be involved in self-consciousness; self-processing; and introspective functions, including emotional awareness and processing (Imperatori et al., 2016; Garrison et al., 2015; Buckner et al., 2008; Greicius et al., 2003). An increase in γ band activity in the frontal and prefrontal areas during VR-guided meditation could reflect the activation of such introspective experiences through meditation. The increase in γ power may also have been due to the activation of attentional networks and visual processing of the meditative VR environment (Braboszcz et al., 2017).

It is also noteworthy that others have reported an increase in γ band power related to meditation (Cahn & Polich, 2006; Braboszcz et al., 2017; Berkovich-Ohana et al., 2012). For example, one study reported an increase in the γ band (25-45 Hz) during meditation compared with the resting state in the temporal and parieto-occipital areas in mindfulness meditation practitioners (Berkovich-Ohana et al., 2012). Another study reported that the proficiency level of the meditator is associated with the increased level of the γ band (60-110 Hz) in the parieto-occipital region in meditative states relative to the mind-wandering state in experienced meditators compared with healthy controls. Although it is noteworthy, in this study, no significant difference was found between the states of meditation and mind wandering (Braboszcz et al., 2017).

VR-Guided Meditation Versus Post-Meditation

In contrast to the pattern of increase in high β and low γ activity in the meditation condition compared with the prior rest condition, here, we observed a pattern of reduced β and γ power in the post condition compared with the meditation condition in the

topographic maps. This was followed by permutation test results in terms of 2 significant clusters of differences in the β cluster (23-36 Hz) and γ cluster (37-50 Hz) in the post versus med condition. These findings suggest a potential regression back to the baseline state activity and further suggest that changes in high β and low γ activity are associated with a VR meditative state. Analysis of single selective channels also supported widespread significant differences in the power of β and γ bandwidths in the frontal, central, and parietal channels (FP2, FC1, CP5, and P5).

As γ band oscillation has also been reported to be associated with attention toward pain and hypervigilance (Tiemann et al., 2012; Tiemann et al., 2010), the significant reduction in γ band activity following the VR meditation experience could potentially show that less attentional capacity is directed toward pain after using a meditative VR environment. However, this is conjectural and requires further verification.

Pre-Meditation Versus Post VR-Guided Meditation

The comparison of the pre and post conditions could provide an indication of a VR-guided meditation effect in our study. These changes were mainly observed in the α frequency range in terms of an increase in α power in the frontal and central areas in the post condition compared with the pre condition. This was accompanied by a significant cluster-based permutation analysis finding over a cluster of channels in the frontal and central areas (8-9.5 Hz) and significant differences in α power in channels such as Fp2, FC1, CP5, and P5. An increase in the θ band in the central areas and a decrease in the θ band in the posterior occipital areas were also observed in the power spectrum analysis; however, these changes were not found to be significant in single-channel analysis. The posterior dominant α rhythm is characteristically present in normal conscious EEG recordings in the occipital region. It is a defining feature of the normal background rhythm of the adult EEG, best observed with the eyes closed and during mental relaxation and is attenuated by eye opening and mental effort. θ waveforms are characteristically observed more in drowsiness and in the early stages of sleep, such as light sleep (the nonrapid eye movement 1 and nonrapid eye movement 2 sleep phases) (Nayak & Anilkumar, 2020). Increases in α-θ bandwidths have previously been reported to be associated with mindfulness meditation, and the α-θ border (7-8 Hz) has also been suggested as an optimal range for indicating visualization activity (Lomas et al., 2015; Belkofer et al., 2014; Faber et al., 2015).

A final observation worthy of note is that there was a reduction in the δ range power in the post condition compared with the pre condition, which was significantly different in the LC and parietal channels (CP5 and P5). Moreover, although changes in the δ range were not significant in the pairwise pre-post comparison, a cluster of channels was identified to be significant in MANOVA. δ is seen more in deep, dreamless sleep, and meditation activities where awareness is more detached (Lomas et al., 2015; Nayak & Anilkumar, 2020). Such a general pattern of reduction in δ power in the post condition compared with the pre condition could possibly be related to the effect of VR-guided meditation on brain activity and would need further work to explore if this is a significant trend.

Coherence

The significant coherence changes suggested that variations in brain connectivity occurred between the different test conditions. Coherence was found predominantly between the frontal and parietal and occipital cortices and in different wave bands, namely, in γ for the pre and med conditions; in θ, α, and β for the med and post conditions; and in δ, α, and β for the pre and post conditions. The γ coherence changes between the pre and med conditions were likely associated with activity during the VR-guided meditation. Between the med and post conditions, it shifted to slower frequencies, possibly suggesting a postmeditation effect. The pre-post comparison showed coherence in the δ, α, and β ranges. The reasons for this are unclear and could be related to the individual responses of the participants after the VR-guided meditation. The coherence values were computed without removing volume conduction effects, such as using the surface Laplacian method. However, significant coherence changes were mainly found between the frontal and parietal regions, the electrodes were far apart, and the coherence contributions due to volume conduction should be small (Srinivasan et al., 1998).

Pain and EEG Signals

In terms of the secondary focus of the study to explore pain changes correlated with EEG variations, we found no significant association between pain reduction and changes in electrophysiological signal. This could be due to the limited sample size of this exploratory study. More electrophysiological studies on a larger sample population could potentially identify EEG correlates associated with pain reduction after VR-guided meditation.

5.4.2. Limitations

As an exploratory study, the sample numbers were small and not necessarily representative of the wider population of patients with CP, which limited the power to identify differences. Therefore, there is a need for neurophysiological studies with larger samples to validate these results and to explore this phenomenon better. In addition, this was a single cohort study with no comparison group, although resting states before and after meditation were used as a no-mindfulness within-subjects control. Finally, the study focused on short-term neurophysiological alterations in the electrophysiology of the brain, and the long-term effects of meditative VR environments are still unknown, which will require longitudinal studies.

5.4.3. Conclusion

These findings suggest that distinct altered neurophysiological brain signals are detectable during VR-guided meditation, predominantly in terms of an increase in the power of the β and γ bands. Changes in the α and θ bands were also identified, predominantly as a pattern in VR-guided meditation compared with the resting baseline, possibly reflecting the specific impact of visual activity during VR-guided meditation. Some changes in coherence were also observed between the frontal and parietal and occipital cortices during VR-guided meditation. No significant association between NRS pain scores and changes in EEG signals was observed. Although this is an exploratory study, the results of this work clearly demonstrate the feasibility of EEG recording and subsequent data processing and analysis during VR experiences in patients using modern VR HMDs. To our knowledge, this is the first exploration of EEG alterations in the brain's electrophysiological signals associated with VR-guided meditation in patients with CP and should provide some valuable initial data to inform future work in this field.

Acknowledgements

The authors would like to acknowledge that the EEG system used in this study was purchased by Dr. Urs Ribary using the Canadian Foundation of Innovation funding. The authors would also like to thank Dr. Diane Gromala, Director of the Pain Studies Lab, School of Interactive Arts and Technology, Simon Fraser University, for supporting this

study, and all participants for their time and effort in taking part in the study. This work was supported by the Lotte and John Hecht Memorial Foundation (grant 4110).

Conflicts of Interest

None declared.

Chapter 6.

Discussion

6.1. Brain Oscillation Variations in Chronic Pain

The literature review in Chapter 2 shows that brain oscillations are closely related to the brain's information processing, and the analysis of oscillations is conceptually suitable for understanding the processes of chronic pain (CP). Despite the heterogeneous types of pain, data, and study results in the literature review, a summary showed that the trend of brain oscillatory activity changes in CP was primarily a slowed PAF. There were also works showing power changes in the theta and alpha bands. The theta power increase and the alpha power decrease could be related to thalamocortical dysrhythmia (TCD), which exhibits decreased inhibition of the thalamus and increased neurons' spikes in the theta band (Llinás et al., 1999). A slowed PAF in the oscillatory activity was also confirmed for the other reviewed pathophysiological conditions, such as dementia, lower cognition and memory performance, and aging in adults. This may imply that PAF could be a biomarker of CP and other pathophysiological conditions.

An important point derived from the literature review is that while performing CP analysis to investigate brain rhythm changes, it is necessary to minimize the effect of other pathophysiological conditions to avoid possible false positive results. This suggests a better understanding of the relationship between those conditions and CP, and a more thorough study design can be helpful.

The literature review also showed that CP analyses often required age-matched patients and controls to compare the differences in brain oscillatory activities. Chapter 4 aimed at this issue and explored an aging model that can be used to include age in CP studies.

In Chapter 3, CP brain oscillatory activity analyses were performed using CP MEG data from OMEGA and SFU. The study results showed CP patients had lower PAF, alpha power and alpha amplitude than matched controls, though significance was not found. Similar results were also found when mixed controls were used in the comparison.

For the SFU data, the patient was compared with a matched control and a group of mixed controls. A slowed PAF was found in the patient in both cases, and the Crawford-Howell single-case test showed significance in slowed PAF in the eyes closed condition of the patient but not the eyes open condition. The average age of the mixed controls was around 20 years younger than the patient; this was a limitation since the slowed PAF is age-related.

The topographies of the SFU data showed the alpha rhythm at the parieto-occipital generation site, where the CP patient had a lower PAF than the matched control. The topographies also revealed the mu wave in the centro-parietal cortex and the tau wave in the temporal lobe. Topography helps to reveal the location of CP sources, as pain is associated with a network of brain areas: primary and secondary somatosensory, anterior cingulate, insular, prefrontal and parietal cortices, and subcortical areas, including the thalamus (Apkarian et al., 2005).

The study using OMEGA data found no significance in the results, partly due to the small sample size limitation. However, using MEG data in a CP study was successfully demonstrated. The use of MEG in CP studies is still relatively rare compared to using EEG or fMRI. As shown in the literature review, pain is not only associated spatially with extended brain areas but also relates to a complex temporal-spectral pattern of brain rhythms: delta, theta, alpha, beta and gamma, as shown in the literature review summary (Table 2.1). MEG has advantages in high spatial and temporal resolutions, and it has the potential to reveal the brain oscillation variations due to CP, as MEG is more sensitive than EEG for tangential sources, which are the majority of cortical sources (Piastra et al., 2021).

6.2. Including Age in Chronic Pain Analysis

The literature review in Chapter 2 revealed that both aging and CP could cause slowed PAF. To avoid false significance in CP studies, age has to be included in the analyses. The study in Chapter 4 aimed at this problem. The study started with a MEG dataset of over 600 subjects. After data preprocessing, a pain-free, healthy control group was obtained with 474 subjects. The alpha rhythm in four brain ROIs: the frontal, central, temporal and parieto-occipital areas, were evaluated based on PAF, absolute and relative peak amplitude, and high and low alpha absolute and relative power. The use of the four

ROIs was verified by the K-sample Anderson-Darling test. Boxplots and support vector regression confirmed the alpha rhythm property variations in aging.

The K-sample Anderson-Darling test results showed that the four brain ROIs had a significant difference of $P<0.001$ in alpha rhythm properties in all ROI comparisons. The PAF comparison test between the frontal and temporal ROIs showed no significance due to the similarity in PAF slowing trends in these ROIs in aging. This evidence showed that choosing the four ROIs in the study was practical in understanding the alpha rhythm variations in brain cortices related to human aging.

The boxplots provided an idea of the alpha rhythm variation trends for the mixed-sex, male and female groups. The results showed a slowed PAF in four ROIs. Other variation trends observed included the relative amplitude and relative power drop in adult aging, but they were less evident and smooth than the PAF trend. The results were further verified with SVR. The frontal, temporal and parieto-occipital PAF in the mixed age group decreased with age with a medium effect size in statistics.

SVR is easy to use and available from scikit-learn (Pedregosa et al., 2011). SVR can take both linear and non-linear kernels to fit different data properties. Also, SVR can take multiple inputs with weights. Unlike OLS linear regression, SVR has adjustable hyperparameters for fine-tuning the regression fittings and is more advanced and suitable for neuroimaging analyses. The case study showed that one could use SVR to achieve the PAF value corresponding to age, such that non-age-matched controls can be used in CP studies. Even matched controls can have inconsistent brain rhythm properties, so the SVR approach using the best-fitting curve can even out irregularities. It may achieve better analysis results than using age-matched controls. The CP case study result showed that the patients had a slower PAF than the SVR-predicted controls in the posterior alpha generation site, though not significant. This might be partly related to the limitation of the pain data since there was an average delay of around 100 days between the interview and MEG scanning, and the pain condition could have been changed.

To our knowledge, the study in Chapter 4 is the first to characterize the correlations between alpha rhythm properties and age in four alpha generation sites using source space MEG and SVR. A novel SVR-prediction approach was proposed for building an aging model for including age in CP studies.

6.3. Brain Oscillation and Synchrony Variations Under Chronic Pain Intervention

In Chapter 5, the study was designed to investigate brain oscillation and synchrony variations pre, during and post a VR-guided meditation. The VR experience was used as an alternative CP intervention. The study examined the waveband power changes in the three meditation conditions through a grand average power spectral density plot, the topography of the power spectrum, selected electrodes investigation, coherence evaluation, and the clustered-base permutation test to verify the results. The relationship between pain level changes and EEG variations in meditation therapy was examined and verified using repeated measures correlation.

The grand average power spectrum plot and the boxplot depicted the overall power changes in the wavebands in the three meditation conditions. Increased δ, β, and γ power in meditation and varying θ and α power within the three conditions were found. The topography showed the power changes in different brain cortices in the three conditions. The topographies depicted that during meditation, an increase in δ power mainly in the central and occipital areas, a decrease in θ power in the frontal area and a decrease in α in occipital and parietal areas. Also, β power increased in the bilateral prefrontal areas, and γ power increased in the frontal and bilateral prefrontal areas. The topographies described the increase and decrease of power in the wavebands and their respective brain areas.

The cluster-based permutation test showed significant signal changes between the three conditions. The pre versus med condition showed a cluster of increased signals occurring across the high β and low γ range (24.5-31 Hz) in the frontal area. The med versus post condition showed two clusters of differences in the high β and low γ cluster (23-36 Hz) and γ cluster (37-50 Hz) in the frontal, central and parietal areas. The pre versus post condition showed a significant α cluster (8-9.5 Hz) in the frontal, central and parietal areas. The selected electrodes depicted results supporting these findings. AF7 and Fp2 showed significance in the frontal area in the high β and low γ range, FP2, FC1, CP5, and P5 showed significance in the frontal, central and parietal areas in the high β and low γ, also Fp2, FC1, CP5, and P5 in the frontal, central and parietal areas in α.

Previous findings in mindfulness meditation studies were increased power and coherence in α, θ, and γ band frequencies (Lomas et al., 2015; Lee et al., 2018; Cahn & Polich, 2006; Delmonte, 1984). The increase in β in this study could be related to muscle motor activity in the motor cortex, drowsiness, stage nonrapid eye movement 1 sleep, and decreases in deeper sleep. The increase in γ power could be associated with the default mode network (DMN) (Berkovich-Ohana et al., 2012), also the activation of attentional networks and visual processing of the meditative VR environment (Braboszcz et al., 2017). The reduction of γ band activity following the VR meditation experience could potentially show that less attentional capacity is directed toward pain after using a meditative VR environment

Significant coherence changes were found predominantly between the frontal and parietal and occipital cortices and in different wavebands, namely, in γ for the pre and med conditions; in θ, α, and β for the med and post-conditions; and in δ, α, and β for the pre and post conditions. The enhanced changes in the frontal and parietal connectivity during meditation could be related to the function of the frontoparietal network (FPN) and DMN. The VR-guided meditation implicated control and attentional processes in FPN, and the goal-directed cognition process of DMN (Uddin et al., 2019).

For the correlations between pain level changes and EEG variations during meditation. No significant relationships between pain scores and EEG power variations were observed. This might be partly due to the limited sample size. The results of this work demonstrate the feasibility of EEG recording in a VR-guided meditation test. The data processing and results proved that signal variations between the pre, during and post-meditation were significantly identified. This study provides novel EEG recording and analysis methods that can be used to investigate neurophysiological changes in VR pain applications

6.4. Conclusion

EEG and MEG can effectively identify brain oscillation variations in neurophysiological conditions. Recent studies have found that using EEG/MEG, brain oscillatory signal variations depicted correlations with CP and aging. In particular, slowed PAF, increased theta and decreased alpha power with CP, and slowed PAF with aging. This thesis verified the shared slowed PAF property in CP and aging, and the SVR

approach was used to correlate age and PAF in the frontal, central, temporal and parieto-occipital ROIs. For CP analysis, SVR can be applied to predict PAF from a group of healthy controls using patients' age. This approach can create an aging model to extend general future large database pathophysiological studies.

VR-guided meditation is a promising alternative approach for CP intervention. EEG was used in this thesis to explore the neurophysiological changes in brain activity during meditation. Specific VR-related EEG variations were identified in PSD and coherence in different wavebands and brain areas pre, during and post meditation. This signifies the potential use of EEG to monitor the effect of VR-guided mediation studies.

6.5. Future Directions

The novel method of using SVR to include age in CP studies may guide further studies to explore (1) including age in other pathophysiological studies, such as dementia, and (2) using other machine learning approaches, like convolutional neural networks (CNNs), to achieve the best accuracy.

The novel EEG recording and analysis methods for VR-guided meditation may guide further studies to explore and identify brain regions and wave bands with respect to VR therapies for CP.

The VR exploratory study found no significant relationships between pain scores and EEG signals. This could be related to the limited sample size used. Future studies on a larger sample could identify the relationships between pain reduction and the effect of VR-guided meditation.

References

Abhang, P. A., Gawali, B. W., Mehrotra, S. C., Abhang, P. A., Gawali, B., & Mehrotra, S. C. (2016). *Introduction to EEG- and Speech-Based Emotion Recognition*. Elsevier Science & Technology. http://ebookcentral.proquest.com/lib/sfu-ebooks/detail.action?docID=4458824

Ahani, A., Wahbeh, H., Nezamfar, H., Miller, M., Erdogmus, D., & Oken, B. (2014). Quantitative change of EEG and respiration signals during mindfulness meditation. *Journal of* NeuroEngineering *and Rehabilitation*, *11*(1), 87. https://doi.org/10.1186/1743-0003-11-87

Angelakis, E., Lubar, J. F., & Stathopoulou, S. (2004). Electroencephalographic peak alpha frequency correlates of cognitive traits. *Neuroscience Letters*, *371*(1), 60–63. https://doi.org/10.1016/j.neulet.2004.08.041

Apkarian, A. V., Bushnell, M. C., Treede, R.-D., & Zubieta, J.-K. (2005). Human brain mechanisms of pain perception and regulation in health and disease. *European Journal of Pain*, *9*(4), 463–463. https://doi.org/10.1016/j.ejpain.2004.11.001

Artificial neural network. (2023). In Wikipedia. https://en.wikipedia.org/w/index.php?title=Artificial_neural_network&oldid=1190122098

Aurlien, H., Gjerde, I. O., Aarseth, J. H., Eldøen, G., Karlsen, B., Skeidsvoll, H., & Gilhus, N. E. (2004). EEG background activity described by a large computerized database. *Clinical Neurophysiology*, *115*(3), 665–673. https://doi.org/10.1016/j.clinph.2003.10.019

Bakdash, J. Z., & Marusich, L. R. (2017). Repeated Measures Correlation. *Frontiers in Psychology*, *8*. https://www.frontiersin.org/articles/10.3389/fpsyg.2017.00456

Baller, E. B., & Ross, D. A. (2017). Your System Has Been Hijacked: The Neurobiology of Chronic Pain. *Biological Psychiatry*, *82*(8), e61–e63. https://doi.org/10.1016/j.biopsych.2017.08.009

Barry, R. J., Clarke, A. R., Johnstone, S. J., Magee, C. A., & Rushby, J. A. (2007). EEG differences between eyes-closed and eyes-open resting conditions. *Clinical Neurophysiology: Official Journal of the International Federation of Clinical Neurophysiology*, *118*(12), 2765–2773. https://doi.org/10.1016/j.clinph.2007.07.028

Bastos, A. M., & Schoffelen, J.-M. (2016). A Tutorial Review of Functional Connectivity Analysis Methods and Their Interpretational Pitfalls. *Frontiers in Systems Neuroscience*, *9*. https://www.frontiersin.org/articles/10.3389/fnsys.2015.00175

Bazanova, O. M. (2011). Individual alpha peak frequency variability and reproducibility in various experimental conditions. *Zhurnal Vysshei Nervnoi Deiatelnosti Imeni I P Pavlova*, *61*(1), 102–111.

Bazanova, O. M. (2012). Alpha EEG Activity Depends on the Individual Dominant Rhythm Frequency, *Journal of Neurotherapy: Investigations in Neuromodulation, Neurofeedback and Applied Neuroscience*, *16:4,* 270-284, DOI: 10.1080/10874208.2012.730786

Bazanova, O. M., & Aftanas, L. I. (2006). Relationships between learnability and individual indices of EEG alpha activity. *Ann. Gen. Psychiatry*, *5*, 74–75. Scopus.

Bazanova, O. M., & Vernon, D. (2014). Interpreting EEG alpha activity. *Neuroscience & Biobehavioral Reviews*, *44*, 94–110. https://doi.org/10.1016/j.neubiorev.2013.05.007

Belkofer, C. M., Van Hecke, A. V., & Konopka, L. M. (2014). Effects of Drawing on Alpha Activity: A Quantitative EEG Study With Implications for Art Therapy. *Art Therapy*, *31*(2), 61–68. https://doi.org/10.1080/07421656.2014.903821

Bell, A. J., & Sejnowski, T. J. (1995). An information-maximization approach to blind separation and blind deconvolution. *Neural Computation*, *7*(6), 1129–1159. https://doi.org/10.1162/neco.1995.7.6.1129

Benjamini, Y., & Hochberg, Y. (1995). Controlling the False Discovery Rate: A Practical and Powerful Approach to Multiple Testing. *Journal of the Royal Statistical Society: Series B (Methodological)*, *57*(1), 289–300. https://doi.org/10.1111/j.2517-6161.1995.tb02031.x

Berger, H. (1929). Über das Elektrenkephalogramm des Menschen. *Archiv für Psychiatrie und Nervenkrankheiten*, *87*(1), 527–570. https://doi.org/10.1007/BF01797193

Berkovich-Ohana, A., Glicksohn, J., & Goldstein, A. (2012). Mindfulness-induced changes in gamma band activity – Implications for the default mode network, self-reference and attention. *Clinical Neurophysiology*, *123*(4), 700–710. https://doi.org/10.1016/j.clinph.2011.07.048

Besl, P. J., & McKay, N. D. (1992). A method for registration of 3-D shapes. *IEEE Transactions on Pattern Analysis and Machine Intelligence*, *14*(2), 239–256. https://doi.org/10.1109/34.121791

Bigdely-Shamlo, N., Mullen, T., Kothe, C., Su, K.-M., & Robbins, K. A. (2015). The PREP pipeline: Standardized preprocessing for large-scale EEG analysis. *Frontiers in Neuroinformatics*, *9*. https://www.frontiersin.org/articles/10.3389/fninf.2015.00016

Boonstra, T. W., Nikolin, S., Meisener, A.-C., Martin, D. M., & Loo, C. K. (2016). Change in Mean Frequency of Resting-State Electroencephalography after Transcranial Direct Current Stimulation. *Frontiers in Human Neuroscience*, *10*. https://www.frontiersin.org/articles/10.3389/fnhum.2016.00270

Boord, P., Siddall, P. J., Tran, Y., Herbert, D., Middleton, J., & Craig, A. (2008). Electroencephalographic slowing and reduced reactivity in neuropathic pain following spinal cord injury. *Spinal Cord*, *46(2)*, Article 2. https://doi.org/10.1038/sj.sc.3102077

Borsook, D. (2012). A Future Without Chronic Pain: Neuroscience and Clinical Research. *Cerebrum: The Dana Forum on Brain Science*, *2012*, 7.

Botella, C., Garcia-Palacios, A., Vizcaíno, Y., Herrero, R., Baños, R. M., & Belmonte, M. A. (2013). Virtual Reality in the Treatment of Fibromyalgia: A Pilot Study. *Cyberpsychology, Behavior, and Social Networking*, *16*(3), 215–223. https://doi.org/10.1089/cyber.2012.1572

Braboszcz, C., Cahn, B. R., Levy, J., Fernandez, M., & Delorme, A. (2017). Increased Gamma Brainwave Amplitude Compared to Control in Three Different Meditation Traditions. *PLOS ONE*, *12*(1), e0170647. https://doi.org/10.1371/journal.pone.0170647

Breiman, L. (2001). Random Forests. Machine Learning, 45(1), 5–32. https://doi.org/10.1023/A:1010933404324

Broyd, S. J., Demanuele, C., Debener, S., Helps, S. K., James, C. J., & Sonuga-Barke, E. J. S. (2009). Default-mode brain dysfunction in mental disorders: A systematic review. *Neuroscience & Biobehavioral Reviews*, *33*(3), 279–296. https://doi.org/10.1016/j.neubiorev.2008.09.002

Buchanan, D. M., Ros, T., & Nahas, R. (2021). Elevated and Slowed EEG Oscillations in Patients with Post-Concussive Syndrome and Chronic Pain Following a Motor Vehicle Collision. *Brain Sciences*, *11(5)*, 537. https://doi.org/10.3390/brainsci11050537

Buckner, R. L., Andrews-Hanna, J. R., & Schacter, D. L. (2008). The Brain's Default Network. *Annals of the New York Academy of Sciences*, *1124*(1), 1–38. https://doi.org/10.1196/annals.1440.011

Bushnell, M. C., Čeko, M., & Low, L. A. (2013). Cognitive and emotional control of pain and its disruption in chronic pain. Nature Reviews Neuroscience, 14(7), Article 7. https://doi.org/10.1038/nrn3516

Buzsáki, G., & Draguhn, A. (2004). Neuronal Oscillations in Cortical Networks. *Science*, *304*(5679), 1926–1929. https://doi.org/10.1126/science.1099745

Cabin, R., & Mitchell, R. (2000). To Bonferroni or Not to Bonferroni: When and How Are the Questions. *Bulletin of the Ecological Society of America*, *81*, 246–248. https://doi.org/10.2307/20168454

Cahn, B. R., & Polich, J. (2006). Meditation states and traits: EEG, ERP, and neuroimaging studies. *Psychological Bulletin*, *132*, 180–211. https://doi.org/10.1037/0033-2909.132.2.180

Canada, H. (2020, November 6). *Canadian Pain Task Force Report: September 2020.* https://www.canada.ca/en/health-canada/corporate/about-health-canada/public-engagement/external-advisory-bodies/canadian-pain-task-force/report-2020.html

Canada, P. H. A. of. (2021, May 5). *Chronic pain*. https://www.canada.ca/en/public-health/services/diseases/chronic-pain.html

Cellier, D., Riddle, J., Petersen, I., & Hwang, K. (2021). The development of theta and alpha neural oscillations from ages 3 to 24 years. *Developmental Cognitive Neuroscience*, *50*, 100969. https://doi.org/10.1016/j.dcn.2021.100969

Chang, C.-C., & Lin, C.-J. (2011). LIBSVM: A library for support vector machines. *ACM Transactions on Intelligent Systems and Technology*, *2*(3), 27:1-27:27. https://doi.org/10.1145/1961189.1961199

Chatrian, G. E., Petersen, M. C., & Lazarte, J. A. (1959). The blocking of the rolandic wicket rhythm and some central changes related to movement. *Electroencephalography and Clinical Neurophysiology*, *11*(3), 497–510. https://doi.org/10.1016/0013-4694(59)90048-3

Chiang, A. K. I., Rennie, C. J., Robinson, P. A., Roberts, J. A., Rigozzi, M. K., Whitehouse, R. W., Hamilton, R. J., & Gordon, E. (2008). Automated characterization of multiple alpha peaks in multi-site electroencephalograms. *Journal of Neuroscience Methods*, *168*(2), 396–411. https://doi.org/10.1016/j.jneumeth.2007.11.001

Chiang, A. K. I., Rennie, C. J., Robinson, P. A., van Albada, S. J., & Kerr, C. C. (2011). Age trends and sex differences of alpha rhythms including split alpha peaks. *Clinical Neurophysiology*, *122*(8), 1505–1517. https://doi.org/10.1016/j.clinph.2011.01.040

Chiesa, A., & Serretti, A. (2010). A systematic review of neurobiological and clinical features of mindfulness meditations. *Psychological Medicine*, *40*(8), 1239–1252. https://doi.org/10.1017/S0033291709991747

Christiansen, S., & Cohen, S. P. (2018). Chronic Pain: Pathophysiology and Mechanisms. In L. Manchikanti, A. D. Kaye, F. J. E. Falco, & J. A. Hirsch (Eds.), *Essentials of Interventional Techniques in Managing Chronic Pain* (pp. 15–25). Springer International Publishing. https://doi.org/10.1007/978-3-319-60361-2_2

Chronic pain in Canada: laying a foundation for action. Government of Canada. (2019). URL: https://physiotherapy.ca/sites/default/files/canadian_pain_task_force_june_2019_report_en.pdf [accessed 2021-05-16]

Ciulla, C., Takeda, T., & Endo, H. (1999). MEG Characterization of Spontaneous Alpha Rhythm in the Human Brain. *Brain Topography*, *11*, 211–222. https://doi.org/10.1023/A:1022233828999

Clark, C. R., Veltmeyer, M. D., Hamilton, R. J., Simms, E., Paul, R., Hermens, D., & Gordon, E. (2004). Spontaneous alpha peak frequency predicts working memory performance across the age span. *International Journal of Psychophysiology*, *53*(1), 1–9. https://doi.org/10.1016/j.ijpsycho.2003.12.011

Classen, J., Gerloff, C., Honda, M., & Hallett, M. (1998). Integrative Visuomotor Behavior Is Associated With Interregionally Coherent Oscillations in the Human Brain. *Journal of Neurophysiology*, *79*(3), 1567–1573. https://doi.org/10.1152/jn.1998.79.3.1567

Cohen, J. (1988). Statistical power analysis for the behavioral sciences (2nd ed). L. Erlbaum Associates.

Cooley, J. W., & Tukey, J. W. (1965). An algorithm for the machine calculation of complex Fourier series. *Mathematics of Computation*, *19*(90), 297–301. https://doi.org/10.1090/S0025-5718-1965-0178586-1

Crawford, J. R., & Garthwaite, P. H. (2004). Statistical Methods for Single-Case Studies in Neuropsychology: Comparing the Slope of a Patient's Regression Line with those of a Control Sample. *Cortex*, *40*(3), 533–548. https://doi.org/10.1016/S0010-9452(08)70145-X

Crawford, J. R., & Howell, D. C. (1998). Comparing an Individual's Test Score Against Norms Derived from Small Samples. *The Clinical Neuropsychologist*, *12*(4), 482–486. https://doi.org/10.1076/clin.12.4.482.7241

Dahlhamer, J. (2018). Prevalence of Chronic Pain and High-Impact Chronic Pain Among Adults—United States, 2016. *MMWR. Morbidity and Mortality Weekly Report*, *67*. https://doi.org/10.15585/mmwr.mm6736a2

Dale, A. M., Fischl, B., & Sereno, M. I. (1999). Cortical Surface-Based Analysis: I. Segmentation and Surface Reconstruction. *NeuroImage*, *9*(2), 179–194. https://doi.org/10.1006/nimg.1998.0395

Dale, A. M., Liu, A. K., Fischl, B. R., Buckner, R. L., Belliveau, J. W., Lewine, J. D., & Halgren, E. (2000). Dynamic Statistical Parametric Mapping: Combining fMRI and MEG for High-Resolution Imaging of Cortical Activity. Neuron, 26(1), 55–67. https://doi.org/10.1016/S0896-6273(00)81138-1

Dascal, J., Reid, M., IsHak, W. W., Spiegel, B., Recacho, J., Rosen, B., & Danovitch, I. (2017). Virtual Reality and Medical Inpatients: A Systematic Review of Randomized, Controlled Trials. *Innovations in Clinical Neuroscience*, *14*(1–2), 14–21.

Davatzikos, C. (2019). Machine learning in neuroimaging: Progress and challenges. NeuroImage, 197, 652–656. https://doi.org/10.1016/j.neuroimage.2018.10.003

Davidson, R. J., & Lutz, A. (2008). Buddha's Brain: Neuroplasticity and Meditation [In the Spotlight]. *IEEE Signal Processing Magazine*, *25*(1), 176–174. https://doi.org/10.1109/MSP.2008.4431873

De Smith, M. J. (2021). *Statistical Analysis Handbook - 2nd* edition, The Winchelsea Press, Drumlin Publications, Drumlin Security Ltd, UK.

De Vries, M., Wilder-Smith, O. H. G., Jongsma, M. L. A., van den Broeke, E. N., Arns, M., van Goor, H., & van Rijn, C. M. (2013). Altered resting state EEG in chronic pancreatitis patients: Toward a marker for chronic pain. Journal of Pain Research, 6, 815–824. Scopus. https://doi.org/10.2147/JPR.S50919

Delmonte, M. M. (1984). Electrocortical Activity and Related Phenomena Associated with Meditation Practice: A Literature Review. *International Journal of Neuroscience*, *24*(3–4), 217–231. https://doi.org/10.3109/00207458409089810

Desikan, R. S., Ségonne, F., Fischl, B., Quinn, B. T., Dickerson, B. C., Blacker, D., Buckner, R. L., Dale, A. M., Maguire, R. P., Hyman, B. T., Albert, M. S., & Killiany, R. J. (2006). An automated labeling system for subdividing the human cerebral cortex on MRI scans into gyral based regions of interest. *NeuroImage*, *31*(3), 968–980. https://doi.org/10.1016/j.neuroimage.2006.01.021

Deuis, J. R., Dvorakova, L. S., & Vetter, I. (2017). Methods Used to Evaluate Pain Behaviors in Rodents. *Frontiers in Molecular Neuroscience*, *10*. https://www.frontiersin.org/article/10.3389/fnmol.2017.00284

Dickinson, A., DiStefano, C., Senturk, D., & Jeste, S. S. (2018). Peak alpha frequency is a neural marker of cognitive function across the autism spectrum. *The European Journal of Neuroscience*, *47*(6), 643–651. https://doi.org/10.1111/ejn.13645

Dosenbach, N. U. F., Nardos, B., Cohen, A. L., Fair, D. A., Power, J. D., Church, J. A., Nelson, S. M., Wig, G. S., Vogel, A. C., Lessov-Schlaggar, C. N., Barnes, K. A., Dubis, J. W., Feczko, E., Coalson, R. S., Pruett, J. R., Barch, D. M., Petersen, S. E., & Schlaggar, B. L. (2010). Prediction of Individual Brain Maturity Using fMRI. *Science*, *329*(5997), 1358–1361. https://doi.org/10.1126/science.1194144

Drucker, H., Burges, C. J. C., Kaufman, L., Smola, A., & Vapnik, V. (1996). Support Vector Regression Machines. *Advances in Neural Information Processing Systems*, *9*. https://proceedings.neurips.cc/paper_files/paper/1996/hash/d38901788c533e8286cb6400b40b386d-Abstract.html

Dunn, B. R., Hartigan, J. A., & Mikulas, W. L. (1999). Concentration and Mindfulness Meditations: Unique Forms of Consciousness? *Applied Psychophysiology and Biofeedback*, *24*(3), 147–165. https://doi.org/10.1023/A:1023498629385

Eccleston, C. (1995). Chronic pain and distraction: An experimental investigation into the role of sustained and shifting attention in the processing of chronic persistent pain. *Behaviour Research and Therapy*, *33*(4), 391–405. https://doi.org/10.1016/0005-7967(94)00057-Q

Engemann, D. A., Kozynets, O., Sabbagh, D., Lemaître, G., Varoquaux, G., Liem, F., & Gramfort, A. (2020). Combining magnetoencephalography with magnetic resonance imaging enhances learning of surrogate-biomarkers. *ELife*, *9*, e54055. https://doi.org/10.7554/eLife.54055

Erlacher, D., & Chapin, H. (2010). Lucid dreaming: Neural virtual reality as a mechanism for performance enhancement. 3(1).

Faber, P. L., Lehmann, D., Gianotti, L. R. R., Milz, P., Pascual-Marqui, R. D., Held, M., & Kochi, K. (2015). Zazen meditation and no-task resting EEG compared with LORETA intracortical source localization. *Cognitive* Processing, *16*(1), 87–96. https://doi.org/10.1007/s10339-014-0637-x

Farias, M., & Wikholm, C. (2016). Has the science of mindfulness lost its mind? *BJPsych Bulletin*, *40*(6), 329–332. https://doi.org/10.1192/pb.bp.116.053686

Faul, F., Erdfelder, E., Lang, A.-G., & Buchner, A. (2007). G*Power 3: A flexible statistical power analysis program for the social, behavioral, and biomedical sciences. *Behavior Research Methods*, *39*(2), 175–191. https://doi.org/10.3758/BF03193146

Fell, J., Axmacher, N., & Haupt, S. (2010). From alpha to gamma: Electrophysiological correlates of meditation-related states of consciousness. *Medical Hypotheses*, *75*(2), 218–224. https://doi.org/10.1016/j.mehy.2010.02.025

Feng, L., Li, H., Cui, H., Xie, X., Xu, S., & Hu, Y. (2021). Low Back Pain Assessment Based on Alpha Oscillation Changes in Spontaneous Electroencephalogram (EEG). Neural Plasticity, 2021, 8537437. https://doi.org/10.1155/2021/8537437

Fisch, L., Leenings, R., Winter, N. R., Dannlowski, U., Gaser, C., Cole, J. H., & Hahn, T. (2021). Editorial: Predicting Chronological Age From Structural Neuroimaging: The Predictive Analytics Competition 2019. *Frontiers in Psychiatry*, *12*, 710932. https://doi.org/10.3389/fpsyt.2021.710932

Fischl, B. (2012). FreeSurfer. *NeuroImage*, *62*(2), 774–781. https://doi.org/10.1016/j.neuroimage.2012.01.021

Franke, K., Luders, E., May, A., Wilke, M., & Gaser, C. (2012). Brain maturation: Predicting individual BrainAGE in children and adolescents using structural MRI. *NeuroImage*, *63*(3), 1305–1312. https://doi.org/10.1016/j.neuroimage.2012.08.001

Froeliger, B., Garland, E., Modlin, L., & McClernon, F. J. (2012). Neurocognitive correlates of the effects of yoga meditation practice on emotion and cognition: A pilot study. *Frontiers in Integrative Neuroscience*, *6*. https://www.frontiersin.org/articles/10.3389/fnint.2012.00048

Fu, H., Garrett, B., Tao, G., Cordingley, E., Ofoghi, Z., Taverner, T., Sun, C., & Cheung, T. (2021). Virtual Reality–Guided Meditation for Chronic Pain in Patients With Cancer: Exploratory Analysis of Electroencephalograph Activity. *JMIR Biomedical Engineering*, *6*(2), e26332. https://doi.org/10.2196/26332

Furman, A. J., Prokhorenko, M., Keaser, M. L., Zhang, J., Chen, S., Mazaheri, A., & Seminowicz, D. A. (2020). Sensorimotor Peak Alpha Frequency Is a Reliable Biomarker of Prolonged Pain Sensitivity. *Cerebral Cortex (New York, NY)*, *30*(12), 6069–6082. https://doi.org/10.1093/cercor/bhaa124

Garrett, B. M., Tao, G., Taverner, T., Cordingley, E., & Sun, C. (2020). Patients perceptions of virtual reality therapy in the management of chronic cancer pain. *Heliyon*, *6*(5). https://doi.org/10.1016/j.heliyon.2020.e03916

Garrett, B., Taverner, T., & McDade, P. (2017). Virtual Reality as an Adjunct Home Therapy in Chronic Pain Management: An Exploratory Study. *JMIR Medical Informatics*, *5*(2), e7271. https://doi.org/10.2196/medinform.7271

Garrett, B., Taverner, T., Gromala, D., Tao, G., Cordingley, E., & Sun, C. (2018). Virtual Reality Clinical Research: Promises and Challenges. *JMIR Serious Games*, *6*(4), e10839. https://doi.org/10.2196/10839

Garrett, B., Taverner, T., Masinde, W., Gromala, D., Shaw, C., & Negraeff, M. (2014). A Rapid Evidence Assessment of Immersive Virtual Reality as an Adjunct Therapy in Acute Pain Management in Clinical Practice. *The Clinical Journal of Pain*, *30*(12), 1089. https://doi.org/10.1097/AJP.0000000000000064

Garrison, K. A., Zeffiro, T. A., Scheinost, D., Constable, R. T., & Brewer, J. A. (2015). Meditation leads to reduced default mode network activity beyond an active task. *Cognitive, Affective, & Behavioral Neuroscience*, *15*(3), 712–720. https://doi.org/10.3758/s13415-015-0358-3

Goldin, P., Ziv, M., Jazaieri, H., Hahn, K., & Gross, J. J. (2013). MBSR vs aerobic exercise in social anxiety: FMRI of emotion regulation of negative self-beliefs. *Social Cognitive and Affective Neuroscience*, *8*(1), 65–72. https://doi.org/10.1093/scan/nss054

Gómez, C., Pérez-Macías, J. M., Poza, J., Fernández, A., & Hornero, R. (2013). Spectral changes in spontaneous MEG activity across the lifespan. *Journal of Neural Engineering*, *10*(6), 066006. https://doi.org/10.1088/1741-2560/10/6/066006

Gong, W., Beckmann, C. F., Vedaldi, A., Smith, S. M., & Peng, H. (2021). Optimising a Simple Fully Convolutional Network for Accurate Brain Age Prediction in the PAC 2019 Challenge. *Frontiers in Psychiatry*, *12*. https://www.frontiersin.org/articles/10.3389/fpsyt.2021.627996

Government of Canada, S. C. (2018, March 21). *Prevalence of chronic pain among individuals with neurological conditions*. https://www150.statcan.gc.ca/n1/pub/82-003-x/2018003/article/54921-eng.htm

Gramfort, A., Luessi, M., Larson, E., Engemann, D. A., Strohmeier, D., Brodbeck, C., Goj, R., Jas, M., Brooks, T., Parkkonen, L., & Hämäläinen, M. (2013). MEG and EEG data analysis with MNE-Python. *Frontiers in Neuroscience*, *7*. https://doi.org/10.3389/fnins.2013.00267

Gramfort, A., Luessi, M., Larson, E., Engemann, D., Strohmeier, D., Brodbeck, C., Parkkonen, L., & Hämäläinen, M. (2014). MNE software for processing MEG and EEG data. *NeuroImage*, *86*, 446–460. https://doi.org/10.1016/j.neuroimage.2013.10.027

Greenwald, J. D., & Shafritz, K. M. (2018). An Integrative Neuroscience Framework for the Treatment of Chronic Pain: From Cellular Alterations to Behavior. *Frontiers in Integrative Neuroscience*, *12*. https://www.frontiersin.org/articles/10.3389/fnint.2018.00018

Greicius, M. D., Krasnow, B., Reiss, A. L., & Menon, V. (2003). Functional connectivity in the resting brain: A network analysis of the default mode hypothesis. *Proceedings of the National Academy of Sciences*, *100*(1), 253–258. https://doi.org/10.1073/pnas.0135058100

Gromala, D., Tong, X., Choo, A., Karamnejad, M., & Shaw, C. D. (2015). The Virtual Meditative Walk: Virtual Reality Therapy for Chronic Pain Management. *Proceedings of the 33rd Annual ACM Conference on Human Factors in Computing Systems*, 521–524. https://doi.org/10.1145/2702123.2702344

Guerrero, M. C., Parada, J. S., & Espitia, H. E. (2021). EEG signal analysis using classification techniques: Logistic regression, artificial neural networks, support vector machines, and convolutional neural networks. *Heliyon*, *7*(6), e07258. https://doi.org/10.1016/j.heliyon.2021.e07258

Hamalainen, M. S., & Sarvas, J. (1989). Realistic conductivity geometry model of the human head for interpretation of neuromagnetic data. *IEEE Transactions on Biomedical Engineering*, *36*(2), 165–171. https://doi.org/10.1109/10.16463

Hanson, R., Mendius. R. (2009). Buddha's Brain: The Practical Neuroscience of Happiness, Love & Wisdom. Oakland, California, United States: New Harbringer Publications, 1-272.

Heeger, D. J., & Ress, D. (2002). What does fMRI tell us about neuronal activity? *Nature Reviews Neuroscience*, *3*(2), Article 2. https://doi.org/10.1038/nrn730

Hemington, K. S., Wu, Q., Kucyi, A., Inman, R. D., & Davis, K. D. (2016). Abnormal cross-network functional connectivity in chronic pain and its association with clinical symptoms. *Brain Structure and* Function, *221*(8), 4203–4219. https://doi.org/10.1007/s00429-015-1161-1

Holm, S. (1979). A Simple Sequentially Rejective Multiple Test Procedure. *Scand J Statist.*, *6*(2), 65-70.

Holsheimer, J., & Feenstra, B. W. A. (1977). Volume conduction and EEG measurements within the brain: A quantitative approach to the influence of electrical spread on the linear relationship of activity measured at different locations. *Electroencephalography and Clinical Neurophysiology*, *43*(1), 52–58. https://doi.org/10.1016/0013-4694(77)90194-8

Hughes, L. E., Henson, R. N., Pereda, E., Bruña, R., López-Sanz, D., Quinn, A. J., Woolrich, M. W., Nobre, A. C., Rowe, J. B., Maestú, F., & the BioFIND Working Group. (2019). Biomagnetic biomarkers for dementia: A pilot multicentre study with a recommended methodological framework for magnetoencephalography. *Alzheimer's & Dementia: Diagnosis, Assessment & Disease Monitoring*, *11*(1), 450–462. https://doi.org/10.1016/j.dadm.2019.04.009

Imperatori, C., Della Marca, G., Brunetti, R., Carbone, G. A., Massullo, C., Valenti, E. M., Amoroso, N., Maestoso, G., Contardi, A., & Farina, B. (2016). Default Mode Network alterations in alexithymia: An EEG power spectra and connectivity study. *Scientific Reports*, *6*(1), Article 1. https://doi.org/10.1038/srep36653

Ivanovski, B., & Malhi, G. S. (2007). The psychological and neurophysiological concomitants of mindfulness forms of meditation. *Acta Neuropsychiatrica*, *19*(2), 76–91. https://doi.org/10.1111/j.1601-5215.2007.00175.x

Jabès, A., Klencklen, G., Ruggeri, P., Antonietti, J.-P., Banta Lavenex, P., & Lavenex, P. (2021). Age-Related Differences in Resting-State EEG and Allocentric Spatial Working Memory Performance. *Frontiers in Aging Neuroscience*, *13*, 704362. https://doi.org/10.3389/fnagi.2021.704362

Jenkins, D. G., & Quintana-Ascencio, P. F. (2020). A solution to minimum sample size for regressions. *PLOS ONE*, *15*(2), e0229345. https://doi.org/10.1371/journal.pone.0229345

Jensen, M. P., Sherlin, L. H., Gertz, K. J., Braden, A. L., Kupper, A. E., Gianas, A., Howe, J. D., & Hakimian, S. (2013). Brain EEG activity correlates of chronic pain in persons with spinal cord injury: Clinical implications. *Spinal Cord*, *51*(1), Article 1. https://doi.org/10.1038/sc.2012.84

Jin, W., Choo, A., Gromala, D., Shaw, C., & Squire, P. (2016). A Virtual Reality Game for Chronic Pain Management: A Randomized, Controlled Clinical Study. *Studies in Health Technology and Informatics*, *220*, 154–160.

Johanson, G. A., & Brooks, G. P. (2010). Initial Scale Development: Sample Size for Pilot Studies. *Educational and Psychological Measurement*, *70*(3), 394–400. https://doi.org/10.1177/0013164409355692

Johnson, L., Lubin, A., Naitoh, P., Nute, C., & Austin, M. (1969). Spectral analysis of the EEG of dominant and non-dominant alpha subjects during waking and sleeping. *Electroencephalography and Clinical Neurophysiology*, *26*(4), 361–370. https://doi.org/10.1016/0013-4694(69)90086-8

Johnson, M. H. (2005). How does distraction work in the management of pain? *Current Pain and Headache Reports*, *9*(2), 90–95. https://doi.org/10.1007/s11916-005-0044-1

Julious, S. A. (2005). Sample size of 12 per group rule of thumb for a pilot study. *Pharmaceutical Statistics*, *4*(4), 287–291. https://doi.org/10.1002/pst.185

Kabat-Zinn, J. (2003). Mindfulness-based interventions in context: Past, present, and future. *Clinical Psychology: Science and Practice*, *10*, 144–156. https://doi.org/10.1093/clipsy.bpg016

Keng, S.-L., Smoski, M. J., & Robins, C. J. (2011). Effects of mindfulness on psychological health: A review of empirical studies. *Clinical Psychology Review*, *31*(6), 1041–1056. https://doi.org/10.1016/j.cpr.2011.04.006

Khera, T., & Rangasamy, V. (2021). Cognition and Pain: A Review. *Frontiers in Psychology*, *12*. https://www.frontiersin.org/articles/10.3389/fpsyg.2021.673962

Klimesch, W. (1996). Memory processes, brain oscillations and EEG synchronization. *International Journal of Psychophysiology*, *24*(1), 61–100. https://doi.org/10.1016/S0167-8760(96)00057-8

Klimesch, W. (1999). EEG alpha and theta oscillations reflect cognitive and memory performance: A review and analysis. *Brain Research Reviews*, *29*(2), 169–195. https://doi.org/10.1016/S0165-0173(98)00056-3

Klimesch, W., Doppelmayr, M., Pachinger, T., & Ripper, B. (1997). Brain oscillations and human memory: EEG correlates in the upper alpha and theta band. *Neuroscience Letters*, *238*(1), 9–12. https://doi.org/10.1016/S0304-3940(97)00771-4

Klymenko, M., Doesburg, S. M., Medvedev, G., Xi, P., Ribary, U., & Vakorin, V. A. (2023). Byte-Pair Encoding for Classifying Routine Clinical Electroencephalograms in Adults Over the Lifespan. *IEEE Journal of Biomedical and Health Informatics*, *27*(4), 1881–1890. https://doi.org/10.1109/JBHI.2023.3236264

Ko, J., Park, U., Kim, D., & Kang, S. W. (2021). Quantitative Electroencephalogram Standardization: A Sex- and Age-Differentiated Normative Database. *Frontiers in Neuroscience*, *15*. https://www.frontiersin.org/articles/10.3389/fnins.2021.766781

Konicar, L., Radev, S., Silvoni, S., Bolinger, E., Veit, R., Strehl, U., Vesely, C., Plener, P. L., Poustka, L., & Birbaumer, N. (2021). Balancing the brain of offenders with psychopathy? Resting state EEG and electrodermal activity after a pilot study of brain self-regulation training. *PLOS ONE*, *16*(1), e0242830. https://doi.org/10.1371/journal.pone.0242830

Köpruner, V., Pfurtscheller, G., & Auer, L. M. (1984). Quantitative EEG in normals and in patients with cerebral ischemia. In G. Pfurtscheller, E. J. Jonkman, & F. Lopes da Silva (Eds.), Brain ischemia: Quantitative EEG and imaging techniques (pp. 29–35). Amsterdam: Elsevier.

Kuner, R., (2004). Nociception. In: Encyclopedic Reference of Molecular Pharmacology. Springer, Berlin, Heidelberg. https://doi.org/10.1007/3-540-29832-0_1136

Lagopoulos, J., Xu, J., Rasmussen, I., Vik, A., Malhi, G. S., Eliassen, C. F., Arntsen, I. E., Sæther, J. G., Hollup, S., Holen, A., Davanger, S., & Ellingsen, Ø. (2009). Increased Theta and Alpha EEG Activity During Nondirective Meditation. *The Journal of Alternative and Complementary Medicine*, *15*(11), 1187–1192. https://doi.org/10.1089/acm.2009.0113

Latremoliere, A., & Woolf, C. J. (2009). Central Sensitization: A Generator of Pain Hypersensitivity by Central Neural Plasticity. *The Journal of Pain*, *10*(9), 895–926. https://doi.org/10.1016/j.jpain.2009.06.012

LeBlanc, B. W., Bowary, P. M., Chao, Y.-C., Lii, T. R., & Saab, C. Y. (2016). Electroencephalographic signatures of pain and analgesia in rats. *Pain*, *157*(10), 2330–2340. https://doi.org/10.1097/j.pain.0000000000000652

Lee, D. J., Kulubya, E., Goldin, P., Goodarzi, A., & Girgis, F. (2018). Review of the Neural Oscillations Underlying Meditation. *Frontiers in Neuroscience*, *12*. https://www.frontiersin.org/articles/10.3389/fnins.2018.00178

Levy, W. J. (1987). Effect of Epoch Length on Power Spectrum Analysis of the EEG. *Anesthesiology*, *66*(4), 489–495. https://doi.org/10.1097/00000542-198704000-00007

Li, A., Montaño, Z., Chen, V. J., & Gold, J. I. (2011). Virtual reality and pain management: Current trends and future directions. *Pain Management*, *1*(2), 147–157. https://doi.org/10.2217/pmt.10.15

Li, S., Kay, S., & Hardicker, N. R. (2007). Virtual reality: Towards a novel treatment environment for ankylosing spondylitis. *Studies in Health Technology and Informatics*, *127*, 190–196.

Lim, M., Kim, J. S., Kim, D. J., & Chung, C. K. (2016). Increased low-and high-frequency oscillatory activity in the prefrontal cortex of fibromyalgia patients. Frontiers in Human Neuroscience, 10(MAR2016). Scopus. https://doi.org/10.3389/fnhum.2016.00111

Liu, S., & Kelliher, L. (2022). Physiology of pain—A narrative review on the pain pathway and its application in the pain management. Digestive Medicine Research, 5(0), Article 0. https://doi.org/10.21037/dmr-21-100

Llinás, R. R., Ribary, U., Jeanmonod, D., Kronberg, E., & Mitra, P. P. (1999). Thalamocortical dysrhythmia: A neurological and neuropsychiatric syndrome characterized by magnetoencephalography. *Proceedings of the National Academy of Sciences of the United States of America*, *96*(26), 15222–15227. https://doi.org/10.1073/pnas.96.26.15222

Lomas, T., Ivtzan, I., & Fu, C. H. Y. (2015). A systematic review of the neurophysiology of mindfulness on EEG oscillations. *Neuroscience & Biobehavioral Reviews*, *57*, 401–410. https://doi.org/10.1016/j.neubiorev.2015.09.018

Maani, C. V., Hoffman, H. G., Morrow, M., Maiers, A., Gaylord, K., McGhee, L. L., & DeSocio, P. A. (2011). Virtual Reality Pain Control During Burn Wound Debridement of Combat-Related Burn Injuries Using Robot-Like Arm Mounted VR Goggles. *Journal of Trauma and Acute Care Surgery*, *71*(1), S125. https://doi.org/10.1097/TA.0b013e31822192e2

Magalhaes, A. A., Oliveira, L., Pereira, M. G., & Menezes, C. B. (2018). Does Meditation Alter Brain Responses to Negative Stimuli? A Systematic Review. *Frontiers in Human Neuroscience*, *12*. https://www.frontiersin.org/articles/10.3389/fnhum.2018.00448

Makeig, S., Bell, A. J., Jung, T.-P., & Sejnowski, T. J. (n.d.). *Independent Component Analysis of Electroencephalographic Data*.

Malloy, K. M., & Milling, L. S. (2010). The effectiveness of virtual reality distraction for pain reduction: A systematic review. *Clinical Psychology Review*, *30*(8), 1011–1018. https://doi.org/10.1016/j.cpr.2010.07.001

Mandal, P. K., Banerjee, A., Tripathi, M., & Sharma, A. (2018). A Comprehensive Review of Magnetoencephalography (MEG) Studies for Brain Functionality in Healthy Aging and Alzheimer's Disease (AD). *Frontiers in Computational Neuroscience*, *12*. https://www.frontiersin.org/article/10.3389/fncom.2018.00060

Mann, H. B., & Whitney, D. R. (1947). On a Test of Whether one of Two Random Variables is Stochastically Larger than the Other. The Annals of Mathematical Statistics, 18(1), 50–60. https://doi.org/10.1214/aoms/1177730491

Maris, E., & Oostenveld, R. (2007). Nonparametric statistical testing of EEG- and MEG-data. *Journal of Neuroscience Methods*, *164*(1), 177–190. https://doi.org/10.1016/j.jneumeth.2007.03.024

McDonald, J.H. (2014). Handbook of Biological Statistics, 3rd ed. Sparky House Publishing, Baltimore, Maryland.

McLaren Health Care News. (2023, March 27). The Five Types of Pain. https://www.mclaren.org/main/news/the-five-types-of-pain-4386

McLain, N. J., Yani, M. S., & Kutch, J. J. (2022). Analytic consistency and neural correlates of peak alpha frequency in the study of pain. *Journal of Neuroscience Methods*, *368*, 109460. https://doi.org/10.1016/j.jneumeth.2021.109460

Melzack, R. & Casey, K. (1968). Chapter 20. Sensory, Motivational, and Central Control Determinants of Pain, *The Skin Senses*, Charles C Thomas (pp. 423–439).

Michel, C. M., & He, B. (2019). EEG source localization. Handbook *of Clinical Neurology*, *160*, 85–101. https://doi.org/10.1016/B978-0-444-64032-1.00006-0

Mierau, A., Klimesch, W., & Lefebvre, J. (2017). State-dependent alpha peak frequency shifts: Experimental evidence, potential mechanisms and functional implications. *Neuroscience*, *360*, 146–154. https://doi.org/10.1016/j.neuroscience.2017.07.037

Mishra, S. K., Khosa, S., Singh, S., Moheb, N., & Trikamji, B. (2017). Changes in functional magnetic resonance imaging with Yogic meditation: A pilot study. *AYU (An International Quarterly Journal of Research in Ayurveda)*, *38*(2), 108. https://doi.org/10.4103/ayu.AYU_34_17

Mohammad, E., & Ahmad, M. (2018). Virtual reality as a distraction technique for pain and anxiety among patients with breast cancer: A randomized control trial. *Palliative and Supportive Care*, *17*. https://doi.org/10.1017/S1478951518000639

Moretti, D. V., Prestia, A., Fracassi, C., Geroldi, C., Binetti, G., Rossini, P. M., Zanetti, O., & Frisoni, G. B. (2011). Volumetric Differences in Mapped Hippocampal Regions Correlate with Increase of High Alpha Rhythm in Alzheimer's Disease. *International Journal of Alzheimer's Disease*, *2011*, e208218. https://doi.org/10.4061/2011/208218

Moriarty, O., McGuire, B. E., & Finn, D. P. (2011). The effect of pain on cognitive function: A review of clinical and preclinical research. *Progress in Neurobiology*, *93*(3), 385–404. https://doi.org/10.1016/j.pneurobio.2011.01.002

Morton, D. L., Sandhu, J. S., & Jones, A. K. (2016). Brain imaging of pain: State of the art. *Journal of Pain Research*, *9*, 613–624. https://doi.org/10.2147/JPR.S60433

Navarro-Haro, M. V., Modrego-Alarcón, M., Hoffman, H. G., López-Montoyo, A., Navarro-Gil, M., Montero-Marin, J., García-Palacios, A., Borao, L., & García-Campayo, J. (2019). Evaluation of a Mindfulness-Based Intervention With and Without Virtual Reality Dialectical Behavior Therapy® Mindfulness Skills Training for the Treatment of Generalized Anxiety Disorder in Primary Care: A Pilot Study. *Frontiers in Psychology*, *10*. https://www.frontiersin.org/articles/10.3389/fpsyg.2019.00055

Nayak, C. S., & Anilkumar, A. C. (2023). EEG Normal Waveforms. In *StatPearls*. StatPearls Publishing. http://www.ncbi.nlm.nih.gov/books/NBK539805/

Niedermeyer, E. (1997). Alpha rhythms as physiological and abnormal phenomena. *International Journal of Psychophysiology*, *26*(1–3), 31–49. https://doi.org/10.1016/S0167-8760(97)00754-X

Niso, G., Rogers, C., Moreau, J. T., Chen, L.-Y., Madjar, C., Das, S., Bock, E., Tadel, F., Evans, A. C., Jolicoeur, P., & Baillet, S. (2016). OMEGA: The Open MEG Archive. *NeuroImage*, *124*, 1182–1187. https://doi.org/10.1016/j.neuroimage.2015.04.028

Niso, G., Tadel, F., Bock, E., Cousineau, M., Santos, A., & Baillet, S. (2019). Brainstorm Pipeline Analysis of Resting-State Data From the Open MEG Archive. *Frontiers in Neuroscience*, *13*. https://doi.org/10.3389/fnins.2019.00284

Nunes, A., & Bloy, L. Annotate muscle artifacts—MNE 1.0.3 documentation. Retrieved 2023, from https://mne.tools/1.0/auto_examples/preprocessing/muscle_detection.html

Nyklíček, I., Dijksman, S. C., Lenders, P. J., Fonteijn, W. A., & Koolen, J. J. (2014). A brief mindfulness based intervention for increase in emotional well-being and quality of life in percutaneous coronary intervention (PCI) patients: The MindfulHeart randomized controlled trial. *Journal of Behavioral Medicine*, *37*(1), 135–144. https://doi.org/10.1007/s10865-012-9475-4

Olejarczyk, E., Bogucki, P., & Sobieszek, A. (2017). The EEG Split Alpha Peak: Phenomenological Origins and Methodological Aspects of Detection and Evaluation. *Frontiers in Neuroscience*, *11*. https://doi.org/10.3389/fnins.2017.00506

Oostenveld, R., Fries, P., Maris, E., & Schoffelen, J.-M. (2010). FieldTrip: Open Source Software for Advanced Analysis of MEG, EEG, and Invasive Electrophysiological Data. *Computational Intelligence and Neuroscience*, *2011*, e156869. https://doi.org/10.1155/2011/156869

Panjwani, U., Selvamurthy, W., Singh, S. H., Gupta, H. L., Mukhopadhyay, S., & Thakur, L. (2000). Effect of Sahaja Yoga Meditation on Auditory Evoked Potentials (AEP) and Visual Contrast Sensitivity (VCS) in Epileptics. *Applied Psychophysiology and Biofeedback*, *25*(1), 1–12. https://doi.org/10.1023/A:1009523904786

Pascual-Marqui, R. D. (2002). Standardized low-resolution brain electromagnetic tomography (sLORETA): Technical details. *Methods and Findings in Experimental and Clinical Pharmacology*, *24 Suppl D*, 5–12.

Pedregosa, F., Varoquaux, G., Gramfort, A., Michel, V., Thirion, B., Grisel, O., Blondel, M., Müller, A., Nothman, J., Louppe, G., Prettenhofer, P., Weiss, R., Dubourg, V., Vanderplas, J., Passos, A., Cournapeau, D., Brucher, M., Perrot, M., & Duchesnay, É. (2011). Scikit-learn: Machine learning in Python. *Journal of Machine Learning Research*, 12(Oct), 2825–2830.

Perrin, F., Pernier, J., Bertrand, O., & Echallier, J. F. (1989). Spherical splines for scalp potential and current density mapping. *Electroencephalography and Clinical* Neurophysiology, *72*(2), 184–187. https://doi.org/10.1016/0013-4694(89)90180-6

Piastra, M. C., Nüßing, A., Vorwerk, J., Clerc, M., Engwer, C., & Wolters, C. H. (2021). A comprehensive study on electroencephalography and magnetoencephalography sensitivity to cortical and subcortical sources. *Human Brain Mapping*, *42*(4), 978–992. https://doi.org/10.1002/hbm.25272

Pinheiro, E. S. dos S., Queirós, F. C. de, Montoya, P., Santos, C. L., Nascimento, M. A. do, Ito, C. H., Silva, M., Santos, D. B. N., Benevides, S., Miranda, J. G. V., Sá, K. N., & Baptista, A. F. (2016). Electroencephalographic Patterns in Chronic Pain: A Systematic Review of the Literature. *PLOS ONE*, *11*(2), e0149085. https://doi.org/10.1371/journal.pone.0149085

Ploner, M., Gross, J., Timmermann, L., Pollok, B., & Schnitzler, A. (2006). Pain Suppresses Spontaneous Brain Rhythms. Cerebral Cortex, 16(4), 537–540. https://doi.org/10.1093/cercor/bhj001

Ploner, M., Sorg, C., & Gross, J. (2017). Brain Rhythms of Pain. Trends *in Cognitive Sciences*, *21*(2), 100–110. https://doi.org/10.1016/j.tics.2016.12.001

Raichle, M. E., MacLeod, A. M., Snyder, A. Z., Powers, W. J., Gusnard, D. A., & Shulman, G. L. (2001). A default mode of brain function. *Proceedings of the National Academy of Sciences of the United States of America*, *98*(2), 676–682. Scopus. https://doi.org/10.1073/pnas.98.2.676

Rathee, S., Bhatia, D., Punia, V., & Singh, R. (2020). Peak Alpha Frequency in Relation to Cognitive Performance. *Journal of Neurosciences in Rural Practice*, *11*(3), 416–419. https://doi.org/10.1055/s-0040-1712585

Rosazza, C., & Minati, L. (2011). Resting-state brain networks: Literature review and clinical applications. *Neurological Sciences*, *32*(5), 773–785. https://doi.org/10.1007/s10072-011-0636-y

Rosenzweig, S., Greeson, J. M., Reibel, D. K., Green, J. S., Jasser, S. A., & Beasley, D. (2010). Mindfulness-based stress reduction for chronic pain conditions: Variation in treatment outcomes and role of home meditation practice. *Journal of Psychosomatic Research*, *68*(1), 29–36. https://doi.org/10.1016/j.jpsychores.2009.03.010

Samson-Dollfus, D., Delapierre, G., Do Marcolino, C., & Blondeau, C. (1997). Normal and pathological changes in alpha rhythms. *International Journal of Psychophysiology*, *26*(1), 395–409. https://doi.org/10.1016/S0167-8760(97)00778-2

Sandwell, D. T. (1987). Biharmonic spline interpolation of GEOS-3 and SEASAT altimeter data. *Geophysical Research Letters*, *14*(2), 139–142. https://doi.org/10.1029/GL014i002p00139

Sarnthein, J., Stern, J., Aufenberg, C., Rousson, V., & Jeanmonod, D. (2006). Increased EEG power and slowed dominant frequency in patients with neurogenic pain. *Brain*, *129*(1), 55–64. https://doi.org/10.1093/brain/awh631

Sawilowsky, S. (2009). New Effect Size Rules of Thumb. *Journal of Modern Applied Statistical Methods*, *8*, 597–599. https://doi.org/10.22237/jmasm/1257035100

Scally, B., Burke, M. R., Bunce, D., & Delvenne, J.-F. (2018). Resting-state EEG power and connectivity are associated with alpha peak frequency slowing in healthy aging. *Neurobiology of Aging*, *71*, 149–155. https://doi.org/10.1016/j.neurobiolaging.2018.07.004

Scapin, S., Echevarría-Guanilo, M. E., Boeira Fuculo Junior, P. R., Gonçalves, N., Rocha, P. K., & Coimbra, R. (2018). Virtual Reality in the treatment of burn patients: A systematic review. *Burns:* Journal *of the International Society for* Burn *Injuries*, *44*(6), 1403–1416. https://doi.org/10.1016/j.burns.2017.11.002

Schaworonkow, N., & Nikulin, V. V. (2022). Is sensor space analysis good enough? Spatial patterns as a tool for assessing spatial mixing of EEG/MEG rhythms. *NeuroImage*, *253*, 119093. https://doi.org/10.1016/j.neuroimage.2022.119093

Schmitt, Y. S., Hoffman, H. G., Blough, D. K., Patterson, D. R., Jensen, M. P., Soltani, M., Carrougher, G. J., Nakamura, D., & Sharar, S. R. (2011). A randomized, controlled trial of immersive virtual reality analgesia, during physical therapy for pediatric burns. *Burns: Journal of the International Society for Burn Injuries*, *37*(1), 61–68. https://doi.org/10.1016/j.burns.2010.07.007

Schoenberg, P. L., & Vago, D. R. (2019). Mapping meditative states and stages with electrophysiology: Concepts, classifications, and methods. *Current Opinion in Psychology*, *28*, 211–217. https://doi.org/10.1016/j.copsyc.2019.01.007

Schölkopf, B., & Smola, A. (2002) Learning with Kernels : Support Vector Machines, Regularization, Optimization, and beyond Adaptive Computation and Machine Learning. MIT Press xviii, Cambridge, Mass, p. 626.

Scholz, F. W., & Stephens, M. A. (1987). K-Sample Anderson-Darling Tests. *Journal of the American Statistical Association*, *82*(399), 918–924. https://doi.org/10.2307/2288805

Schopflocher, D., Taenzer, P., & Jovey, R. (2011). *The* Prevalence *of Chronic Pain in Canada* [Research article]. Pain Research and Management. https://doi.org/10.1155/2011/876306

Seabold, S., & Perktold, J. (2010). Statsmodels: Econometric and Statistical Modeling with Python. *Proceedings of the 9th Python in Science Conference*, 92–96. https://doi.org/10.25080/Majora-92bf1922-011

Seay, A. F., Gromala, D., Hodges, L., & Shaw, C. (2002). The meditation chamber: A debriefing. *ACM SIGGRAPH 2002 Conference Abstracts and Applications*, 263. https://doi.org/10.1145/1242073.1242276

Seeley, W. W. (2019). The Salience Network: A Neural System for Perceiving and Responding to Homeostatic Demands. *Journal of Neuroscience*, *39*(50), 9878–9882. https://doi.org/10.1523/JNEUROSCI.1138-17.2019

Shafto, M. A., Tyler, L. K., Dixon, M., Taylor, J. R., Rowe, J. B., Cusack, R., Calder, A. J., Marslen-Wilson, W. D., Duncan, J., Dalgleish, T., Henson, R. N., Brayne, C., & Matthews, F. E. (2014). The Cambridge Centre for Ageing and Neuroscience (Cam-CAN) study protocol: A cross-sectional, lifespan, multidisciplinary examination of healthy cognitive ageing. *BMC Neurology*, *14*. https://doi.org/10.1186/s12883-014-0204-1

Sikka, P., Revonsuo, A., Noreika, V., & Valli, K. (2019). EEG Frontal Alpha Asymmetry and Dream Affect: Alpha Oscillations over the Right Frontal Cortex during REM Sleep and Presleep Wakefulness Predict Anger in REM Sleep Dreams. *Journal of Neuroscience*, *39*(24), 4775–4784. https://doi.org/10.1523/JNEUROSCI.2884-18.2019

Sitnikova, T. A., Hughes, J. W., Ahlfors, S. P., Woolrich, M. W., & Salat, D. H. (2018). Short timescale abnormalities in the states of spontaneous synchrony in the functional neural networks in Alzheimer's disease. *NeuroImage : Clinical*, *20*, 128–152. https://doi.org/10.1016/j.nicl.2018.05.028

Siuly, S., Li, Y., & Zhang, Y. (2016). *EEG Signal Analysis and Classification*. Springer International Publishing. https://doi.org/10.1007/978-3-319-47653-7

Slepian, D. (1978). Prolate spheroidal wave functions, fourier analysis, and uncertainty — V: The discrete case. *The Bell System Technical Journal*, *57*(5), 1371–1430. https://doi.org/10.1002/j.1538-7305.1978.tb02104.x

Sprecher, K. E., Riedner, B. A., Smith, R. F., Tononi, G., Davidson, R. J., & Benca, R. M. (2016). High Resolution Topography of Age-Related Changes in Non-Rapid Eye Movement Sleep Electroencephalography. *PLOS ONE*, *11*(2), e0149770. https://doi.org/10.1371/journal.pone.0149770

Srinivasan, R., Nunez, P. L., & Silberstein, R. B. (1998). Spatial filtering and neocortical dynamics: Estimates of EEG coherence. *IEEE Transactions on Biomedical Engineering*, *45*(7), 814–826. https://doi.org/10.1109/10.686789

Stern, J., Jeanmonod, D., & Sarnthein, J. (2006). Persistent EEG overactivation in the cortical pain matrix of neurogenic pain patients. *NeuroImage*, *31*(2), 721–731. https://doi.org/10.1016/j.neuroimage.2005.12.042

Sullivan, G. M., & Feinn, R. (2012). Using Effect Size—Or Why the P Value Is Not Enough. *Journal of Graduate Medical Education*, *4*(3), 279–282. https://doi.org/10.4300/JGME-D-12-00156.1

Talbot, K., Madden, V. J., Jones, S. L., & Moseley, G. L. (2019). The sensory and affective components of pain: Are they differentially modifiable dimensions or inseparable aspects of a unitary experience? A systematic review. BJA: British Journal of Anaesthesia, 123(2), e263–e272. https://doi.org/10.1016/j.bja.2019.03.033

Taulu, S., & Kajola, M. (2005). Presentation of electromagnetic multichannel data: The signal space separation method. *Journal of Applied Physics*, *97*(12), 124905. https://doi.org/10.1063/1.1935742

Taulu, S., & Simola, J. (2006). Spatiotemporal signal space separation method for rejecting nearby interference in MEG measurements. *Physics in Medicine and Biology*, *51*(7), 1759–1768. https://doi.org/10.1088/0031-9155/51/7/008

Taylor, J. R., Williams, N., Cusack, R., Auer, T., Shafto, M. A., Dixon, M., Tyler, L. K., Cam-CAN, & Henson, R. N. (2017). The Cambridge Centre for Ageing and Neuroscience (Cam-CAN) data repository: Structural and functional MRI, MEG, and cognitive data from a cross-sectional adult lifespan sample. *NeuroImage*, *144*, 262–269. https://doi.org/10.1016/j.neuroimage.2015.09.018

Tiemann, L., Schulz, E., Gross, J., & Ploner, M. (2010). Gamma oscillations as a neuronal correlate of the attentional effects of pain. *PAIN*, *150*(2), 302. https://doi.org/10.1016/j.pain.2010.05.014

Tiemann, L., Schulz, E., Winkelmann, A., Ronel, J., Henningsen, P., & Ploner, M. (2012). Behavioral and Neuronal Investigations of Hypervigilance in Patients with Fibromyalgia Syndrome. *PLOS ONE*, *7*(4), e35068. https://doi.org/10.1371/journal.pone.0035068

Tipping, M. E. (2001). Sparse Bayesian learning and the relevance vector machine. *Journal of Machine Learning Research*, *1*, 211–244. https://doi.org/10.1162/15324430152748236

Tran, Y., Boord, P., Middleton, J., & Craig, A. (2004). Levels of brain wave activity (8–13 Hz) in persons with spinal cord injury. Spinal Cord, 42(2), Article 2. https://doi.org/10.1038/sj.sc.3101543

Travis, F., & Shear, J. (2010). Focused attention, open monitoring and automatic self-transcending: Categories to organize meditations from Vedic, Buddhist and Chinese traditions. *Consciousness and Cognition*, *19*(4), 1110–1118. https://doi.org/10.1016/j.concog.2010.01.007

Treede, R.-D., Rief, W., Barke, A., Aziz, Q., Bennett, M. I., Benoliel, R., Cohen, M., Evers, S., Finnerup, N. B., First, M. B., Giamberardino, M. A., Kaasa, S., Kosek, E., Lavand'homme, P., Nicholas, M., Perrot, S., Scholz, J., Schug, S., Smith, B. H., … Wang, S.-J. (2015). A classification of chronic pain for ICD-11. *PAIN*, *156*(6), 1003. https://doi.org/10.1097/j.pain.0000000000000160

Uddin, L. Q., Yeo, B. T. T., & Spreng, R. N. (2019). Towards a Universal Taxonomy of Macro-scale Functional Human Brain Networks. *Brain Topography*, *32*(6), 926–942. https://doi.org/10.1007/s10548-019-00744-6

Unde, S. A., & Shriram, R. (2014). Coherence Analysis of EEG Signal Using Power Spectral Density. *2014 Fourth International Conference on Communication Systems and Network Technologies*, 871–874. https://doi.org/10.1109/CSNT.2014.181

Uusitalo, M. A., & Ilmoniemi, R. J. (1997). Signal-space projection method for separating MEG or EEG into components. *Medical & Biological Engineering & Computing*, *35*(2), 135–140. https://doi.org/10.1007/BF02534144

Vapnik, V. N. (1995). The nature of statistical learning theory / Vladimir N. Vapnik. Springer.

Venuturupalli, R. S., Chu, T., Vicari, M., Kumar, A., Fortune, N., & Spielberg, B. (2019). Virtual Reality–Based Biofeedback and Guided Meditation in Rheumatology: A Pilot Study. *ACR Open Rheumatology*, *1*(10), 667–675. https://doi.org/10.1002/acr2.11092

Virtanen, P., Gommers, R., Oliphant, T. E., Haberland, M., Reddy, T., Cournapeau, D., Burovski, E., Peterson, P., Weckesser, W., Bright, J., van der Walt, S. J., Brett, M., Wilson, J., Millman, K. J., Mayorov, N., Nelson, A. R. J., Jones, E., Kern, R., Larson, E., … van Mulbregt, P. (2020). SciPy 1.0: Fundamental algorithms for scientific computing in Python. *Nature Methods*, *17*(3), Article 3. https://doi.org/10.1038/s41592-019-0686-2

Welch, P. (1967). The use of fast Fourier transform for the estimation of power spectra: A method based on time averaging over short, modified periodograms. *IEEE Transactions on Audio and Electroacoustics*, *15*(2), 70–73. https://doi.org/10.1109/TAU.1967.1161901

Williamson, A., & Hoggart, B. (2005). Pain: A review of three commonly used pain rating scales. *Journal of Clinical Nursing*, *14*(7), 798–804. https://doi.org/10.1111/j.1365-2702.2005.01121.x

Winkler, I., Debener, S., Müller, K.-R., & Tangermann, M. (2015). On the influence of high-pass filtering on ICA-based artifact reduction in EEG-ERP. *2015 37th Annual International Conference of the IEEE Engineering in Medicine and Biology Society (EMBC)*, 4101–4105. https://doi.org/10.1109/EMBC.2015.7319296

Winter, W. R., Nunez, P. L., Ding, J., & Srinivasan, R. (2007). Comparison of the effect of volume conduction on EEG coherence with the effect of field spread on MEG coherence. Statistics in Medicine, 26(21), 3946–3957. https://doi.org/10.1002/sim.2978

Witjes, B., Baillet, S., Roy, M., Oostenveld, R., J.P.M. Huygen, F., & C. de Vos, C. (2021). Magnetoencephalography reveals increased slow-to-fast alpha power ratios in patients with chronic pain. *Pain Reports*, *6*(2), e928. https://doi.org/10.1097/PR9.0000000000000928

Wolitzky, K., Fivush, R., Zimand, E., Hodges, L., & Rothbaum, B. O. (2005). Effectiveness of virtual reality distraction during a painful medical procedure in pediatric oncology patients. *Psychology & Health*, *20*(6), 817–824. https://doi.org/10.1080/14768320500143339

Woolf, C. J. (2011). Central sensitization: Implications for the diagnosis and treatment of pain. *Pain*, *152*(3 Suppl), S2–S15. https://doi.org/10.1016/j.pain.2010.09.030

Wydenkeller, S., Maurizio, S., Dietz, V., & Halder, P. (2009). Neuropathic pain in spinal cord injury: Significance of clinical and electrophysiological measures. *European Journal of Neuroscience*, *30*(1), 91–99. https://doi.org/10.1111/j.1460-9568.2009.06801.x

Xifra-Porxas, A., Ghosh, A., Mitsis, G. D., & Boudrias, M.-H. (2021). Estimating brain age from structural MRI and MEG data: Insights from dimensionality reduction techniques. *NeuroImage*, *231*, 117822. https://doi.org/10.1016/j.neuroimage.2021.117822

Xu, C., Qu, H., Wang, G., Xie, B., Shi, Y., Yang, Y., Zhao, Z., Hu, L., Fang, X., Yan, J., & Feng, L. (2015). A novel strategy for forensic age prediction by DNA methylation and support vector regression model. *Scientific Reports*, *5*(1), 17788. https://doi.org/10.1038/srep17788

Yang, S., & Chang, M. C. (2019). Chronic Pain: Structural and Functional Changes in Brain Structures and Associated Negative Affective States. International Journal of Molecular Sciences, 20(13), 3130. https://doi.org/10.3390/ijms20133130

Yokosawa, K., Murakami, Y., & Sato, H. (2020). Appearance and modulation of a reactive temporal-lobe 8–10-Hz tau-rhythm. *Neuroscience Research*, *150*, 44–50. https://doi.org/10.1016/j.neures.2019.02.002

Zebhauser, P. T., Hohn, V. D., & Ploner, M. (2022). Resting-state electroencephalography and magnetoencephalography as biomarkers of chronic pain: A systematic review. *PAIN*, 10.1097/j.pain.0000000000002825. https://doi.org/10.1097/j.pain.0000000000002825

Zhang, S., & Seymour, B. (2014). Technology for Chronic Pain. *Current Biology*, *24*(18), R930–R935. https://doi.org/10.1016/j.cub.2014.07.010

Appendix A.

A Study of Multiple Alpha Peaks

This study used the CamCAN Magnetoencephalography (MEG) datasets (Shafto et al., 2014; Taylor et al., 2017) to investigate the multiple alpha peak properties in four alpha rhythm generation sites: frontal, central, temporal, and parieto-occipital regions of interest (ROIs). As described in Chapter 4, source space PSD was plotted for the control group (N= 474, 246 males and 228 females, mean = 53.90, SD = 18.29) and pain group (N=22, 12 males and 10 females, mean = 64.03, SD = 15.64).

Multiple or split alpha peaks are common in the EEG/MEG spectrum. The split alpha peaks could be generated from independent or interconnected sites in the cortex (Olejarczyk et al., 2017; Chiang et al., 2011). For example, Figures A1 to A3 show the PSD and topographies of a selected subject, and two peaks are observed in the alpha band. The topographies of the low alpha and high alpha bands show that the central and parieto-occipital ROIs were the signal generation sites, respectively.

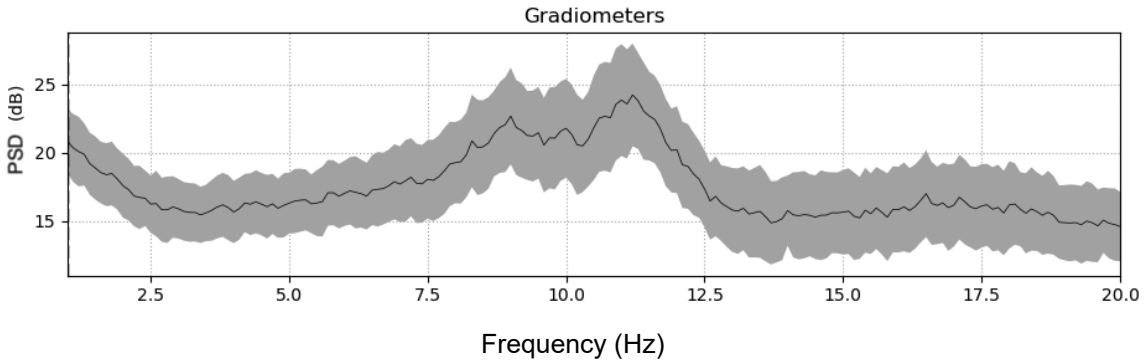

Figure A1. Source power spectral density (PSD) plot of a subject showing two peaks in the alpha band. The PSD unit is dB.

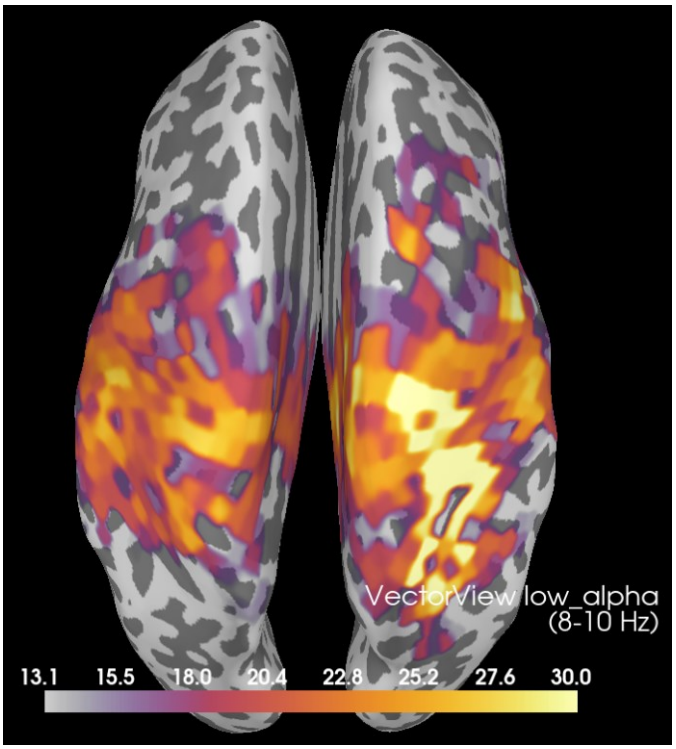

Figure A2. **Topography of the peak in the central ROI in the low alpha range (8-10 Hz). The colour bar unit is dB.**

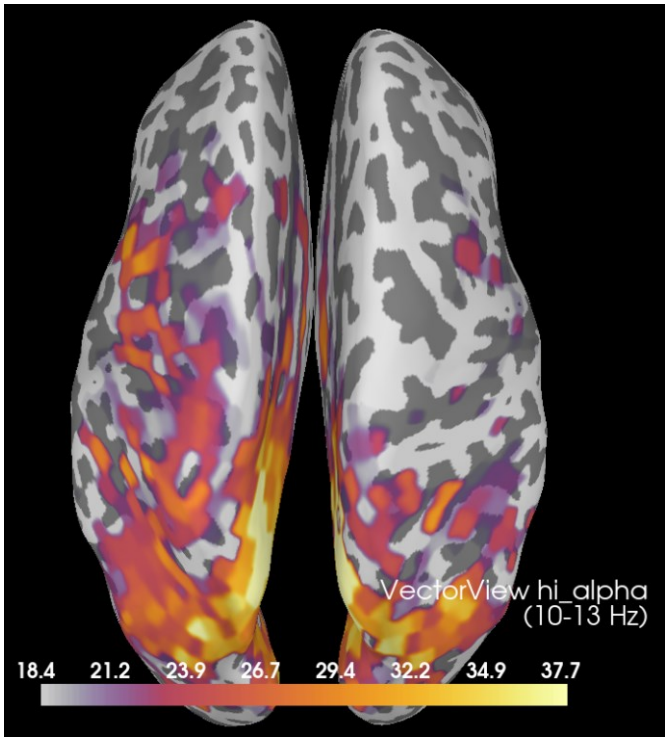

Figure A3. **Topography of the peak in the parieto-occipital ROI in the high alpha range (10-13 Hz).**

For this study, the PSD computed from the CamCAN datasets was smoothed using a 9-point boxcar equivalent to a window of 0.9 Hz to minimize false peaks due to noise extrema (Chiang et al., 2008). Scipy's (Virtanen et al., 2020) *find_peak* function was then used to find the number of peaks. The prominence parameter of SciPy's "find_peaks" was set to 0.15. If an alpha rhythm peak prominence was less than this threshold, it was assumed that no peak was found.

Table A1 lists the results for all subjects. The frontal and central ROIs have the highest percentage of no peak of 11.6% and 9.0%, likely due to the relatively weak amplitudes in these two regions and, in some cases, not being distinguishable from noise. For single peaks, the parieto-occipital region has the highest percentage of 77.3%. The central and temporal ROIs have a higher percentage of double peaks of more than 25%. The percentage of triple peaks is less than 3% in all ROIs, with the highest of 2.8% in the central ROI. No four or more peaks were detected in the PSD.

Table A2 shows the difference between all subjects in Table A1(A) and controls in Table A1(B). A difference of 1.3% or less is found in each category. This is likely because the controls dominated with 83.5% of all subjects. Comparing controls in Table A1(B) with the pain group in Table A1(E), the controls have a higher no-peak percentage in the frontal and central ROIs, and the pain group has a higher no-peak percentage in the temporal and parieto-occipital ROIs. Table A3 shows this percentage difference.

Tables A1(C) and (D) show the number of peaks in the male and female controls. Table A4 shows the difference in percentage between these two groups. The male control group has a 4.4% higher two-peak rate in the frontal ROI, and the female control group has a 6.0% higher two-peak rate in the central ROI.

A null hypothesis was set that no difference existed between the mean number of peaks in the four ROIs. ANOVA tests showed significance for all subjects, controls, male controls and female controls, but not the pain group, as shown in Table A1, whereas a Bonferroni corrected $\alpha = 0.0083$ was assumed. A post hoc test was done for controls using Bonferroni. The comparisons of central vs temporal, central vs parieto-occipital, and temporal vs parieto-occipital failed to reject the null hypothesis. MANOVA tests were done for all subjects and controls with sex as an additoinal factor, and no significance was found. This implies that sex is not a factor in the number of peaks.

Table A1. **The number of alpha peaks found in the regions of interest (ROIs) in the CamCAM MEG database. Frontal: the frontal ROI. Central: the central ROI. Temporal: the temporal ROI. PO: the parieto-occipital ROI.**

A: All (ANOVA of the four ROIs, p = 1.46e-05)								
No. Peaks	**Frontal**	**Percentage**	**Central**	**Percentage**	**Temporal**	**Percentage**	**PO**	**Percentage**
0	66	11.6%	51	9.0%	15	2.6%	11	1.9%
1	382	67.3%	340	59.9%	400	70.4%	439	77.3%
2	112	19.7%	161	28.3%	144	25.4%	113	19.9%
3	8	1.4%	16	2.8%	9	1.6%	5	0.9%
Total	568	100.0%	568	100.0%	568	100.0%	568	100.0%
B: Controls (ANOVA of the four ROIs, p = 2.08e-05)								
No. Peaks	**Frontal**	**Percentage**	**Central**	**Percentage**	**Temporal**	**Percentage**	**PO**	**Percentage**
0	50	10.5%	39	8.2%	7	1.5%	6	1.3%
1	325	68.6%	284	59.9%	340	71.7%	368	77.6%
2	94	19.8%	137	28.9%	119	25.1%	95	20.0%
3	5	1.1%	14	3.0%	8	1.7%	5	1.1%
Total	474	100.0%	474	100.0%	474	100.0%	474	100.0%
C: Male Controls (ANOVA of the four ROIs, p = 0.0059)								
No. Peaks	**Frontal**	**Percentage**	**Central**	**Percentage**	**Temporal**	**Percentage**	**PO**	**Percentage**
0	26	10.6%	17	6.9%	1	0.4%	1	0.4%
1	165	67.1%	157	63.8%	178	72.4%	193	78.5%
2	54	22.0%	64	26.0%	63	25.6%	48	19.5%
3	1	0.4%	8	3.3%	4	1.6%	4	1.6%
Total	246	100.0%	246	100.0%	246	100.0%	246	100.0%
D: Female Controls (ANOVA of the four ROIs, p = 0.0059)								
No. Peaks	**Frontal**	**Percentage**	**Central**	**Percentage**	**Temporal**	**Percentage**	**PO**	**Percentage**
0	24	10.5%	22	9.6%	6	2.6%	5	2.2%
1	160	70.2%	127	55.7%	162	71.1%	175	76.8%
2	40	17.5%	73	32.0%	56	24.6%	47	20.6%

3	4	1.8%	6	2.6%	4	1.8%	1	0.4%
Total	228	100.0%	228	100.0%	228	100.0%	228	100.0%
E: Pain Group (ANOVA of the four regions, p = 0.92)								
No. Peaks	**Frontal**	**Percentage**	**Central**	**Percentage**	**Temporal**	**Percentage**	**PO**	**Percentage**
0	1	4.5%	1	4.5%	1	4.5%	1	4.5%
1	16	72.7%	15	68.2%	15	68.2%	17	77.3%
2	4	18.2%	6	27.3%	6	27.3%	4	18.2%
3	1	4.5%	0	0.0%	0	0.0%	0	0.0%
Total	22	100.0%	22	100.0%	22	100.0%	22	100.0%

Table A2. The difference in the number of peaks between all subjects in Table A1(A) and controls in Table A1(B).

No. Peaks	Frontal	Central	Temporal	PO
0	1.1%	0.8%	1.2%	0.7%
1	-1.3%	-0.1%	-1.3%	-0.3%
2	-0.1%	-0.6%	0.2%	-0.1%
3	0.4%	-0.1%	-0.1%	-0.2%

Table A3. The difference in the number of peaks between the control and pain groups.

No. Peaks	Frontal	Central	Temporal	PO
0	6.0%	3.7%	-3.1%	-3.3%
1	-4.2%	-8.3%	3.5%	0.4%
2	1.6%	1.6%	-2.2%	1.9%
3	-3.5%	3.0%	1.7%	1.1%

Table A4. The difference in the number of peaks between the male and female controls.

No. Peaks	Frontal	Central	Temporal	PO
0	0.0%	-2.7%	-2.2%	-1.8%
1	-3.1%	8.1%	1.3%	1.7%
2	4.4%	-6.0%	1.0%	-1.1%
3	-1.3%	0.6%	-0.1%	1.2%

Appendix B.

Effect of SSP Projectors on Raw Data

This analysis demonstrates raw MEG noise reduction using the signal-space projection (SSP) technique. The PSD plots below demonstrate the effect of the number of projectors used in SSP for environmental noise reduction. The system-provided projectors were discarded, and the projectors were created from the empty-room MEG recording.

Reference:
https://mne.tools/stable/auto_tutorials/preprocessing/50_artifact_correction_ssp.html

- Number of gradiometer projectors: 0
- Number of magnetometer projectors: 0 to 15

The aim is to select the minimum number of projectors required to separate the environmental noise, since a large number of projectors will lower the rank of the data matrix. Figure B1 shows the PSD of magnetometers with the number of projectors from 0 to 15. The top plot shows the PSD of gradiometers. Gradiometers are less noise-prone, and we used gradiometers in the top plot as a reference. The other plots show the effect of the number of projectors used. Where the number of projectors equals 6 or 7 seems optimal.

A

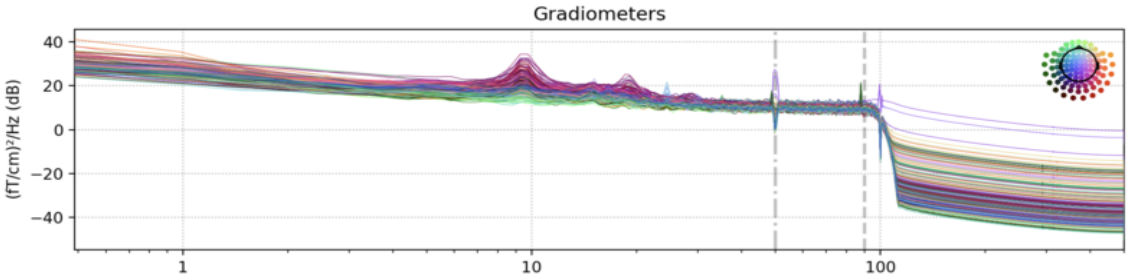
Gradiometers
(fT/cm)²/Hz (dB)
40
20
0
−20
−40
1
10
100

B

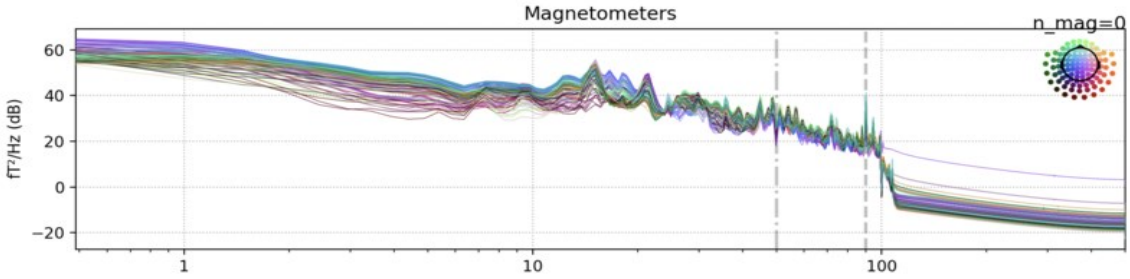
Magnetometers
n_mag=0
fT²/Hz (dB)
60
40
20
0
−20
1
10
100

C

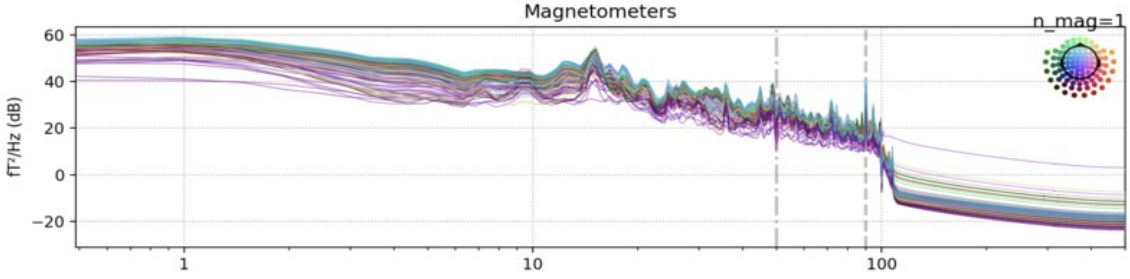
Magnetometers
n_mag=1
fT²/Hz (dB)
60
40
20
0
−20
1
10
100

D

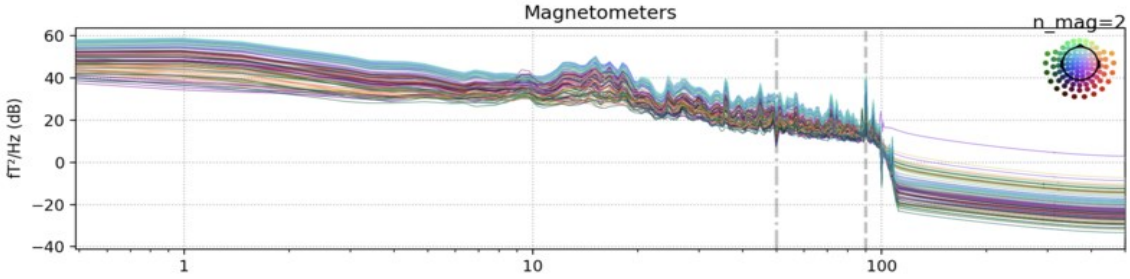
Magnetometers
n_mag=2
fT²/Hz (dB)
60
40
20
0
−20
−40
1
10
100

E

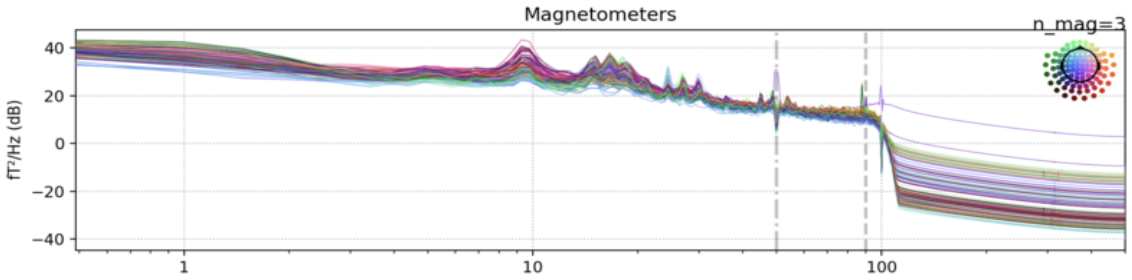
Magnetometers
n_mag=3
fT²/Hz (dB)
40
20
0
−20
−40
1
10
100

F

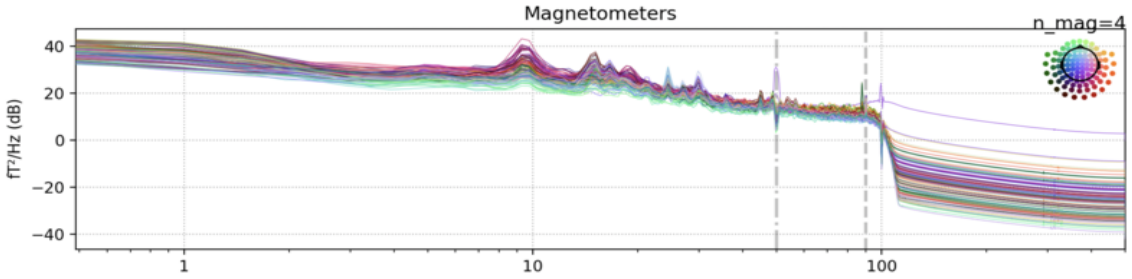
Magnetometers
n_mag=4
fT²/Hz (dB)
40
20
0
−20
−40
1
10
100

G

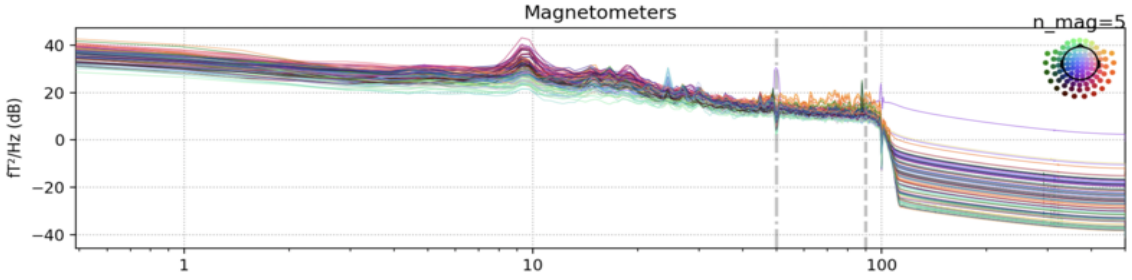
Magnetometers
n_mag=5
fT²/Hz (dB)
40
20
0
−20
−40
1
10
100

H

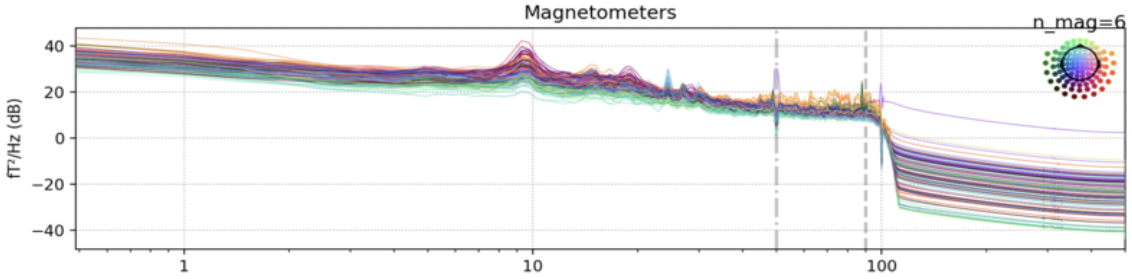
Magnetometers
n_mag=6
fT²/Hz (dB)
40
20
0
−20
−40
1
10
100

I

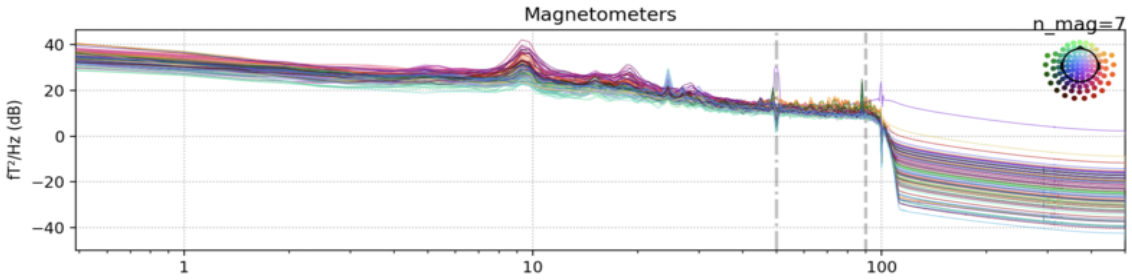
Magnetometers
n_mag=7
fT²/Hz (dB)
40
20
0
−20
−40
1
10
100

J

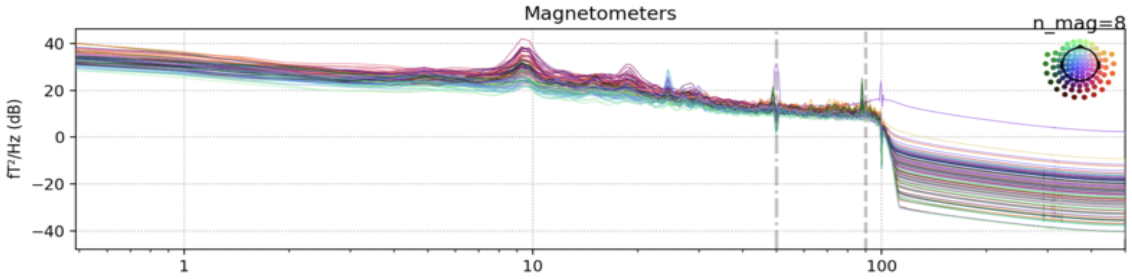
Magnetometers
n_mag=8
fT²/Hz (dB)
40
20
0
−20
−40
1
10
100

K

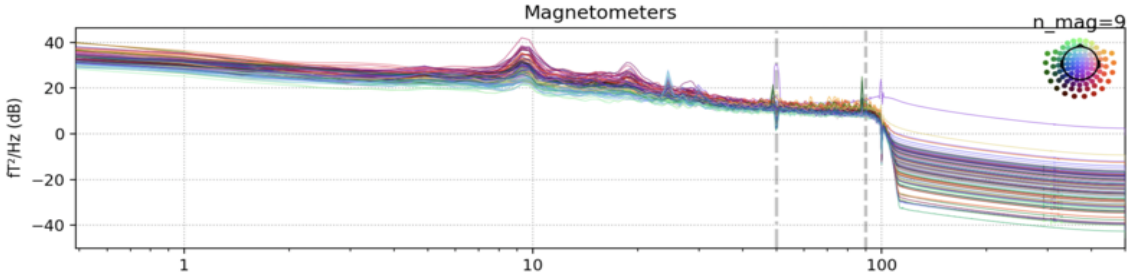
Magnetometers
n_mag=9
fT²/Hz (dB)
40
20
0
−20
−40
1
10
100

L

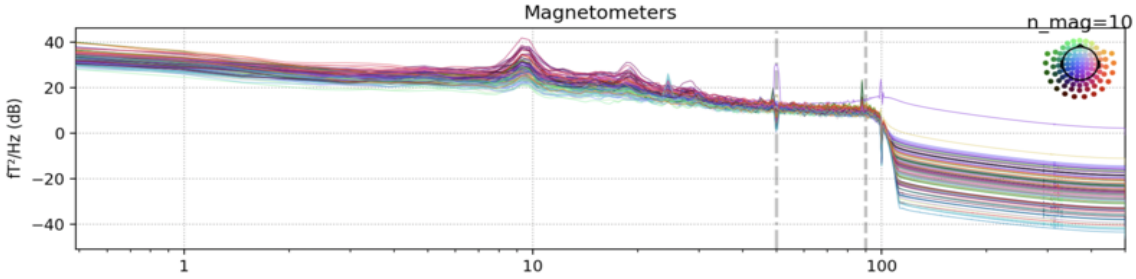
Magnetometers
n_mag=10
fT²/Hz (dB)
40
20
0
−20
−40
1
10
100

M

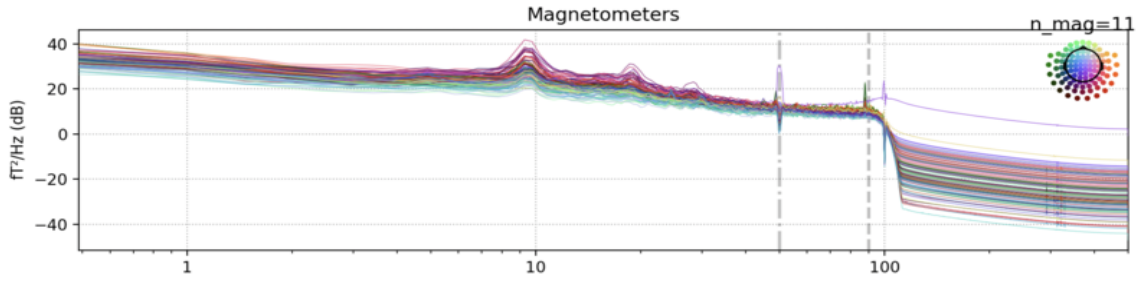
Magnetometers
n_mag=11
fT²/Hz (dB)
40
20
0
−20
−40
1
10
100

N

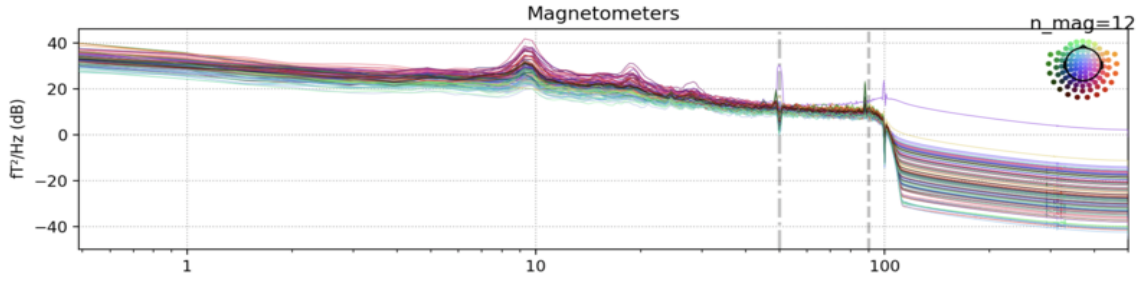
Magnetometers
n_mag=12
fT²/Hz (dB)
40
20
0
−20
−40
1
10
100

O

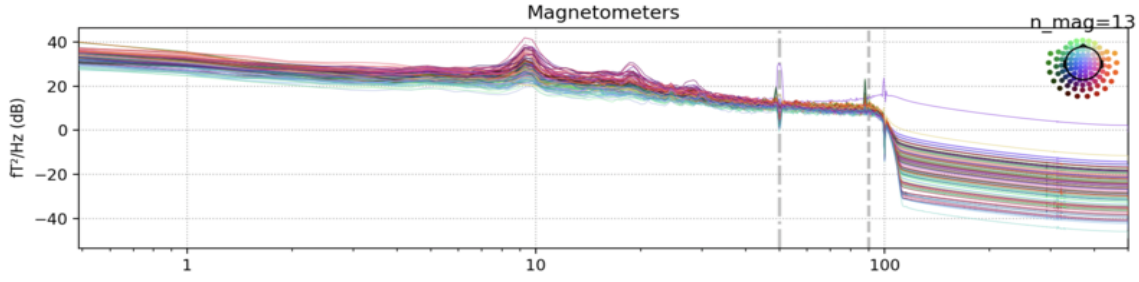
Magnetometers
n_mag=13
fT²/Hz (dB)
40
20
0
−20
−40
1
10
100

P

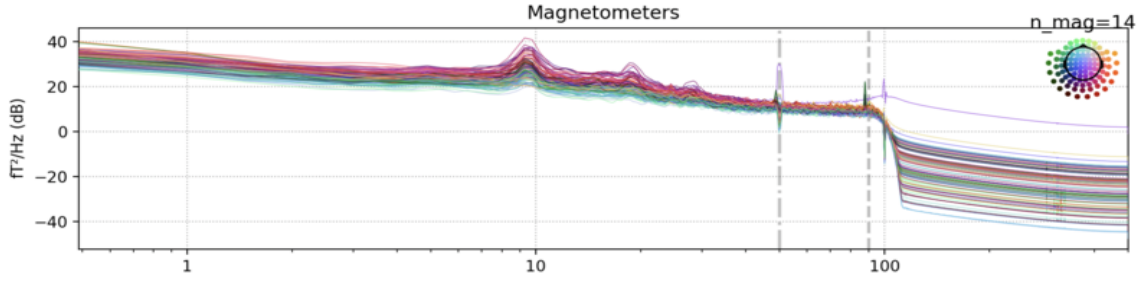
Magnetometers
n_mag=14
fT²/Hz (dB)
40
20
0
−20
−40
1
10
100

Q

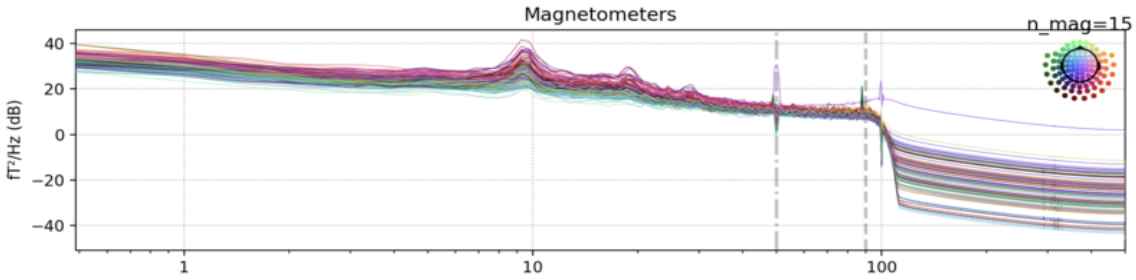

Figure B1. (A) PSD of gradiometers. (B)-(Q) PSD of magnetometers with the number of projectors from 0 to 15.

Appendix C.

Parcellation

Aparc Parcellation is used in Chapter 4 in labelling the source positions. Figure C1 shows the Aparc parcellation label map. Figure C2 shows the Aparc.a2009s label map. Table C1 shows the labels used in the brain areas in the Apace pacellation.

Reference: Desikan et al., 2006

Figure C1. A subject with Aparc parcellation (68 labels).

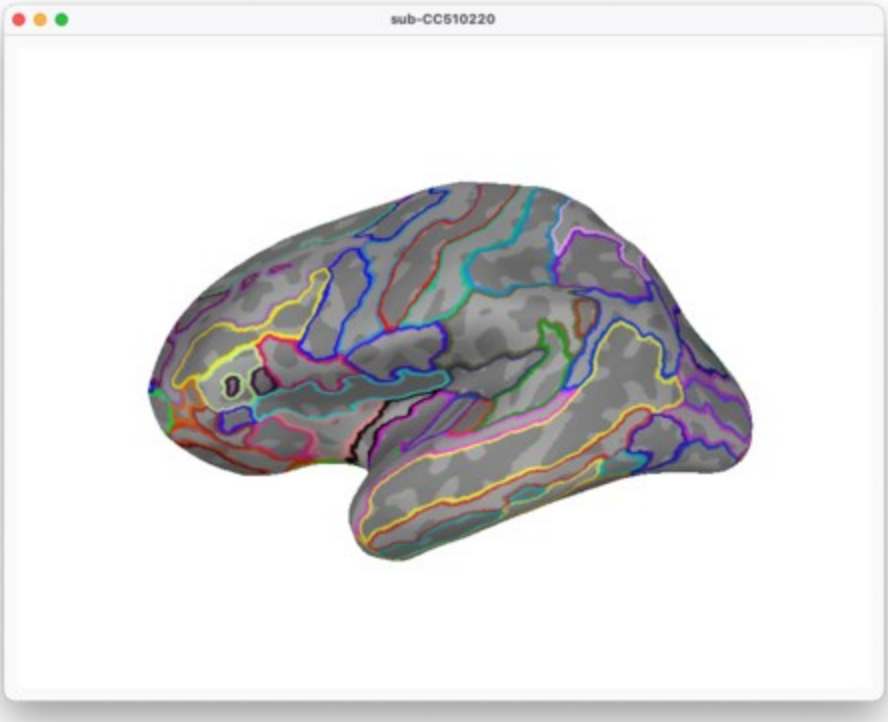

Figure C2. A subject with Aparc.a2009s parcellation.

Table C1. Aparc labels used in five brain regions of interest.

Region of Interest	# Labels
Frontal	**18**
Superior Frontal	
Rostral and Caudal Middle Frontal	
Pars Opercularis, Pars Triangularis, and Pars Orbitalis	
Lateral and Medial Orbitofrontal	
Frontal Pole	
Central	**6**
Precentral	
Paracentral	
Postcentral	
Parietal	**8**
Superior Parietal	

Inferior Parietal	
Supramarginal	
Precuneus	
Temporal	**18**
Superior, Middle, and Inferior Temporal	
Banks of the Superior Temporal Sulcus	
Fusiform	
Transverse Temporal	
Entorhinal	
Temporal Pole	
Parahippocampal	
Occipital	**8**
Lateral Occipital	
Lingual	
Cuneus	
Pericalcarine	

Appendix D.

Boxplots of Alpha Rhythm Properties versus Control Age Group

Boxplots of all the alpha rhythm properties versus age group in Chapter 4 are shown below, with initial outliers removed to help zooming in on the y-axis.

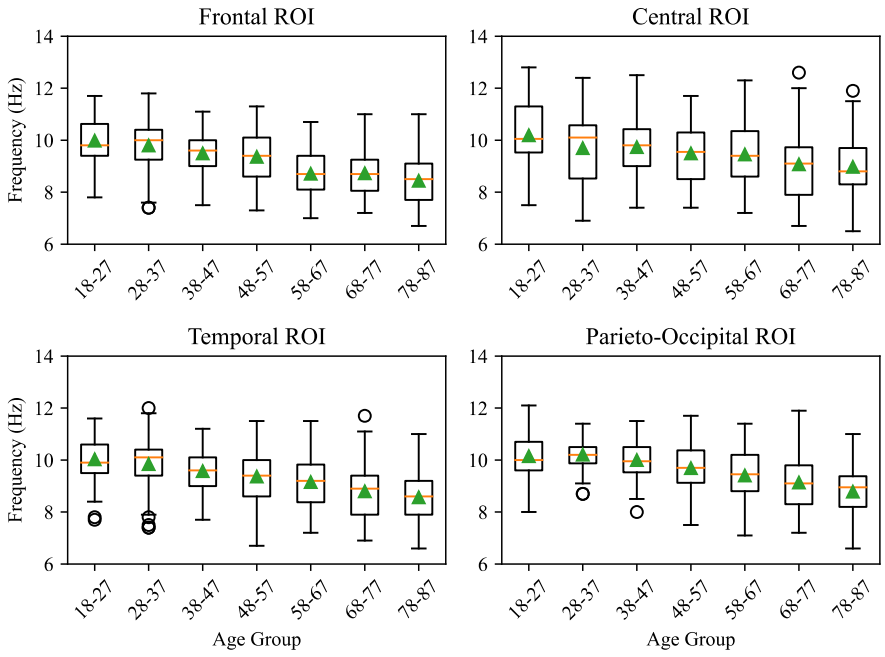

Figure D1. Peak alpha frequency versus control age group

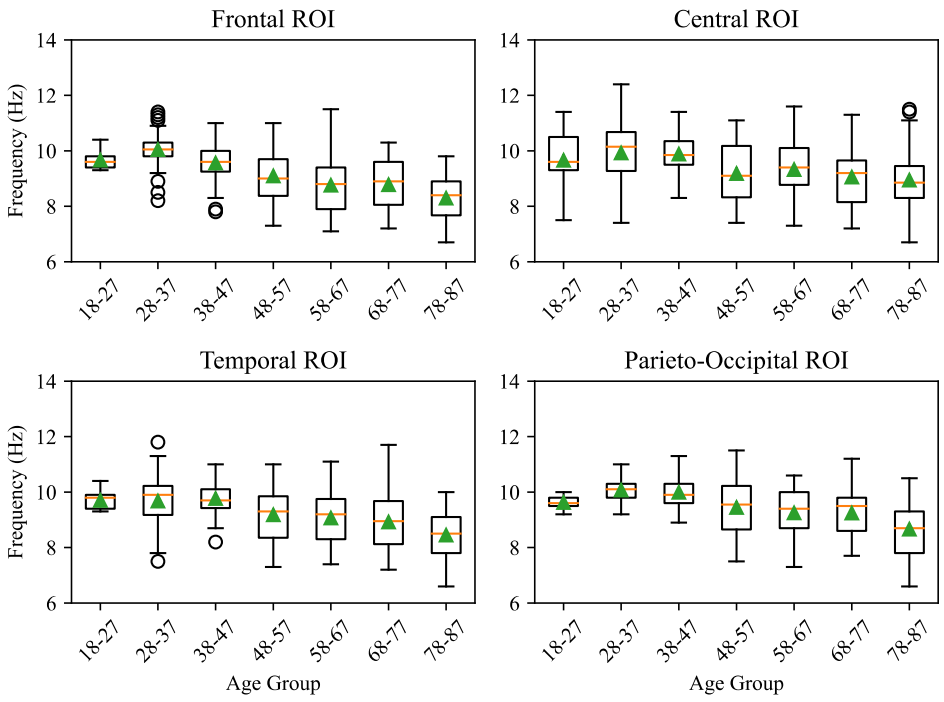

Figure D2. Peak alpha frequency versus male control age group

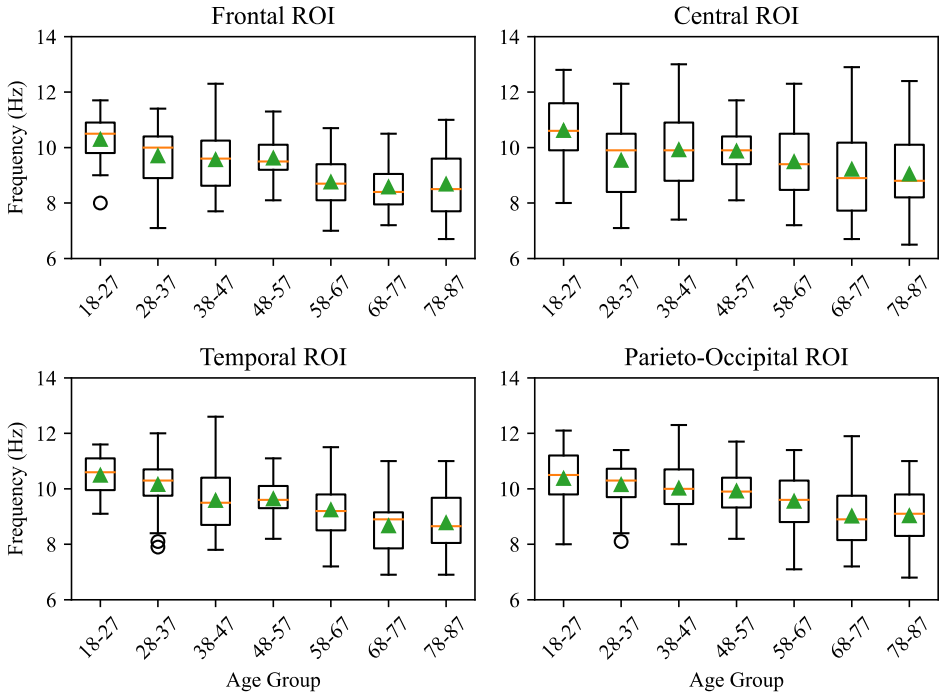

Figure D3. Peak alpha frequency versus female control age group

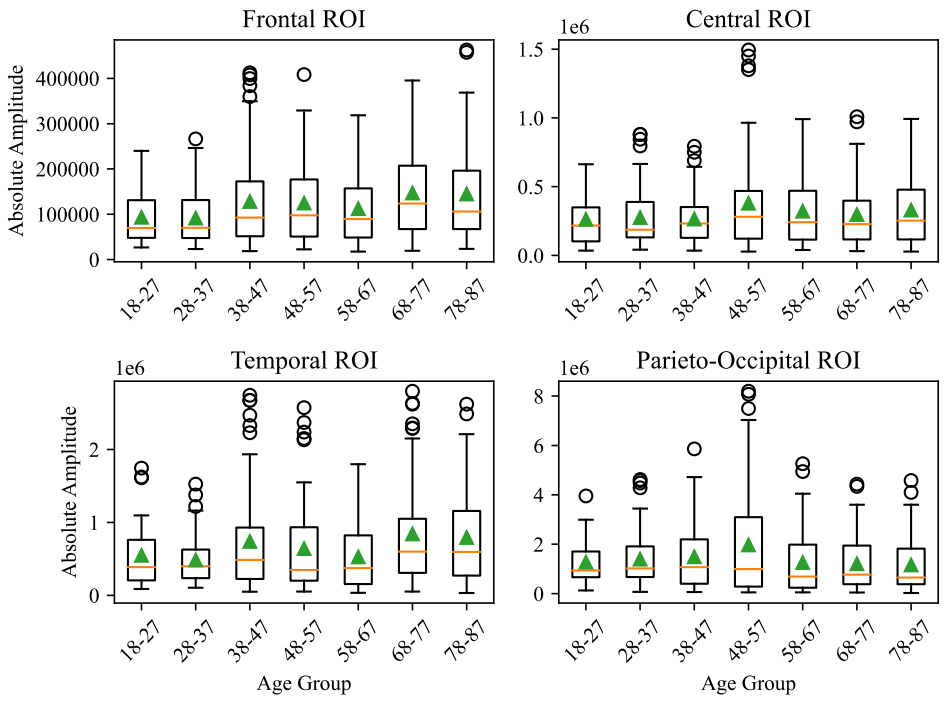

Figure D4. Peak alpha absolute amplitude versus control age group

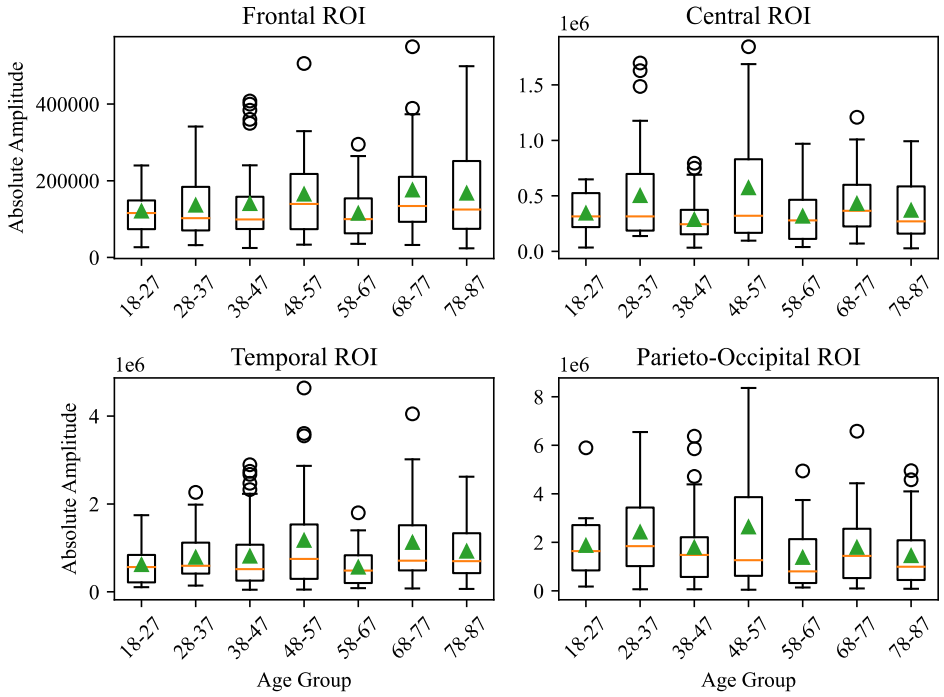

Figure D5. Peak alpha absolute amplitude versus male control age group

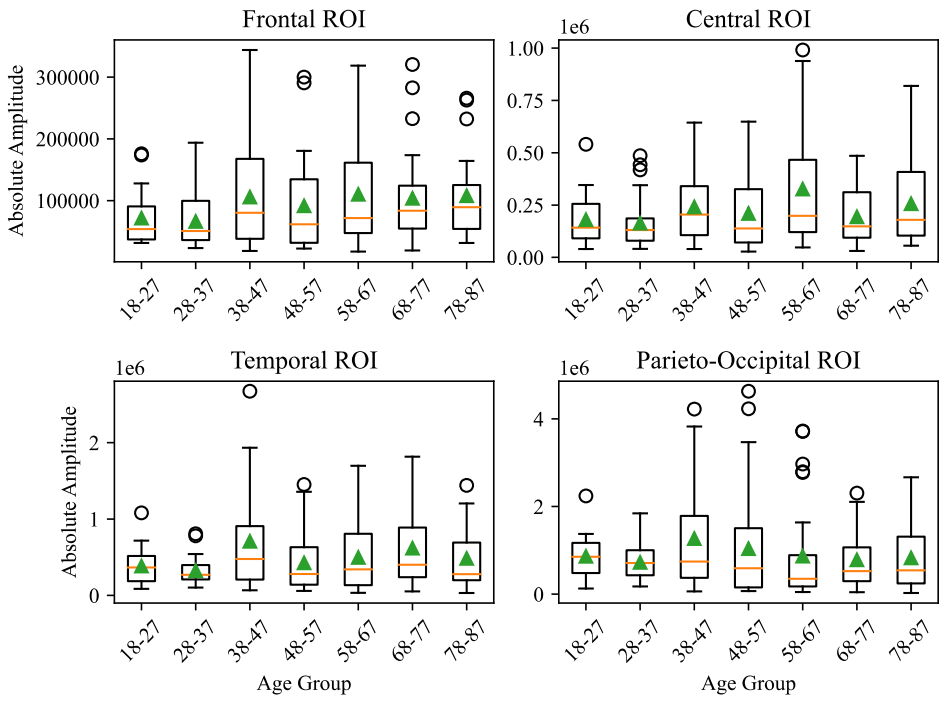

Figure D6. Peak alpha absolute amplitude versus female control age group

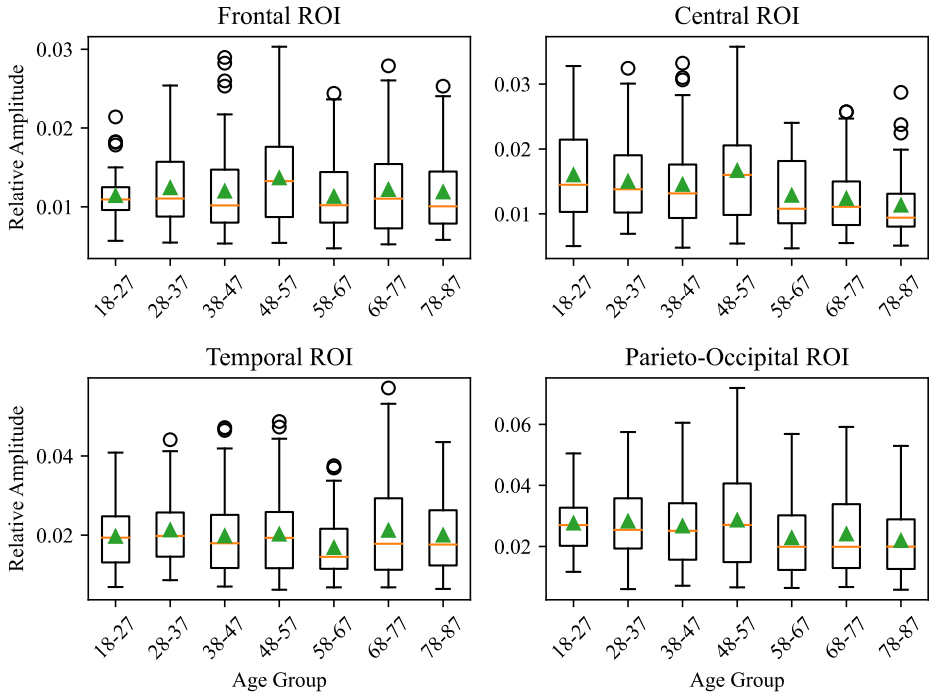

Figure D7. Peak alpha relative amplitude versus control age group

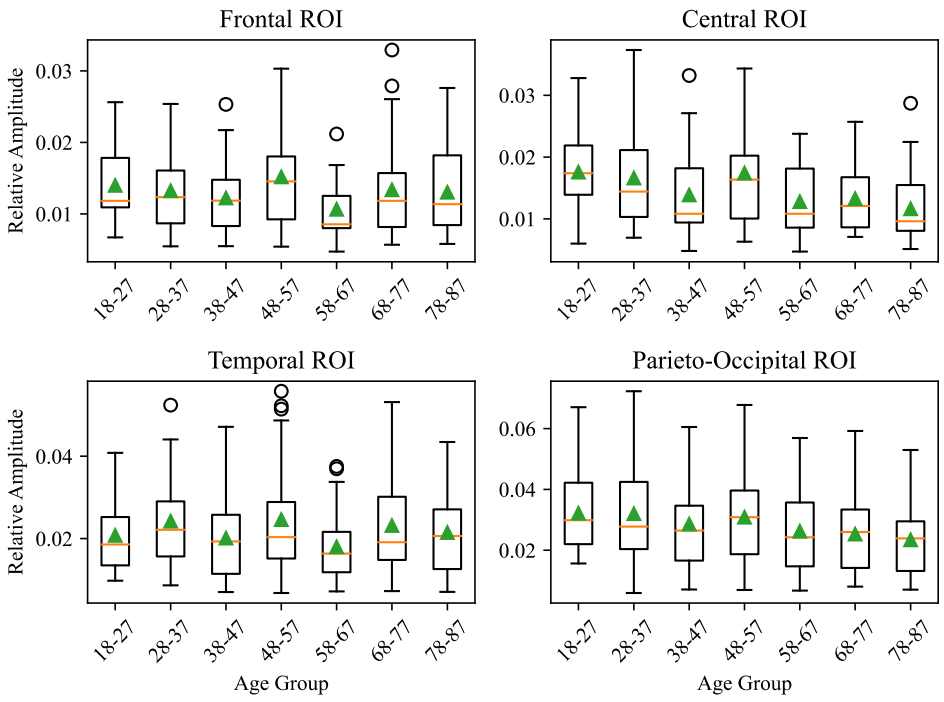

Figure D8. Peak alpha relative amplitude versus male control age group

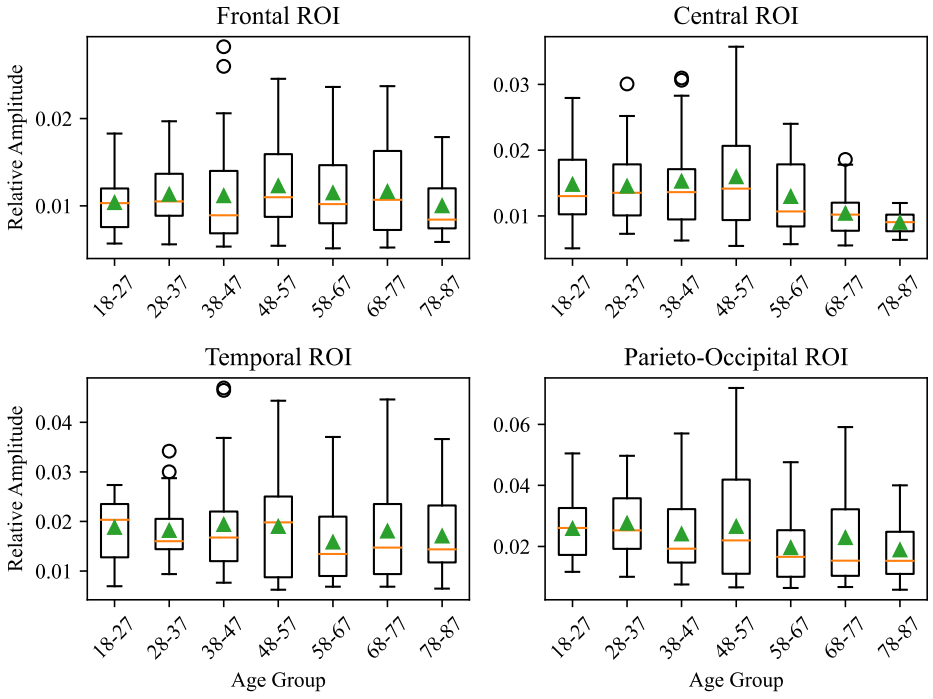

Figure D9. Peak alpha relative amplitude versus female control age group

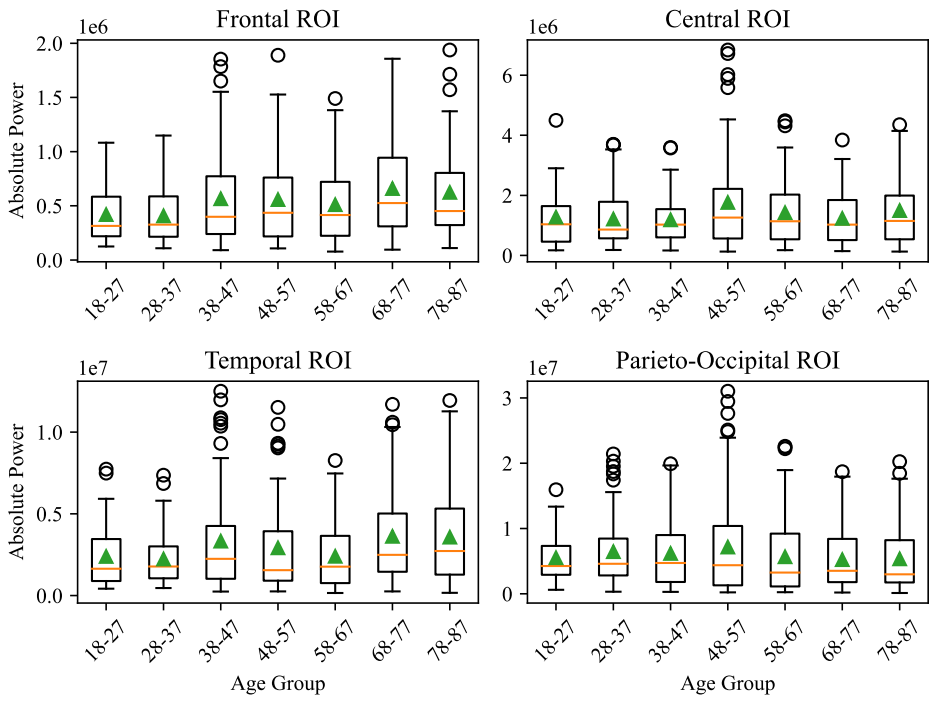

Figure D10. High alpha absolute power versus control age group

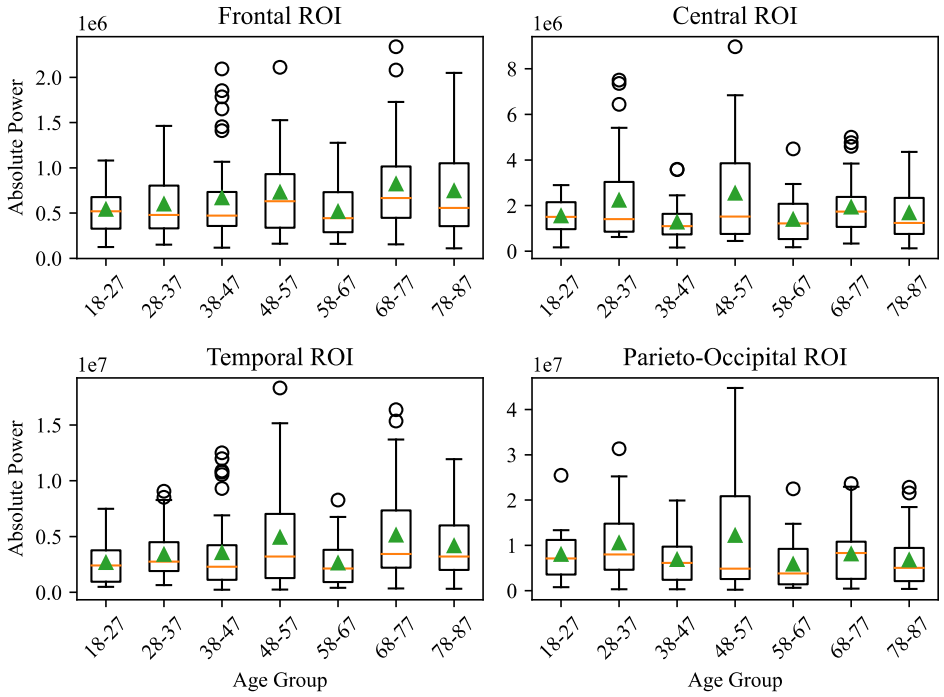

Figure D11. High alpha absolute power versus male control age group

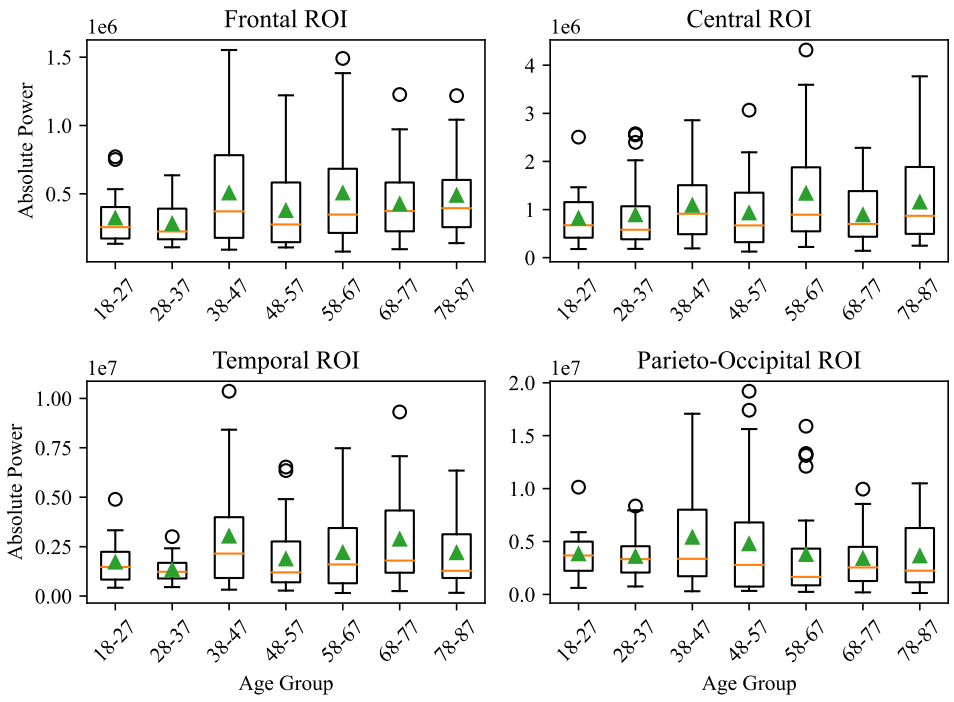

Figure D12. High alpha absolute power versus female control age group

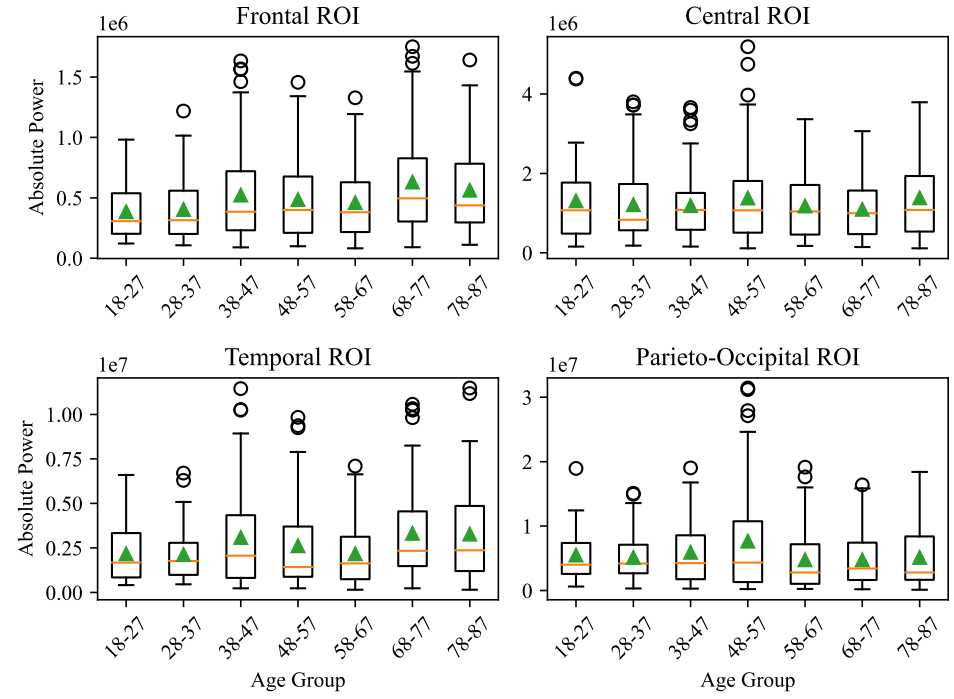

Figure D13. Low alpha absolute power versus control age group

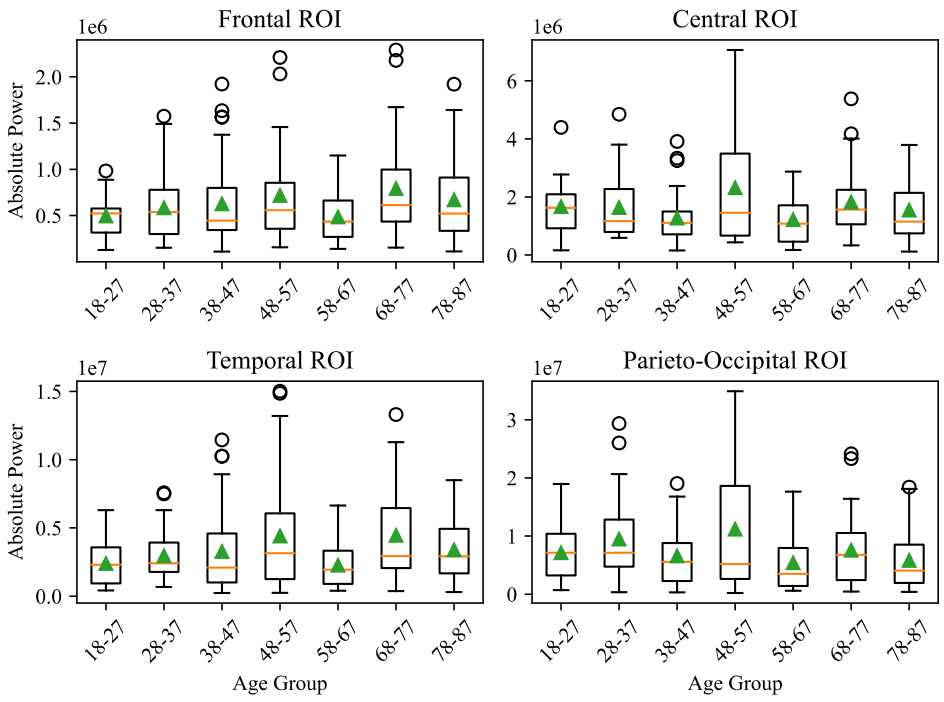

Figure D14. Low alpha absolute power versus male control age group

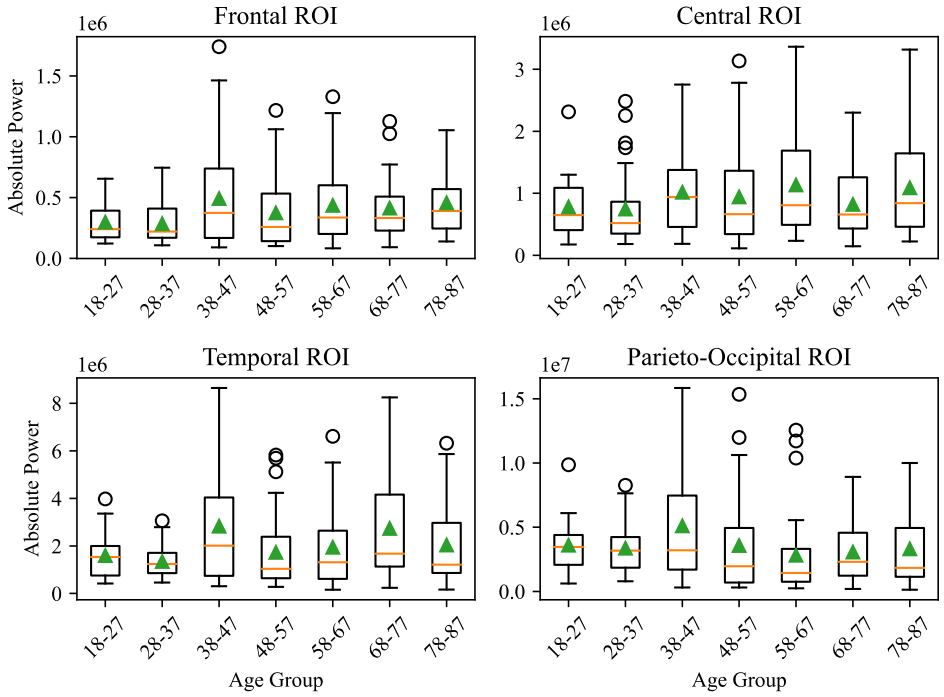

Figure D15. Low alpha absolute power versus female control age group

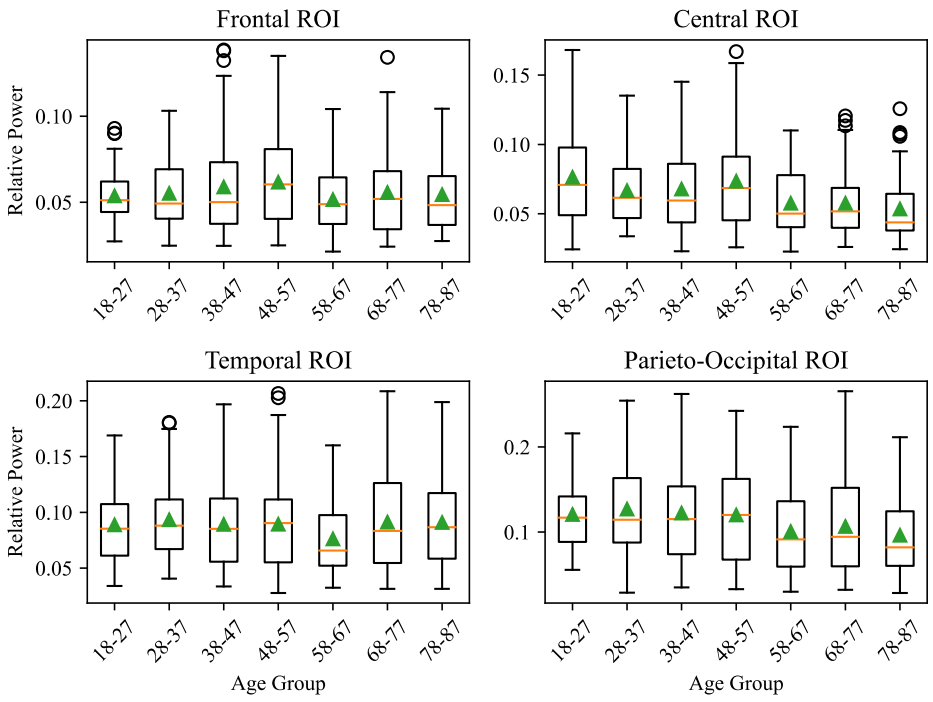

Figure D16. High alpha relative power versus control age group

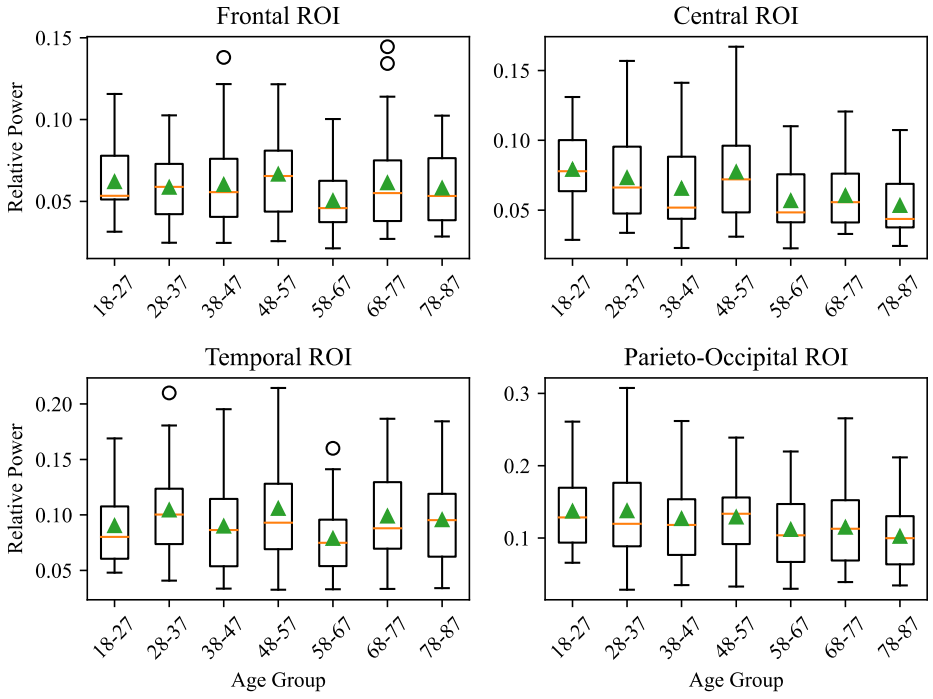

Figure D17. High alpha relative power versus male control age group

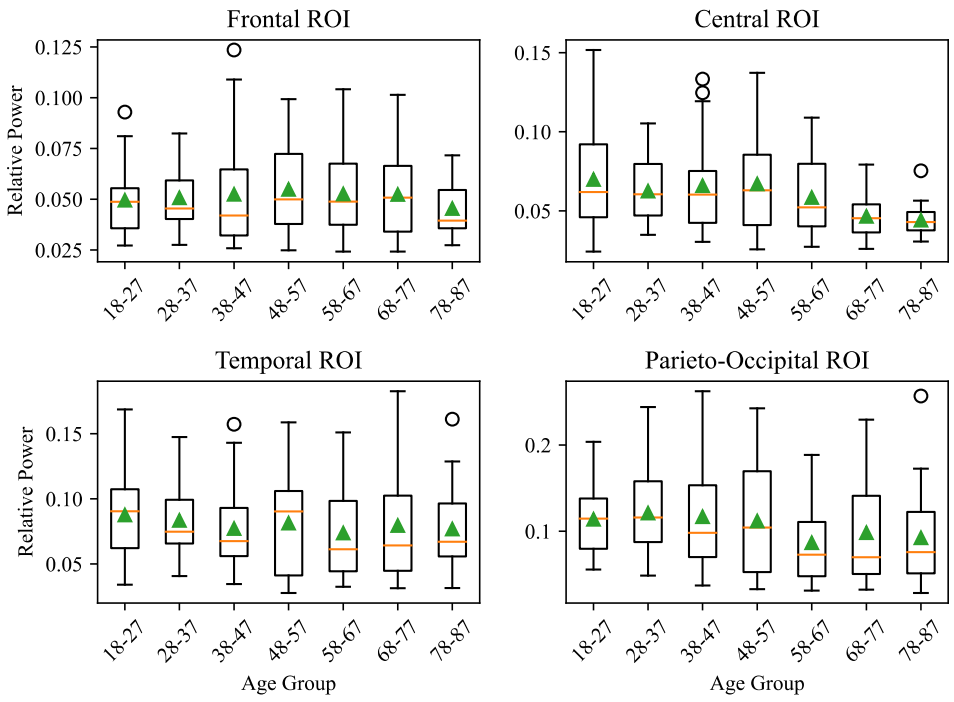

Figure D18. High alpha relative power versus female control age group

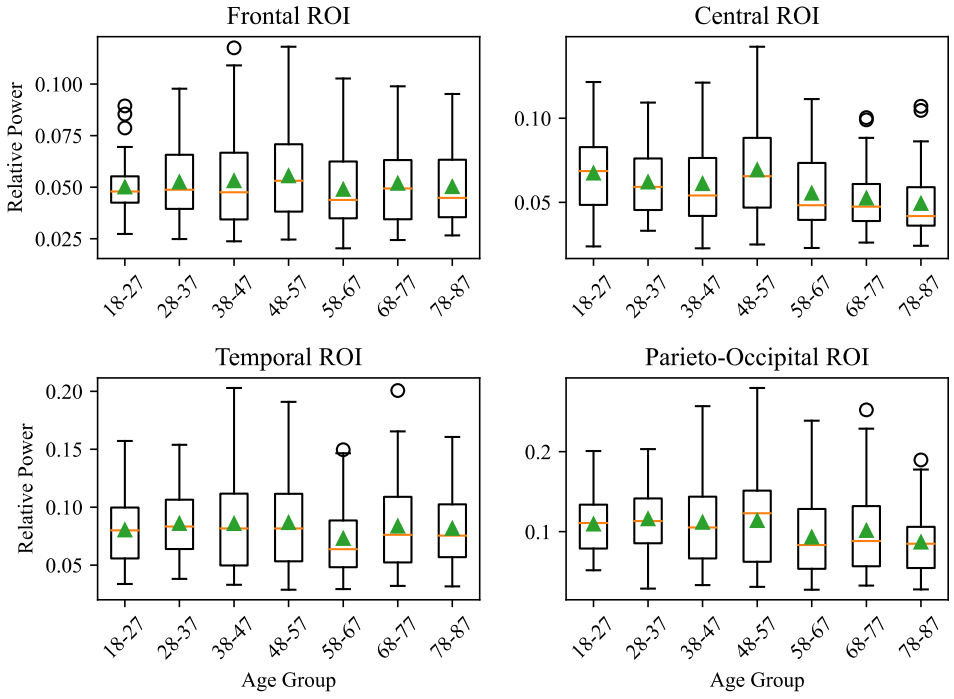

Figure D19. Low alpha relative power versus control age group

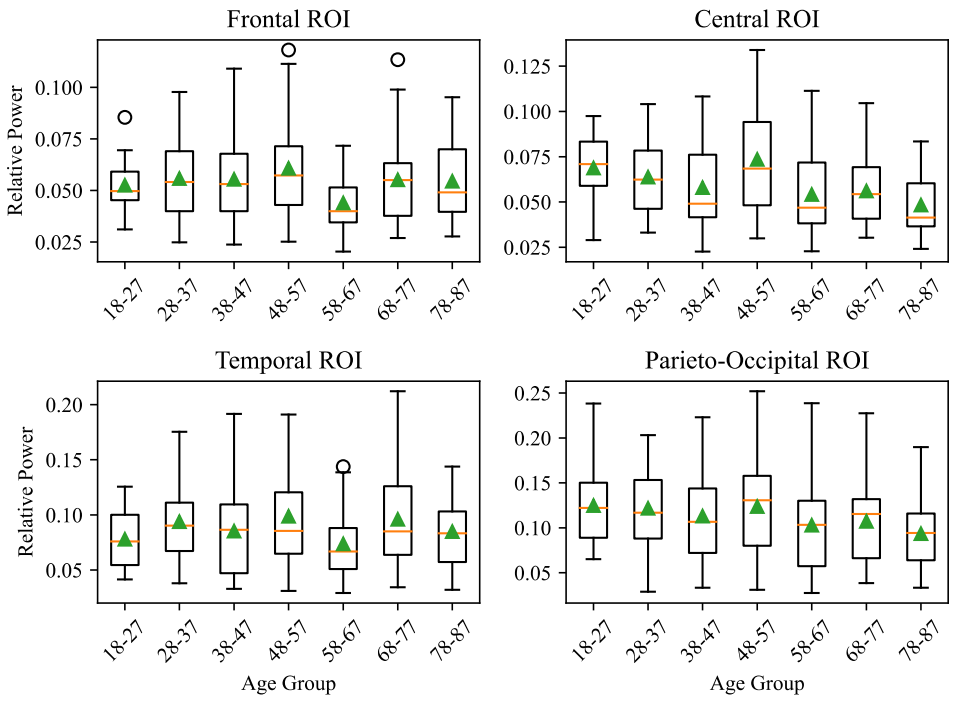

Figure D20. Low alpha relative power versus male control age group

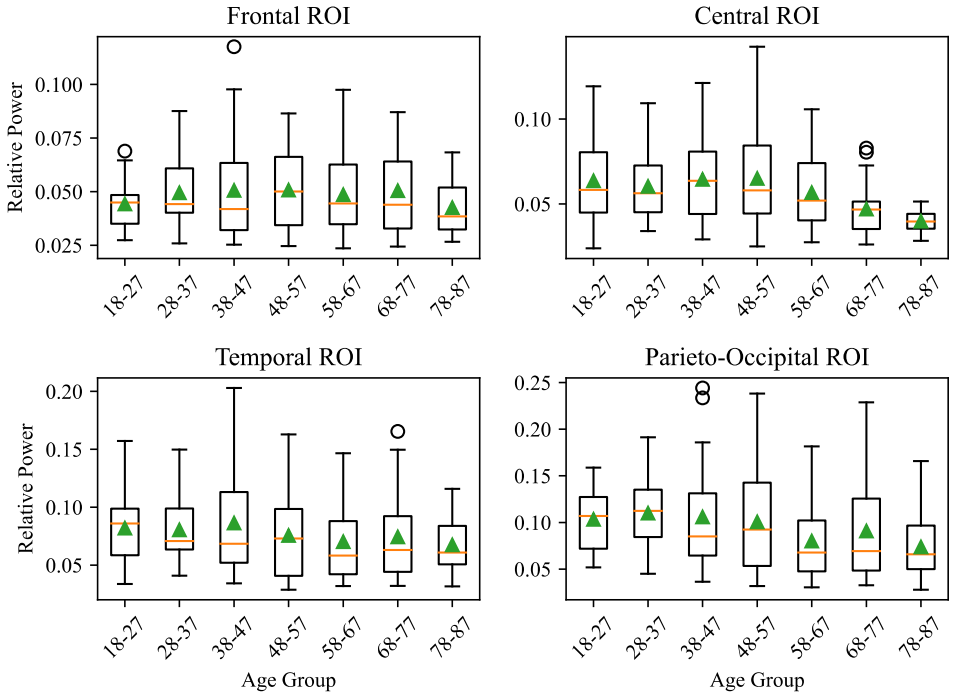

Figure D21. Low alpha relative power versus female control age group